2018

PROTEIN SUPPRESSION OF FLAVIN SEMIQUINONE AS A MECHANISTICALLY IMPORTANT CONTROL OF REACTIVITY: A STUDY COMPARING FLAVOENZYMES WHICH DIFFER IN REDOX PROPERTIES, SUBSTRATES, AND ABILITY TO BIFURCATE ELECTRONS

John Patrick Hoben
University of Kentucky, jphoben@gmail.com
Digital Object Identifier: https://doi.org/10.13023/etd.2018.505

STUDENT AGREEMENT:

I represent that my thesis or dissertation and abstract are my original work. Proper attribution has been given to all outside sources. I understand that I am solely responsible for obtaining any needed copyright permissions. I have obtained needed written permission statement(s) from the owner(s) of each third-party copyrighted matter to be included in my work, allowing electronic distribution (if such use is not permitted by the fair use doctrine) which will be submitted to UKnowledge as Additional File.

I hereby grant to The University of Kentucky and its agents the irrevocable, non-exclusive, and royalty-free license to archive and make accessible my work in whole or in part in all forms of media, now or hereafter known. I agree that the document mentioned above may be made available immediately for worldwide access unless an embargo applies.

I retain all other ownership rights to the copyright of my work. I also retain the right to use in future works (such as articles or books) all or part of my work. I understand that I am free to register the copyright to my work.

REVIEW, APPROVAL AND ACCEPTANCE

The document mentioned above has been reviewed and accepted by the student's advisor, on behalf of the advisory committee, and by the Director of Graduate Studies (DGS), on behalf of the program; we verify that this is the final, approved version of the student's thesis including all changes required by the advisory committee. The undersigned agree to abide by the statements above.

John Patrick Hoben, Student

Dr. Anne-Frances Miller, Major Professor

Dr. Mark Lovell, Director of Graduate Studies

PROTEIN SUPPRESSION OF FLAVIN SEMIQUINONE AS A MECHANISTICALLY IMPORTANT CONTROL OF REACTIVITY: A STUDY COMPARING FLAVOENZYMES WHICH DIFFER IN REDOX PROPERTIES, SUBSTRATES, AND ABILITY TO BIFURCATE ELECTRONS

DISSERTATION

A dissertation submitted in partial fulfillment of the requirements for the degree of Doctor of Philosophy in the College of Arts and Sciences at the University of Kentucky.

By
John Patrick Hoben
Lexington, Kentucky

Director: Anne-Frances Miller, Ph.D., Professor of Chemistry
Lexington, Kentucky
2018

ABSTRACT OF DISSERTATION

PROTEIN SUPPRESSION OF FLAVIN SEMIQUINONE AS A MECHANISTICALLY IMPORTANT CONTROL OF REACTIVITY: A STUDY COMPARING FLAVOENZYMES WHICH DIFFER IN REDOX PROPERTIES, SUBSTRATES, AND ABILITY TO BIFURCATE ELECTRONS

A growing number of flavoprotein systems have been observed to bifurcate pairs of electrons. Flavin-based electron bifurcation (FBEB) results in products with greater reducing power than that of the reactants with less reducing power. Highly reducing electrons at low reduction midpoint potential are required for life processes of both aerobic and anaerobic metabolic processes. For electron bifurcation to function, the semiquinone (SQ) redox intermediate needs to be destabilized in the protein to suppress its ability to trap electrons. This dissertation examines SQ suppression across a number of flavin systems for the purpose of better understanding the nature of SQ suppression within FBEB and elucidates potential mechanistic roles of SQ.

The major achievement of this work is advancing the understanding of SQ suppression and its utility in flavoproteins with the capacity to bifurcate pairs of electrons. Much of these achievements are highlighted in Chapter 6. To contextualize these mechanistic studies, we examined the kinetic and thermodynamic properties of non-bifurcating flavoproteins (Chapters 2 and 3) as well as bifurcating flavoproteins (Chapters 4 and 5). Proteins were selected as models for SQ suppression with the aim of elucidating the role of an intermediate SQ in bifurcation.

The chemical reactions of flavins and those mediated by flavoproteins play critical roles in the bioenergetics of all lifeforms, both aerobic and anaerobic. We

highlight our findings in the context of electron bifurcation, the recently discovered third form of biological energy conservation.

Bifurcating NADH-dependent ferredoxin-NADP+ oxidoreductase I (NfnI) and the non-bifurcating flavoproteins nitroreductase, NADH oxidase, and flavodoxin were studied by transient absorption spectroscopy to compare electron transfer rates and mechanisms in the picosecond range. Different mechanisms were found to dominate SQ decay in the different proteins, producing lifetimes ranging over 3 orders of magnitude. The presence of a short-lived SQ alone was found to be insufficient to infer bifurcating activity. We established a model wherein the short SQ lifetime in NfnI results from efficient electron propagation. Such mechanisms of SQ decay may be a general feature of redox active site ensembles able to carry out bifurcation.

We also investigated the proposed bifurcating electron transfer flavoprotein (Etf) from *Pyrobaculum aerophilum* (*Pae*), a hyperthermophilic archaeon. Unlike other Etfs, we observed a stable and strong charge transfer band (λ_{max}= 724 nm) for *Pae*'s Etf upon reduction by NADH. Using a series of reductive titrations to probe bounds for the reduction midpoint potential of the two flavins, we argue that the heterodimer alone could participate in a bifurcation mechanism.

KEYWORDS: Flavin, Nitroreductase, NADOX, Electron Transfer Flavoprotein, Suppressed Semiquinone, Bifurcation

John Patrick Hoben

November 27, 2018

PROTEIN SUPPRESSION OF FLAVIN SEMIQUINONE AS A MECHANISTICALLY IMPORTANT CONTROL OF REACTIVITY: A STUDY COMPARING FLAVOENZYMES WHICH DIFFER IN REDOX PROPERTIES, SUBSTRATES, AND ABILITY TO BIFURCATE ELECTRONS

By
John Patrick Hoben

Dr. Anne-Frances Miller

Director of Dissertation

Dr. Mark Lovell

Director of Graduate Studies

November 27, 2018

To
Francis Eugene Berrill, William Justin Phifer, and David Arthur Jones…
as well as others who never had an opportunity to finish what they started at a Land-Grant University

ACKNOWLEDGEMENTS

I have been fortunate to work with a full cast of talented, thoughtful, and helpful people. At the helm coaching along the way has been one of the most supportive research mentors I have ever had, Professor Anne-Frances Miller. Many thanks are owed to Professor Miller as well as so many others. The extent of my gratitude will not be fully captured by my words here. However, perhaps I can best honor those that have helped me by continuing to share my skills and publish lessons learned.

Nearly every piece of glassware in the Miller Lab and nearly every instrument in the department has been a victim of my use in the pursuit of this dissertation. The opportunity to truly dive deep into chemical experimentation and instrumentation has been intellectually stimulating but also challenging and, looking back, selfish at times. The molecular world which captured so much of my attention and time required of me a focus and shutter speed orders of magnitude away from my family, friends, and previous colleagues. Perhaps in the fall of 2011 I did not fully grasp the gravity of Professor Art Cammers' words that I must be like a monk regarding my return to the department for doctoral studies.

Early on in the program, John Layton was instrumental in helping me use a number of nuclear magnetic resonance instruments and provided a parental level of care and attention. In those early years, I had many desperate requests for Jeff Babbitt who successfully forged custom anaerobic glassware and optical cells from that were critical to these results. Later on, Art Sebesta, Dr. Sarah Peak, Professor David Atwood, and Professor Mark Watson were instrumental in enabling the set up and maintenance of Schlenk lines and gloveboxes. Professor Testa, Professor Rymond, Dr. David Heidary, and Dr. Ting Wang enabled my use of contemporary molecular biological tools and thinking. The research and my perspective on it presented herein have been, in part, shaped

by the committee (Professors Steven Van Lanen, Arthur Cammers, Mark Lovell, and Anne-Frances Miller) as well as the outsider examiner (Professor Mark Coyne). Many more folks on campus have been helpful in ways beyond the bench, and I am forever thankful to have had a whole team of support.

Collaboration in the Biological and Electron Transfer and Catalysis (BETCy) EFRC, an Energy Frontier Research Center (Department of Energy, DE-SC0012518) has been a whirlwind of professional development, if not travel and demanding benchwork. Special consideration is owed to the teams at Washington State University (John Peters Lab- Dr. Oleg Zadvornyy and Dr. Jacob Artz), University of Georgia (Mike Adams Lab- Dr. Diep Nguyen, Dr. Gerritt Schut), The National Renewable Energy Lab (Paul King Lab- Mike “IUPAC” Ratzloff, Dr. Cara “Laser” Lubner, and Dr. David “Special Agent” Mulder), Arizona State University (Anne Jones Lab- David Jennings and Garrett Williams), and Montana State University (Eric Boyd Lab- Saroj Poudel; Brian Bothner Lab- Dr. Monika Tokmina-Lukaszewska, Dr. Amaya Garcia Costas, and Dr. George Gauss). Although each of these collaborators provided invaluable guidance, I was most humbled by the time Dr. Gerritt Schut took to bring me up to speed not only at the bench but also in my thinking.

On a more personal note, much appreciation is owed to my parents (Ellen Berrill Hoben and Thomas James Hoben) who stood strong when I wanted to quit. Other sources of strength were derived from members of the Bluegrass (The Berrills, West Green, C4, Connie, Aunt Susan), Benton (Beth King, The Evans), and Saco Bay (The Hobens) Family Tree as well as affiliate members of the Knob and River Regions. For those not yet affiliated but equally deserving, you are appreciated. Thank you.

TABLE OF CONTENTS

ACKNOWLEDGEMENTS iii

List of Tables viii

List of Figures ix

List of Schemes xii

CHAPTER 1 INTRODUCTION 1

1.1 Flavoprotein Introduction 1

1.2 Nitroreductase 3

1.3 Bifurcating Systems: Role Of Flavin 5

1.4 Summary of Work 7

CHAPTER 2 ANAEROBIC METHOD FOR *IN-SITU* DETECTION OF *p*-AMINOBENZOIC ACID FORMATION BY NITROREDUCTASE 15

2.1 Introduction 15

2.2 Experimental 16

Materials 16

Over-expression and purification of wild-type NR 16

Anaerobic Method 17

2.3 Results 18

2.4 Discussion 19

2.5 Conclusion 20

2.6 Abbreviations 21

CHAPTER 3 CLONING AND PARTIAL CHARACTERIZATION OF A THERMOPHILIC NR HOMOLOGUE FROM *THERMUS THERMOPHILUS* 27

3.1 Introduction 27

3.2 Experimental 28

Materials 28

Cloning of wild-type NADOX 28

Cloning of 6xHis-NADOX 30
Over-expression and purification of wild-type NADOX 30
Over-expression and purification of 6xHis-NADOX 32
Kinetic Assays 32
Assays of Anaerobic Reduction of WT-NADOX 33
3.3 Results 34
Cloning and expression 34
Enzyme Kinetics 35
Anaerobic Reduction of WT-NADOX 37
3.4 Discussion 37
3.5 Conclusion 39
3.6 Abbreviations 39
CHAPTER 4 EQUILIBRIUM AND ULTRAFAST KINETIC STUDIES MANIPULATING ELECTRON TRANSFER: A SHORT-LIVED FLAVIN SEMIQUINONE IS NOT SUFFICIENT FOR ELECTRON BIFURCATION 51
4.1 Introduction 51
4.2 Experimental 54
Reagents 54
Production of flavodoxin 55
Nitroreductase production 55
Production of wild-type NADOX 55
Production of Nfn 56
Redox titration of NADOX 56
Transient Absorption Spectroscopy 57
Reduction Potentials of Exogenous Donors 59
Steady-State Absorbance and Fluorescence 59
4.3 Results 60
4.4 Discussion 67
4.5 Conclusion 71

CHAPTER 5 INITIAL CHARACTERIZATION OF THE REDOX PROPERTIES OF *PYROBACULUM AEROPHILUM* ELECTRON-TRANSFERRING FLAVOPROTEIN....88
5.1 Introduction....88
5.2 Experimental Procedures....90
Materials....90
Buffer Exchange and Removal of Excess Flavin for As Isolated Samples and Following Flavin Reconstitution....90
Flavin Occupancy....91
Redox Titrations....91
Fluorescence....94
5.3 Results....94
Flavin Occupancy....94
Reductive Titrations and Redox States of the Individual Flavins....95
Assessment of the energies (E°') associated with reduction....98
Reductions Monitored by Redox Standards....100
5.4 Discussion....105
5.5 Conclusion....107
CHAPTER 6 SUMMARY AND OUTLOOK....127
REFERENCES....136
CURRICULUM VITAE....149

LIST OF TABLES

Table 2.1: Analysis of *p*-HABA reaction with NADH using MBTH.....22

Table 3.1: PCR primers 40

Table 3.2: Purification of WT-NADOX. 41

Table 3.3: Purification of 6xHis-NADOX. 42

Table 3.4: WT-NADOX response to exogenous FMN at 25°C 43

Table 3.5: Specific activity for wild-type NADOX in the presence and absence of 2,4-dinitrotoluene (2,4-DNT). 44

Table 3.6: Specific activity for wild-type NADOX for one-electron acceptors. 45

Table 4.1. Processes and lifetimes in proteins 72

Table 4.2. Effects of exogenous donors on NR ASQ decay and OX recovery 73

Table 5.1: Flavin occupancy. 108

LIST OF FIGURES

Figure 1.1: Flavin Structure. 10

Figure 1.2: Representative equilibrium absorbance spectra for the four flavin redox states: oxidized (OX), hydroquinone (HQ), anionic semiquinone (ASQ), and neutral semiquinone (NSQ). 11

Figure 1.3: Comparison of semiquinone (SQ) suppression (dashed line) versus stabilization (solid line) 12

Figure 2.1: Absorbance spectra of MBTH assay components (a) and of reaction mixtures (b). 23

Figure 2.2: MBTH response to 0-1 mM *p*-ABA (a) and mixtures of *p*-HABA and *p*-ABA (b). 24

Figure 3.1: 6xHis-NADOX PCR products resulting from two different annealing temperatures 46

Figure 3.2: SDS/PAGE of WT-NADOX purification steps.. 47

Figure 3.3: SDS/PAGE of 6xHis-NADOX purification steps. 48

Figure 3.4: WT-NADOX response to FMN.....49

Figure 3.5: Anaerobic reduction of WT-NADOX 50

Figure 4.1. Recovery of oxidized flavin.....74

Figure 4.2. Transient absorption spectroscopy (TAS) of NR 75

Figure 4.3. Electron transfer (ET) processes and overlay of the flavin sites.76

Figure 4.4. Recovery of oxidized flavin for NR (455 nm; *black-gray*) and decay of ASQ (375 nm; *red-pink*) in the presence of exogenous electron donors.....77

Figure 4.5. Fluorescence quenching (a and b) and formation of a charge transfer band near 550 nm (c and d) upon binding of the exogenous donors BA (a and c) or PAB (b and d) to NR.....78
Figure 4.6. Structural mechanistic model. 80
Figure 4.S2. Select absorbance transients for the identification of distinct dynamic phases following photoexcitation.....82
Figure 4.S3. Phase-associated difference spectra (PADS) corresponding to photogenerated species 83
Figure 4.S4. Overlay of the active sites of NADOX (*magenta*) and NR with benzoic acid bound (*blue*).....84
Figure 4.S5. Recovery of oxidized flavin (455 nm, *black-grey*) and decay of anionic semiquinone (375 nm, *red-pink*) for nitroreductase (NR) in the presence of 25 or 2500 µM 2-(phenylamino)benzoic acid (PAB). 85
Figure 4.S6. Structures of the exogenous donors used.....86
Figure 4.S7. Derivation of equation describing fluorescence quenching. .87
Figure 5.1: Electron flow in the proposed pathway for *Pae* EtfABCX.....109
Figure 5.2: Reduction of 13 µM as isolated *Pae* EtfAB (jph-5-59; UG-116) with the one electron reductant dithionite.....110
Figure 5.3: Dithionite reduction of 11 µM reconstituted *Pae* EtfAB (jph-5-78; UG-116) (a) followed by NAD^+ addition. 111
Figure 5.4: Reduction of 30 µM 'as isolated Pae EtfAB' (jph-5-60; UG-116) with the two electron reductant NADH. 112
Figure 5.5: Potentiometric dithionite titration of reconstituted 6.5 µM *Pae* EtfAB (jph-5-37; UG-102).....113

Figure 5.6: Plot of absorbance at 368 nm divided by absorbance at 454 nm (A_{368}/A_{454}) for the potentiometric dithionite titration of reconstituted 6.5 µM *Pae* EtfAB (jph-5-37; UG-102). 115
Figure 5.7: Thionine in the oxidized and reduced states.....116
Figure 5.8: Potentiometric dithionite titration of 6.5 µM reconstituted *Pae* EtfAB (jph-5-44; UG-102) in the presence of near equimolar thionine 117
Figure 5.9: Plot of the linear best fit of $\ln(E_{ox}/E_{red})$ versus $\ln(S_{ox}/_{red})$ used in the calculation of *E°'* ($E_{ASQ/HQ}$) for reconstituted *Pae* EtfAB (jph-5-44; UG-102) in the presence of equimolar thionine. 119
Figure 5.10: Phenosafranin in the oxidized and reduced states. 120
Figure 5.11: Potentiometric reductive titration for reconstituted *Pae* EtfAB (jph-5-59; UG-102) (a) and the resulting difference spectra (b) in the presence of equimolar phenosafranin by a xanthine/xanthine oxidase reducing system.. 121
Figure 5.12: Plot of the linear best fit of $\ln(E_{ox}/E_{red})$ versus $\ln(S_{ox}/_{red})$ used in the calculation of *E°'* 123
Figure 5.13: Graphical depiction of the redox transitions observed and their assignment to each flavin site.....124
Figure 6.1: Transient absorbance spectroscopy results from global analysis 135

LIST OF SCHEMES

Scheme 1.1: Redox and ionization states of free FMN (R= CH2(CHOH)3CH2OH2PO3). 13

Scheme 1.2: Enzymatic reactions for Type I vs. Type II nitroreductases. 14

Scheme 2.1: Type I NR performs multiple rounds of pyridine nucleotide-dependent two-electron reductions of substituted aromatics. 26

Scheme 5.1: Flavin-based electron bifurcation (FBEB) 125

Scheme 5.2: Formation of the proposed charge transfer (CT) complex. 126

CHAPTER 1 INTRODUCTION

1.1 Flavoprotein Introduction

The chemical reactions of flavin and those mediated by flavoproteins play critical roles in the bioenergetics of aerobic and anaerobic organisms. Oxidoreductases, a subgroup of flavoproteins that facilitate redox reactions, are the focus of this dissertation. Flavin mononucleotide (FMN) and flavin adenine dinucleotide (FAD) are two of the more common cofactors that flavoprotein active sites bind (**Figure 1.1**). Both FMN and FAD are biological derivatives of riboflavin (vitamin B_2) with extended functional groups at the N10 position. In many flavoproteins, cofactor specificity depends on the N10 functional group identity (1,2). Starting with the isoalloxazine ring system as the base structural unit of flavins, FMN has a phosphorylated ribose group, whereas FAD contains an additional adenine nucleotide (adenosine monophosphate) linking the ribose chain by a diphosphate group.

Understanding of flavoproteins, first discovered in the 1930s (3,4), has grown to encompass a sub-discipline of within enzymology (5-7). Flavin cofactors endow enzymes with the ability to catalyze a wide variety of reactions beyond those of other cofactors, which typically catalyze a single reaction type (8). The ability to catalyze a wide variety of reactions results from the isoalloxazine tricyclic ring system and, upon binding, the cofactor's interaction with the protein backbone and amino acid side chains. Isoalloxazine is generally considered amphipathic, with the xylene ring being hydrophobic and the pyrimidine ring being hydrophilic (8). Generally, the xylene ring interacts with hydrophobic areas of protein binding pockets whereas the redox active

pyrimidine ring (uracil-like) can form multiple hydrogen bonds, akin to nucleobases, and also can form ionic bonds. One- and two-electron transfers (the focus of this thesis), O_2 activation, dehydrogenations, photo(bio)chemistry, isomerizations, redox signaling, and many more reactions are performed by flavoenzymes (9).

The flavin cofactor can access three redox states: oxidized, semiquinone, and fully reduced/hydroquinone (**Scheme 1.1**). As a result, flavoenzymes are able to catalyze and mediate one- and/or two-electron transfers. Additionally, the semiquinone and the hydroquinone states have biologically relevant pKa's (8.5 and 6.8, respectively for free FMN) (10). The redox and protonation states significantly influence a range of the flavin's physicochemical properties. Notably, flavin ultraviolet-visible (UV-Vis) absorbance provides a simple but powerful diagnostic for spectroscopic identification of the redox state and, for the semiquinone, the protonation state (**Figure 1.2**). Visually, flavins are yellow when fully oxidized (OX, λ_{max}= ~450 nm), red in the anionic semiquinone state (ASQ, λ_{max}= ~370 nm), blue in the neutral semiquinone state (NSQ, λ_{max}= ~580 nm), and colorless in the two-electron fully reduced hydroquinone state (HQ, λ_{max}= <500 nm). Typically, redox reactions for flavins proceed via two half-reactions: either the oxidative half-reaction where HQ is oxidized by an acceptor (e.g.- NAD^+) or the reductive half-reaction where OX is reduced by a substrate (e.g. NAD(P)H).

Most flavoenzymes are classified as oxidoreductases, which include reductases, monooxygenases/hydroxylases, electron transferases, dehydrogenases/transhydrogenases, and oxidases (6,9). Oxidoreductases catalyze the transfer of electrons from a reductant to an oxidant and

flavoenzymes are unique in that they are able to catalyze both one or two electron redox reactions using electrons from strict two-electron donors (e.g.- NAD(P)H). An oxidoreductase with many homologs, nitroreductase, is discussed in the following section (11).

1.2 Nitroreductase

Nitroreductases are oxidoreductase flavoenzymes that catalyze the reduction of nitrogen-containing compounds utilizing FAD or FMN as tightly bound cofactors and NAD(P)H as the reductant. Homologs of these enzymes are found across most kingdoms of life and represent a large family of related enzymes (11,12). Furthermore, nitroreductases can be classified as Type I (oxygen-insensitive, “classical”) and Type 2 (oxygen-sensitive), based on their ability to reduce nitro groups in the presence of oxygen via one- or two-electron transfers (13). Type I nitroreductases suppress flavin SQ and are therefore more relevant as models for the study of electron bifurcation than Type II, which do not suppress flavin SQ. Therefore, Type II will only briefly be discussed.

Type II nitroreductases reduce nitro groups via a single-electron transfer in the presence of oxygen (**Scheme 1.2**). Single-electron reduction forms a nitro radical-anion that reacts with oxygen, resulting in a superoxide radical. This superoxide radical then transfers the one-electron back to the nitro group, resulting in a “futile redox cycle.” Under anaerobic conditions, Type II nitroreductases facilitate the overall two-electron reduction like their Type I counterparts.

Type I nitroreductases facilitate sequential two-electron transfers (**Scheme 1.2**). There are two major groups of Type I nitroreductases: Group A and Group B. These designations relate to the nitroreductases’ similarity to

Escherichia coli two nitroreductases NfsA (Group A) and NfsB (Group B). Group A represents the major oxygen-insensitive nitroreductase utilizing NADPH as a reductant, whereas Group B represents the minor oxygen-insensitive nitroreductase able to utilize NADH or NADPH as a reductant (14).

In Type I nitroreductases, the first two-electron transfer to the nitro group results in the formation of a nitrosoaromatic intermediate that is then further reduced to a hydroxylamine by a second two-electron transfer. Some nitroreductases have been shown to produce amines as final products starting from nitroaromatic substrates (15-18). However, the few reports of amine formation employ workup conditions and analytical methods that limit the ability to distinguish between enzymatic versus non-enzymatic amine products (19,20). Such chemistry is, in part, the focus of Chapter 2 where we sought to detect the formation of *p*-aminobenzoic acid formation by nitroreductase (NR) from *Enterobacter cloacae* (Type I, Group B).

Enterobacter cloacae's NR is homodimeric (216 amino acids, 24.5 kDa) with FMN or FAD as a tightly bound cofactor (13,21,22). Utilizing a ping-pong (double-displacement) kinetic mechanism, NR is first reduced by NAD(P)H to produce modified enzyme: doubly reduced NR where the bound flavin is in the HQ state (23). Following $NAD(P)^+$ dissociation, the nitroaromatic secondary substrate binds and is reduced by NR. One turn of the catalytic cycle results in a nitrosoaromatic intermediate and a second turn, using a total of two NAD(P)H equivalents, results in a hydroxylamine product (24). Only one substrate is able to bind at a time with product dissociation preceding secondary substrate binding.

The unusually large substrate repertoire of NR has led to an expanding body of work that seeks to advance both applications (e.g., biodegradation, biosynthesis, prodrug therapy, etc.) and fundamental understanding of NR (e.g., physiological relevance, flavin cofactor reactivity, enzyme dynamics, etc.) (25-29). Despite NR's promiscuity, it strictly facilitates two-electron reductions. Previous work has determined that this is a result of the thermodynamic properties of the FMN cofactor (22). The oxygen insensitivity of NR (and other Type I nitroreductases) can be explained by the thermodynamic suppression of the SQ state (**Figure 1.3**). In the case of NR, the SQ is highly energetic and its formation is thermodynamically unfavorable.

1.3 Bifurcating Systems: Role Of Flavin

Flavin-based electron bifurcation (FBEB), first discovered in 2008, is now considered to be the third fundamental mechanism of energy conservation in biology (30,31). The previously established mechanisms (i.e., substrate-level phosphorylation and electron transport-linked phosphorylation) have long been a subject of study but may not fully capture the scope of bioenergetics within microbes (32). Substrate-level phosphorylation results in the formation of energy-rich ATP or GTP via conversion from ADP and GDP. Common to aerobes and anaerobes alike, substrate-level phosphorylation occurs during glycolysis and the Krebs cycle (aerobic organisms only) and results in a net gain of 2 ATP per glucose molecule (33). Electron transport-linked phosphorylation results in the production of 30 to 36 ATP per glucose molecule (33). To drive electron transport-linked phosphorylation, an electrochemical proton gradient facilitates the synthesis of ATP from ADP. The proton gradient is established as electrons

move down the electron transport chain, and protons are pumped to the intermembrane space of mitochondria resulting in a higher concentration of H^+ ions outside of the mitochondrial matrix.

In FBEB, two electrons are transferred with each electron going to different acceptors. Flavin-based electron bifurcation pairs an energetically favorable reaction (exergonic) with a less favorable reaction (endergonic). Often in FBEB, one equivalent of ferredoxin (E_m= -320 mV) is produced as the reduced product for each equivalent of NAD(P)H oxidized (E_m= -420 mV) (32). Overall, a medium power reducing agent is utilized to produce a stronger reducing agent. This allows organisms to use available and abundant reducing equivalents for the production of products with greater reducing power. Flavin-based electron bifurcation was first discovered in the FAD-containing crotonyl-CoA reductases from *Clostridium tetanomorphum* and *Clostridium pascui* (30). This flavoenzyme is comprised of three α-subunits (40 kDa) as butyryl-CoA dehydrogenase (Bcd) and the β-subunit (36 kDa) and γ-subunit (28 kDa) as the subunits of an electron-transferring flavoprotein (Etf) (30). It was proposed that one of the two flavin sites of the Etf-Bcd complex could bifurcate two electrons from NADH, with one electron going to the more positive acceptor crotonyl-CoA and the other going to the more negative acceptor ferredoxin. Follow-up studies on the Etf-Bcd complex have substantiated the proposed paths of electrons following bifurcation at flavin (34,35).

More recently, FBEB has been proposed and/or observed in other flavoenzyme systems, notably, the Etf homologs of microbes (36-38). However, detailed mechanistic information on the kinetics and thermodynamics of electron transfer from the bifurcating flavin to acceptors is largely unknown. Early

mechanistic findings indicate that the capacity for a flavin site to perform bifurcation is related to thermodynamic suppression of SQ by the protein active site (**Figure 1.3**) (31,39). This dissertation examines SQ suppression across a number of flavin systems for the purpose of better understanding the nature of SQ suppression within FBEB and elucidates potential mechanistic roles of SQ.

In Chapter 4, we focus on a different class of bifurcating system: transhydrogenase NADH-dependent ferredoxin-$NADP^+$ oxidoreductase I (Nfn) from *Pyrococcus furiosus*. We return to considering Etf protein complexes in Chapter 5 with the initial characterization of the Etf heterodimeric core from the microaerophilic crenarchaeote *Pyrobaculum aerophilum* - the first hyperthermophile to demonstrate the capacity to bifurcate. Our aim in studying various classes of proteins with homology to known bifurcating systems was to identify mediating factors and mechanisms at the level of the electron which allow for bifurcation.

1.4 Summary of Work

Flavoenzymes perform an array of catalysis and signaling functions and our work provides specific insight into the redox properties and kinetics governing SQ suppression and the ability to bifurcate electrons. In this work, we explore the redox reactions and states that flavin environments enable. We examine both kinetic and thermodynamic properties of non-bifurcating (NR and NADOX) as well as bifurcating (NfnI and EtfAB) systems. Chapters 2 and 3 focus on NR and its thermophilic homolog, NADOX, in the context of models for flavin environments that suppress SQ and perform strict two-electron reductions.

Chapters 4 and 5 continue the consideration of suppressed SQ but transition to examine potential mechanisms of bifurcation.

Chapter 2 addresses the difficulty in evaluating amine production by flavoenzyme NR. To evaluate the feasibility of using NR to produce substantial quantities of aromatic amines, an anaerobic *in-situ* method was developed. Using 3-methyl-2-benzothiazolinone hydrazine (MBTH), amines are detected colorimetrically by the formation of a strongly absorbing chromophore. The method can be adapted for use as a screen to detect the production of amines by NR homologs and mutants.

Chapter 3 examines an NR homolog, NADH oxidase (NADOX), from the extremophile *Thermus thermophius.* NADOX may share NR's large substrate repertoire but has been much less studied. The work contained in Chapter 3 describes the subcloning of the NADOX gene into overexpression vectors, the purification of the wild type and His-tagged holoenzymes, as well as the initial characterization of catalytic activity and redox properties. We propose that NADOX performs much of the same chemistry as NR but across a broader range of pH, temperature, and chaotropic agent concentrations. Further, we hypothesize that the extreme stability of NADOX should allow the enzyme to be more tolerant of mutations compared to NR. Through mutation of key active-site residues of NADOX, we hope to modulate the substrate repertoire, reduction potential, and extent of flavin cofactor semiquinone formation.

Chapter 4 investigates the requirements for electron bifurcation to occur and highlights what is necessary versus what is sufficient. Utilizing the flavoenzyme Nfn, we demonstrate that while a short-lived ASQ is expected from

the high energy SQ it is not sufficient in determining the capacity for electron bifurcation; although, the existence of an ASQ state may be necessary.

Chapter 5 reports on the initial characterization of the redox properties of the Etf from *Pyrobaculum aerophilum* and flavin oxidation states for each of the two flavins that could participate in a bifurcation mechanism.

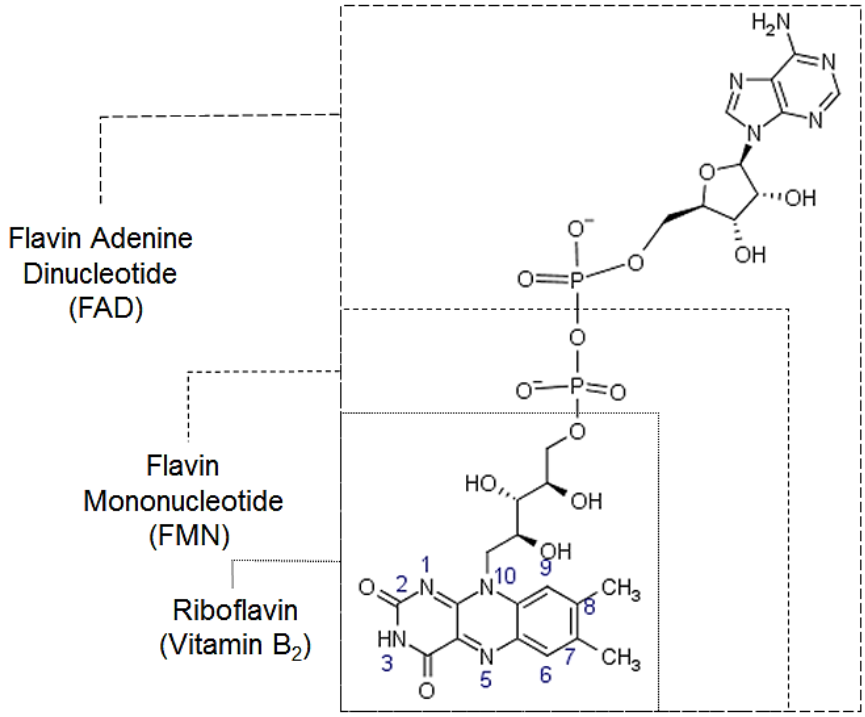

Figure 1.1: Flavin Structure. Starting with the isoalloxazine tricyclic ring system, the three common biological flavins differ by the length of the prosthetic groups attached at the N10 position with flavin adenine dinucleotide (FAD) being the longest. The dashed boxes indicate the terminal atom for a given flavin.

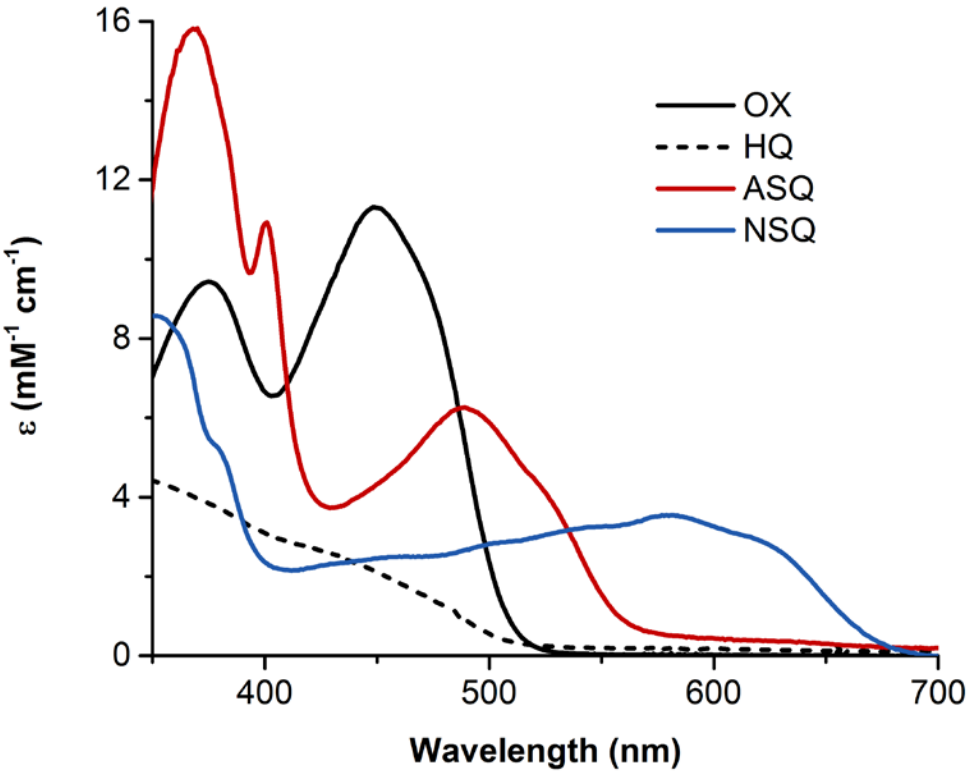

Figure 1.2: Representative equilibrium absorbance spectra for the four flavin redox states: oxidized (OX), hydroquinone (HQ), anionic semiquinone (ASQ), and neutral semiquinone (NSQ).

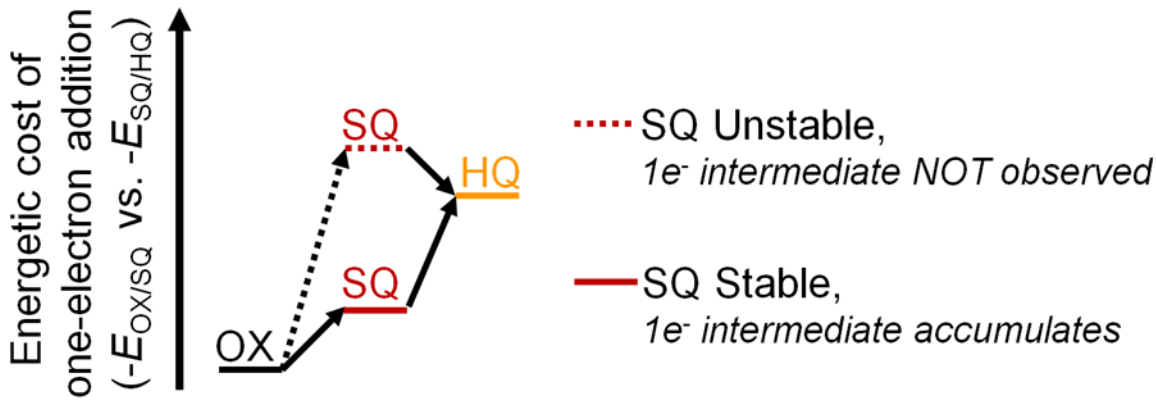

Figure 1.3: Comparison of semiquinone (SQ) suppression (dashed line) versus stabilization (solid line). The y-axis is meant to convey the energetic cost associated with the one-electron reduction steps. A more positive midpoint potential stabilizes the SQ when considering the one-electron oxidized (OX) to SQ redox couple energy (EOX/SQ) compared to the hydroquinone (HQ) redox couple energy (ESQ/HQ). The solid line represents flavin sites similar to flavodoxin whereas the dashed line represents the current working model for bifurcating flavin sites.

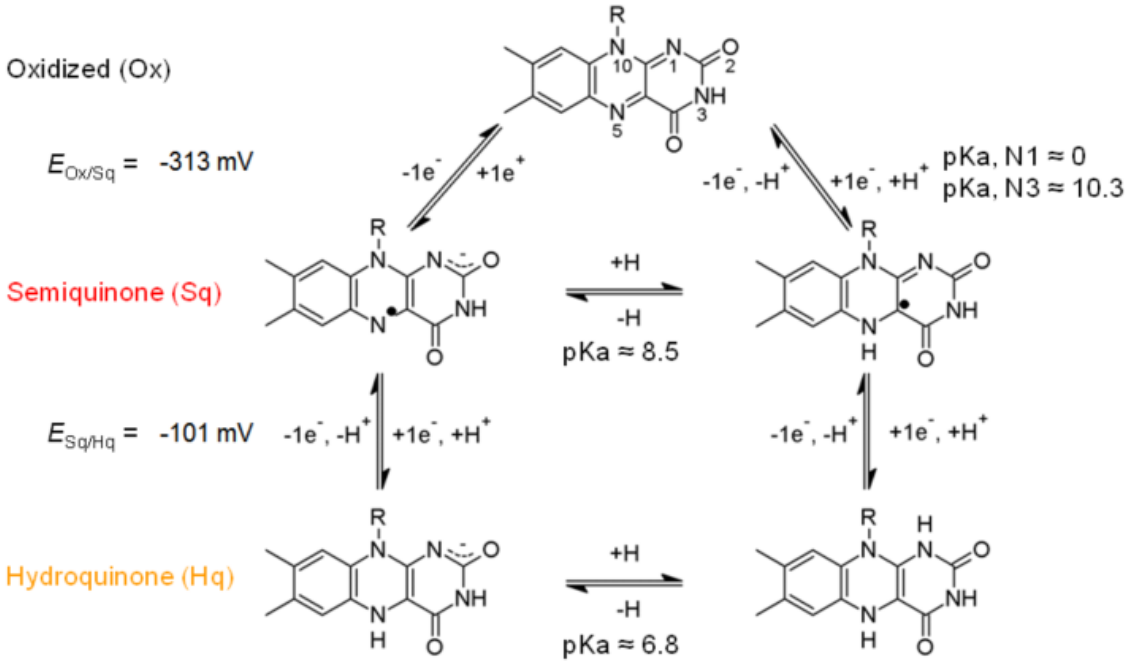

Scheme 1.1: Redox and ionization states of free FMN (R= CH2(CHOH)3CH2OH2PO3). The midpoint potentials for one-electron potentials (*E*°') are shown for the OX to SQ ($E_{OX/SQ}$) and SQ to HQ ($E_{SQ/HQ}$) reduction steps as determined at pH 7 and 20 °C (10). Unlike free FMN, the electron transfer enzyme flavodoxin stabilizes SQ which will accumulate during a reductive titration as a result of the midpoint potentials: $E_{OX/SQ}$= -148 mV; $E_{OX/HQ}$ = -439 mV (40). The difference between the one-electron couples ($E_{OX/SQ}$ and $E_{SQ/HQ}$) determines the equilibrium concentration of SQ (41):

$$E_{SQ/HQ} - E_{OX/SQ} = -59 \text{ mV} \log K \qquad \text{eq. 1.1}$$

$$K = \frac{[SQ]^2}{[OX]\,[HQ]} \qquad \text{eq. 1.2}$$

The SQ is 8% of the equilibrium concentration for free FMN at pH 7 while flavodoxin stablilizes nearly 100% of the SQ.

Adapted from Mayhew, S. G. (1999) The effects of pH and semiquinone formation on the oxidation-reduction potentials of flavin mononucleotide - A reappraisal. *Eur. J. Biochem.* **265**, 698-702.

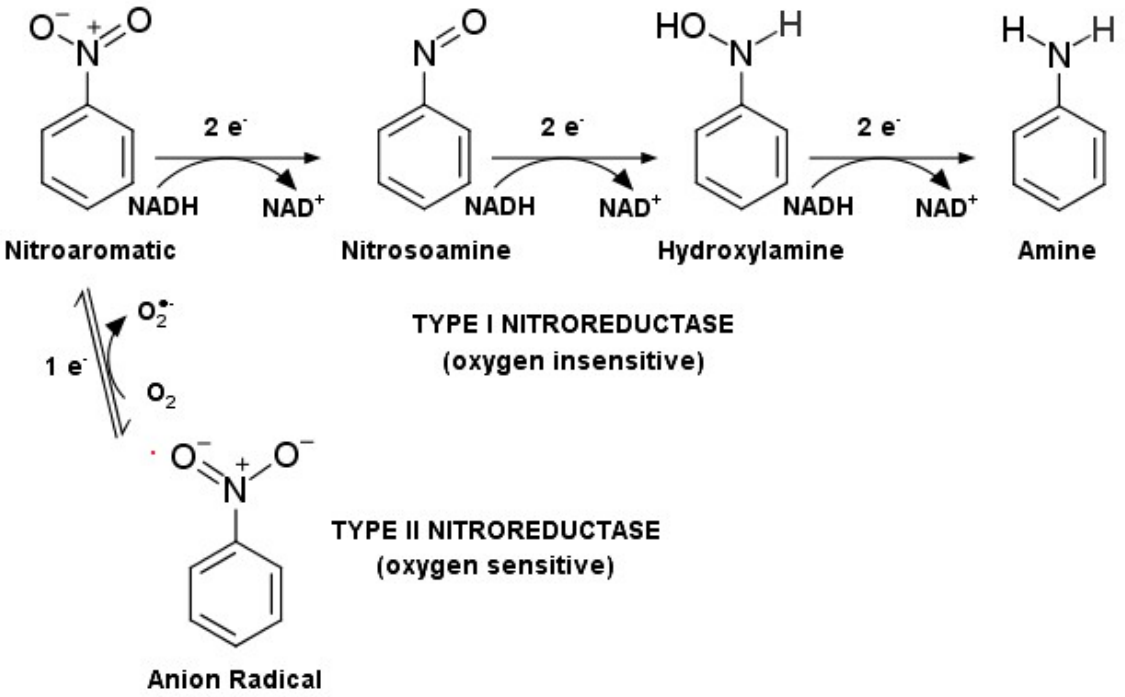

Scheme 1.2: Enzymatic reactions for Type I vs. Type II nitroreductases.

Adapted from Koder, R. L., Haynes, C. A., Rodgers, M. E., Rodgers, D. W., and Miller, A. F. (2002) Flavin thermodynamics explain the oxygen insensitivity of enteric nitroreductases. Biochemistry 41, 14197-14205.

CHAPTER 2 ANAEROBIC METHOD FOR *IN-SITU* DETECTION OF *P*-AMINOBENZOIC ACID FORMATION BY NITROREDUCTASE

NOTE: Chapter 2 includes previously published work from:

Pitsawong, W., Hoben, J. P., and Miller, A. F. (2014) Understanding the Broad Substrate Repertoire of Nitroreductase Based on Its Kinetic Mechanism. *J. Biol. Chem.* **289**, 15203-15214.

Such content is denoted by use of quotation marks and is presented in accordance with the policies set forth by the American Society for Biochemistry and Molecular Biology to allow reuse of any material published in its journals (the Journal of Biological Chemistry, Molecular & Cellular Proteomics and the Journal of Lipid Research).

2.1 Introduction

The large substrate repertoire of nitroreductase (NR) presents a rare opportunity to use a single enzyme for the biodegradation and biosynthesis of many chemicals. Starting from substituted nitroaromatic compounds, as well as a smaller number of known nitroalkenes, cyclohexenones, and quinones, *Enterobacter cloacae* NR (EC 1.6.99.7) and its many bacterial homologues catalyze the NADH- and NADPH-dependent reduction using a flavin mononucleotide (FMN) or flavin adenine dinucleotide (FAD) cofactor (13,23). Reduction of nitroaromatic (**Scheme 2.1a**) compounds by NR yields the corresponding reactive aromatic nitroso- (**Scheme 2.1b**) and hydroxylamino (**Scheme 2.1c**) products (**Scheme 2.1d**). Amine formation for some NRs has been previously reported (15,16,42). However, direct quantification of products has been complicated due to the sensitivity of aromatic hydroxylamines and amines to O_2 and water. The few reports of amine formation employ workup conditions and analytical methods that limit the ability to distinguish between enzymatically- versus non-enzymatically-formed amine products (15,16,18,42).

Thus, a convenient method is needed to quantify amine formation resulting from NR activity and distinguishing this from effects of spontaneous reactions.

To detect aromatic amines, with minimal interference from aromatic hydroxylamines, the 3-methyl-2-benzothiazolinone hydrazone (MBTH) assay was adopted. This assay has been primarily used to detect phenols (43) but can also detect aromatic amines (44). The reaction of the chromogen MBTH and the analyte aromatic amine is outlined in **Scheme 2.1**. The reactions leading to chromophore production are irreversible, and the products are not air-sensitive. The chromogenic reaction can be conducted by simple addition of reagents following the enzymatic reaction, and the entire process can be conducted in a glove box so that any aromatic amines formed will not be oxidized, nor will hydroxylamines that are the necessary precursors to amine production. Because there is relatively little manipulation involved, the method can be adapted for use as a screen to detect and quantify production of amines by NR homologues and mutants.

2.2 Experimental

Materials

"NADH (100% purity) was purchased from Roche. *p*-Nitrobenzoic acid (*p*-NBA) was from Acros Organics. *p*-hydroxylaminobenzoic acid (*p*-HABA) was the generous gift of K. Ferguson and A. S. Bommarius (School of Chemical & Biomolecular Engineering, Georgia Institute of Technology) and was determined to be 99% pure based on NMR. All other reagents were purchased from Sigma-Aldrich."

Over-expression and purification of wild-type NR

Wild-type NR from *E. cloacae* was expressed as previously described (45) and purified using the modified procedure reported in a previous dissertation

(46). “The concentration of holo-NR was evaluated based on the extinction coefficient of the bound flavin, $\varepsilon_{454} = 14.3 \times 10^3\ M^{-1}cm^{-1}$” (45).

Anaerobic Method

“The possible formation of aromatic amines was assessed by MBTH which reacts with aromatic amines to produce a strongly-absorbing chromophore ($\varepsilon_{550nm} > 2\ mM^{-1}cm^{-1}$) (43,44).”

“All manipulations were performed under inert atmosphere (N_2) in a glove box ($[O_2] \leq 10$ ppm) at room temperature. With the exception of concentrated enzyme solutions, all reagents and materials were equilibrated in the glove-box overnight in advance of use. Enzyme solutions were rendered anaerobic by 5-10 pump-purge cycles of ~30 seconds each followed by equilibration in the glove-box for 1 hour. Enzymatic reactions and controls were run for 0, 0.25., 0.5., or 10 hours in 50 mM potassium phosphate pH 7.50 containing 1.25 mM NADH, 0-1 mM *p*-ABA and/or 0-1 mM *p*-HABA. Enzymatic reactions contained 17.5 µM NR. At the end of the reaction time, enzyme was removed by ultrafiltration using a centrifugal filter (EMD-millipore, 10 kDa cutoff).” This step was also executed for control samples. Removal of the protein also resulted in a lower background level of chromophore production. This was, therefore, attributed to reactions between the MBTH and amine functionalities of the protein. “The published protocol for quantifying substituted aromatic compounds using MBTH was optimized to accommodate the presence of NADH. In anaerobic conditions, 1.5 mM MBTH and 6.5 mM $Ce(SO_4)_2$ in the presence of 0.5-1 mM *p*-ABA produced the largest increase in absorbance at 550 nm.“ To perform the assay, 500 µL of the enzymatic reaction was loaded into a centrifugal filter and spun at 1000x g for 15 to 20 minutes. The filtrate (400 µL) was placed in a 1.5 mL tube and then 160 µL of a fresh 6.75 mM MBTH stock solution in water was added and mixed slowly by pipetting with caution to avoid the formation of air bubbles. Next, 160 µL of a fresh 29.25 mM $Ce(SO_4)_2$ stock in 0.4% H_2SO_4 (aqueous) was added slowly with mixing by pipetting to slowly introduce the acidic oxidizing stock solution into the

filtrate and MBTH mixture. Again, caution was taken to avoid the formation of air bubbles. Stocks of MBTH and $Ce(SO_4)_2$ were prepared within 2 hours of use on the bench and immediately moved into the glovebox. After 30 minutes, 650 µL of the assay mixture was placed into a screw cap cuvette, tightened, and then wrapped with common polytetrafluoroethylene (PTFE) tape. For analysis by ultraviolet-visible (UV-Vis) spectroscopy (Cary 300, Agilent Technologies), the sealed cuvette was removed from the glovebox within 35 minutes of initiating the formation of the chromophore upon addition of $Ce(SO_4)_2$.

"The total time between termination of the reaction by protein removal and reading of the colorimetric assay results did not exceed 40 minutes." One-way analysis of variance (ANOVA) was performed using OriginPro 9.0 software.

2.3 Results

The intensely-colored adduct resulting from the reaction of *p*-ABA with MBTH was detected with high sensitivity via its absorbance at 550 nm in a window between the optical signatures of NADH and FMN (**Figure 2.1b**). The MBTH assay has the important advantage that chromophore production is specific to aromatic amines but not hydroxylamines. Initial attempts to use fluorescamine for amine detection were abandoned due to reaction with *p*-HABA. The rate of reaction of 450 µM fluorescamine with 45 µM *p*-ABA is faster (k_{app} = 661 ± 1 s^{-1}) than with 45 µM *p*-HABA (k_{app} = 283 ± 1 s^{-1}). However, the MBTH assay was ultimately chosen due to its specificity for *p*-ABA.

"The absorbance at 550 nm responded linearly to *p*-ABA concentration in the range of 0.05 - 0.3 mM *p*-ABA (**Figure 2.2a**). To simulate the possible outcome of an enzymatic reaction beginning with 0.3 mM *p*-HABA and converting some amount to *p*-ABA, a second standard curve was constructed varying the mole fractions of *p*-ABA and *p*-HABA contributing to a total of 0.3 mM (**Figure 2.2b**). The resulting response curve again revealed that the A_{550nm} increased with increasing amounts of *p*-ABA and decreasing amounts of *p*-HABA. Because high concentrations of *p*-HABA appear to diminish the amount of MBTH available

for reaction with *p*-ABA, controls were constructed to have the same initial concentration of *p*-HABA as experimental samples. Based on these data and their standard errors we expect accumulation of more than 0.05 mM *p*-ABA to produce a significant A_{550} increase above background (**Figure 2.2b**)."

To evaluate the extent to which any amine accumulation was enzyme-catalyzed, "we compared the outcome of MBTH assays on samples in which NR was allowed to react with *p*-HABA vs. controls wherein NR was omitted." "**Table 2.1** shows slightly higher absorbance for the reactions initially containing 0.3 mM *p*-HABA compared to those initially containing 1 mM *p*-HABA. The higher absorbances are consistent with **Figure 2.2b** and point to possible consumption of a small amount of MBTH by *p*-HABA. However, among reactions begun with the same starting *p*-HABA concentration, no significant differences were found across treatments by one-way ANOVA at 0.3 mM *p*-HABA (p=0.097) or at 1 mM *p*-ABA (p=0.097) (**Table 2.1**). The fact that omission of NR from the 10 hour controls did not significantly affect absorbance at 550 nm indicates that there was little if any accumulation of aromatic amine due to enzymatic activity."

2.4 Discussion

Significant quantities of amine product could not be detected as a result of enzymatic reaction. However, initial stopped-flow spectroscopic studies indicated possible enzymatic reduction of *p*-HABA for the oxidative half-reaction (Warintra Pitsawong, data not published). Considering that small amounts of *p*-nitrosobenzoic acid (*p*-NBA) contaminants in the *p*-HABA could be responsible for the oxidation of reduced NR, we sought instead to directly measure product formation. This is a departure from most assays of NR activity that exploit the strong optical signature of NADH and monitor NR activity via consumption of NADH (19,23).

As noted (19), interest in NR is, in part, due to its possible utility as a biocatalyst for producing aromatic amines from corresponding nitroaromatics

(16). However our current results confirm earlier findings that significant quantities of aromatic amines do not accumulate under the action of *E. cloacae* NR (23). Further work is warranted to better understand the basis for the ability of *Mycobacterium smegmatis* nitroreductase (NfnIB) to reduce a benzothiazinone drug (BTZ043) to the corresponding amine (17). Similarly, a nitroreductase from *Klebsiella* sp. C1 has been reported to have the ability to fully reduce one of the nitro groups in trinitrotoluene (TNT), but not the nitro groups at C4 and C6 (15). In the case of *M. smegmatis* NfnIB, the flavin midpoint potential is very similar to that of NR(25,47). Thus, redox tuning alone does not appear to control the final product formed.

It is possible that amines can be generated from some substrates but not others. For example electron withdrawal by nitro groups at C4 and C6 of TNT and activation of the third nitro group at C2 may help to explain the observation of amine formation by *M. smegmatis* NfnIB (15). To understand why some nitroreductases appear to produce aromatic amine products while others do not, further study is needed to compare the amount of amine formed from different substrate-enzyme combinations.

Published studies have often used different substrates for different NRs in aerobic conditions. Comparison of the nitroreductase activity of different NR homologues for a common panel of substrates in both aerobic and anaerobic conditions would contribute greatly to the current study. Such a comparison using our highly sensitive and selective assay for aromatic amine production would also help to clarify the basis for reported differences in product formation.

2.5 Conclusion

Our development of a sensitive and selective chromogenic assay to detect aromatic amines affirms that *p*-NOBA and thus also *p*-NBA are not converted to *p*-ABA by *E. cloacae* NR in significant quantities. Improvements in the assay included the removal of protein by ultrafiltration prior to detection and the optimization of the ratio of MBTH to $Ce(SO_4)_2$. We found that a 1 to 4.3 ratio of

MBTH to $Ce(SO_4)_2$ provided the best result for testing 0-1 mM *p*-ABA. Moreover, the assay provides a valuable tool for determining whether a given enzyme-substrate combination can produce aromatic amine products.

2.6 Abbreviations

[1]: ANOVA, analysis of variance; MBTH, 3-methyl-2-benzothiazolinone hydrazone; NR, nitroreductase; *p*-ABA, para-aminobenzoic acid; *p*-HABA, para-hydroxylaminobenzoic acid; *p*-NBA, para-nitrobenzoic acid; *p*-NOBA, para-nitrosobenzoic acid; TNT, trinitrotoluene.

Table 2.1: Analysis of *p*-HABA reaction with NADH using MBTH. Samples were held at 29 °C in 50 mm potassium phosphate pH 7.50 containing 1.25 mM NADH, 17.5 µM NR, 0.3 or 1 mM *p*-HABA. Enzymatic reactions were terminated by protein removal using a centrifugal filter (EMD-Millipore, 10 kDa cutoff). Aromatic amines were detected using the absorbance of the product of the reaction with 1.5 mM MBTH and 6.5 mM $Ce(SO_4)_2$.

Reaction Time	*p*-HABA (mM)	Absorbance (550 nm)
0 hr	0.3	0.111(2)[a]
10 hrs[b]	0.3	0.120(8)
10 hrs control (no NR)	0.3	0.120(3)
0.5 hr	1	0.065(2)[a]
10 hrs	1	0.080(3)
10 hrs control (no NR)	1	0.074(11)

[a] Standard deviations based on 3 repetitions are provided in parentheses. No significant differences were found across treatments by one-way ANOVA at 0.3 mM *p*-HABA ($F(2,6)= 3.52$, $p=0.097$) or at 1 mM *p*-ABA ($F(2,6)=3.53$, $p=0.097$).

[b] Partial enzyme precipitation was observed after 6 hours at 29 °C however aliquots of enzyme allowed to stand in buffer under the same conditions for 24 hours retained 76% activity.

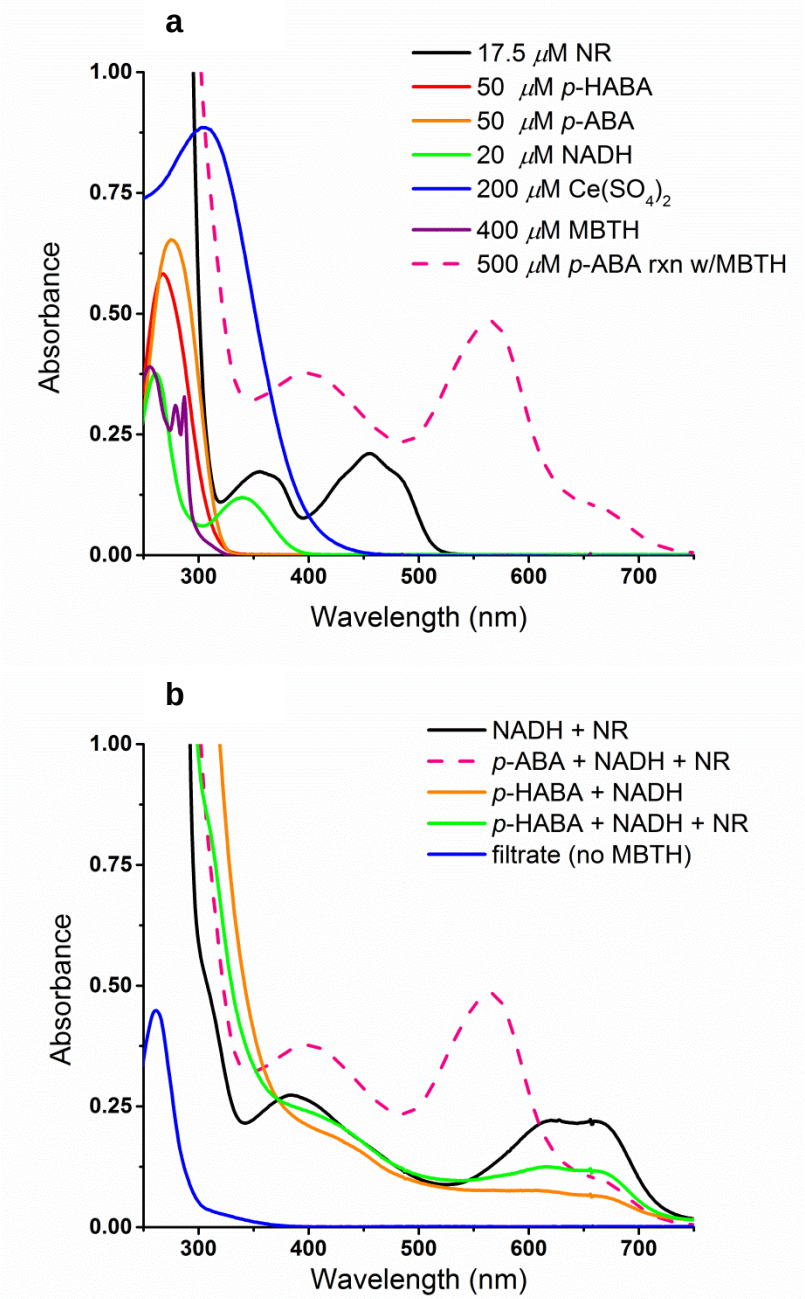

Figure 2.1: Absorbance spectra of MBTH assay components (a) and of reaction mixtures (b). The reaction mixtures (1.25 mM NADH, 17.5 µM NR, 0.5 mM *p*-ABA, and/or 1 mM *p*-HABA) were reacted for 10 hours at 29 ^{0}C prior to reaction with 1.5 mM MBTH and 6.5 mM $Ce(SO_4)_2$ for 0.5 hr at 29 ^{0}C.

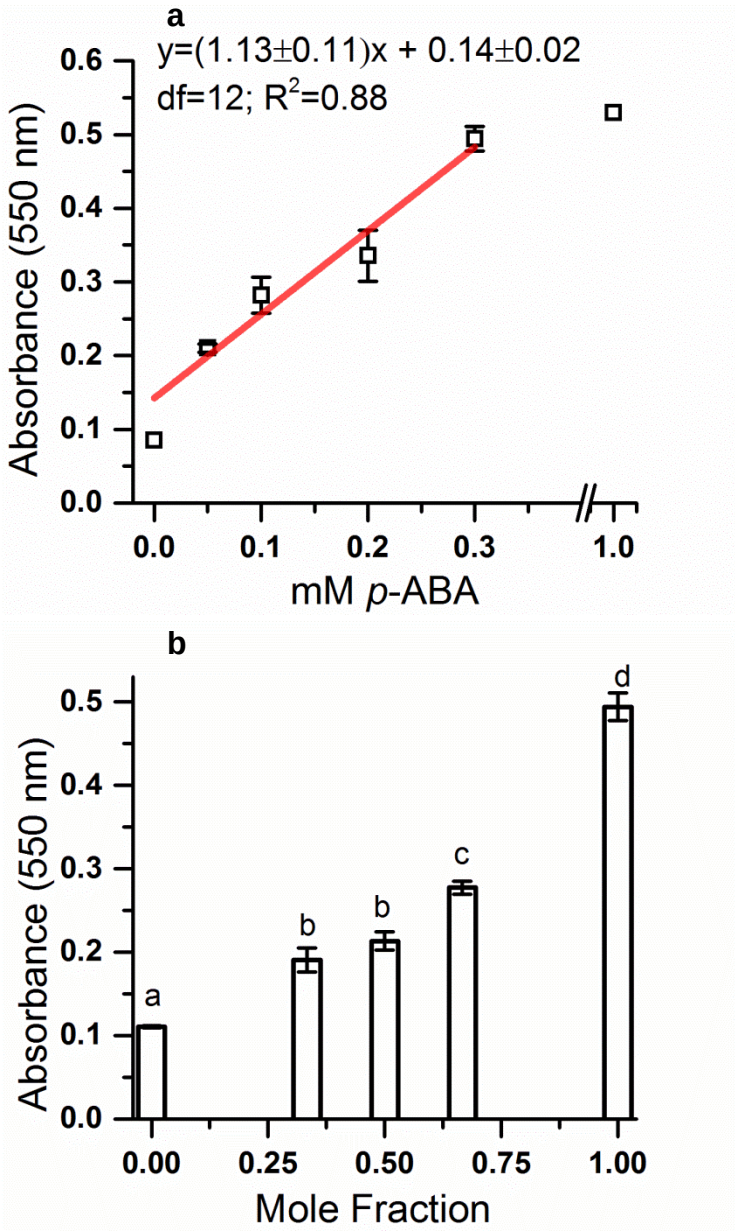

Figure 2.2: MBTH response to 0-1 mM *p*-ABA (**a**) and mixtures of *p*-HABA and *p*-ABA (**b**). The red solid line is the linear portion of the response. Mole fractions were used to simulate possible enzyme catalyzed reduction of 0.3 mM *p*-HABA to produce increasing yields of *p*-ABA. Solutions totaling 0.3 mM *p*-ABA and/or *p*-HABA were varied with respect to the mole fraction of *p*-ABA were augmented with 1.25 mM NADH and 17.5 µM NR and incubated for 15 minutes at 29 °C before being assayed for aromatic amine content using MBTH. The mole

fraction is expressed as a function of the amine content: [*p*-ABA] / ([*p*-ABA]+[*p*-HABA]). Significant differences were found among the mole fractions by one-way ANOVA: $F(4,10)= 157$, $p<0.001$, $LSD_{0.05}= 0.030$. The averages and standard errors are shown for the result of 3 replications.

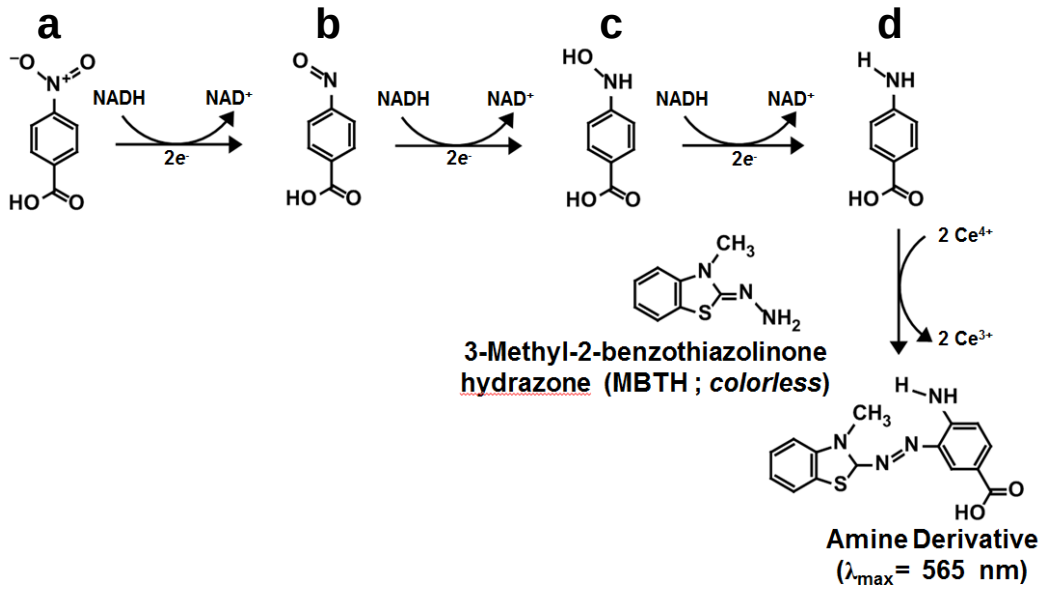

Scheme 2.1: Type I NR performs multiple rounds of pyridine nucleotide-dependent two-electron reductions of substituted aromatics and may be capable of producing significant amounts of amine products. Reduction of nitroaromatic (**a**) compounds by NR yields the corresponding reactive aromatic nitroso- (**b**) and hydroxylamino (**c**) products. Use of MBTH provides a method to directly detect amines (**d**) colorimetrically *in-situ* by the formation of a detectable amine derivative (43,44).

CHAPTER 3 CLONING AND PARTIAL CHARACTERIZATION OF A THERMOPHILIC NR HOMOLOGUE FROM *THERMUS THERMOPHILUS*

3.1 Introduction

How flavoproteins control the ability of flavin to perform one- versus two-electron chemistry remains unclear and even more difficult to implement in protein design (7). Some large flavoproteins (e.g.- human NADPH-cytochrome P450 reductase, 77 kDa) can perform both one- and two-electron chemistry by binding multiple cofactors in different domains (48). One of the most widely studied flavoproteins, flavodoxin, is only able to perform one-electron chemistry but participates in a number of metabolic pathways. In contrast, nitroreductase (NR) is an example of a flavoprotein which only performs two-electron chemistry but has an unusually large substrate repertoire. The unusually large substrate repertoire of NR has led to an expanding body of work that seeks to advance both applications (e.g., biodegradation, biosynthesis, prodrug therapy, etc.) and fundamental understanding of NR (e.g., physiological relevance, flavin cofactor reactivity, enzyme dynamics, etc.) (25-29). An NR homolog, NADH oxidase (NADOX), from the extremophile *Thermus thermophilus* may share NR's large substrate repertoire but has been much less studied.

Using NADOX as a model system, it may be possible to modulate the substrate repertoire, reduction potential, and semiquinone (SQ) population. The NR homolog from *T. thermophilus* was selected for this study because it has been shown to be stable (49,50) and tolerant of mutations (51). Thus, we anticipated that it would be a much better system than NR for protein design.

Previous NADOX research has been hampered by limited protein availability. Žoldák et al. report using 50 L growths as starting points for purifying the enzyme even though their work employed fluorescence spectroscopy, a low sample requirement technique, as the main experimental method (52). Herein

we report the sub-cloning of the gene into overexpression vectors, the development of a purification scheme, and the initial characterization of the resulting wild-type (WT-) and histidine-tagged (6xHis-) NADOX.

3.2 Experimental

Materials

The plasmid (pKK223-3) containing the WT-NADOX gene (TTHA0425) from *T. thermophilus* HB8 (ATCC 27634) was a gift from Professor Erdmann (Laboratorium für Biochemie, Universität Bayreuth, Federal Republic of Germany). Manganese superoxide dismutase (MnSOD) was the kind gift of Dr. Ting Wang (Department of Chemistry, University of Kentucky). Wild-type NR from *E. cloacae* was expressed as previously described (45) and purified using the modified procedure reported in a previous dissertation (46). The concentration of holo-NR was evaluated based on the extinction coefficient of the bound flavin, $\varepsilon_{454} = 14.3 \times 10^3\ M^{-1}cm^{-1}$ (45). NADH (100% purity) was purchased from Roche. Primers were ordered from Integrated DNA Technologies (Rapid HPLC Oligo service). All other reagents were purchased from Sigma-Aldrich unless noted otherwise (FMN: Catalog #F6750; lysozyme: Catalog #L6876; DNAse: Catalog #D4527).

Cloning of wild-type NADOX

The forward primer was designed to introduce an EcoRI restriction site, a ribosome binding site, and a silent mutation to convert a rare Ala codon to a more common Ala codon (Ala3, GCG) better able to support over-expression in *E. coli*: 5'-T TTT GAA TTC GAA GGA GAT ATA CAT ATG GAA GCG ACC CTT CCC GT-3'. The reverse primer was designed to introduce a HindIII restriction site and a silent mutation to introduce a stop codon that is more common for *E. coli* (TAA): 5'-TT TTT TAA GCT TTT AGC GCC AGA GGA CCA CC-3'.

High fidelity DNA polymerase (Phusion #M0530, New England Biolabs) was used to clone NADOX from pKK223-3, isolated from *E. coli* JM109 host cells, by PCR. After multiple rounds of optimization, the following conditions were found to provide the best results: 50 µL reactions containing 1 unit DNA polymerase, 200 µM dNTP, 0.5 µM of each primer, and 1 ng template DNA (pKK223-3). Difficulties with the ligation reaction were overcome by not exposing the DNA to UV light, and the use of 'touch down' polymerase chain reaction PCR (TD-PCR) to obtain clean PCR products (53). Optimal conditions for TD-PCR were obtained with a high annealing temperate program:

Initial denaturation: 98ºC, 3 min

Annealing: 72^0C, 30 sec (10 cycles)
67^0C, 30 sec (10 cycles)
62^0C, 30 sec (10 cycles)
Final Extension: 72^0C, 5 min

Hold: 4^0C, ∞

Insert double digestion was performed using 40 units of EcoRI-HF (#R3101, New England Biolabs) and 40 units of HindIII-HF (#R3104, New England Biolabs) with 400 ng of clean PCR product in 50 µL reactions incubated overnight at 37 ºC. Heat inactivation for HindIII was performed at 80ºC for 20 min. Plasmid double digestion was similarly performed for 2 µg pET-21 a(+) (#69740-3, EMD Biosciences).

Prior to ligation, digested insert and plasmid were gel purified. Gels and gel extractions (QIAquick kit #28704, Qiagen) were run in duplicate to prevent exposure to UV light for bands to be used for ligation. Ligation seemed to produce the most transformants when a 3:1 ratio of 100 ng digested vector to 33 ng digested insert was used.

After an initial denaturation (65 ºC, 5 min) of insert and plasmid DNA, 41 µL reactions were performed with 400 units of T4 DNA ligase (#M0202, New

England Biolabs) at 16 ºC overnight to produce plasmid p234NADOX (Table 3.1). Standard heat shock transformation (42 ºC, 45 sec) of TOP10 cells (#C4040, Invitrogen) was most successful when using 100 µl of cells (concentrated to OD_{600} = 1.5) with 5 µl (16 ng) of the ligation reaction. The ligated plasmid was propagated using the TOP10 (#C4040, Invitrogen) host and verified by restriction analysis and agarose gel electrophoresis (EcoRI, HindIII, and/or NdeI). Standard plasmid extraction (QuickLyse Miniprep Kit #27405, Qiagen) of transformed TOP10 cell was used to generate material for the transformation of an over-expression host, E. coli T7 Express lysY/I^q (C3013#, New England Biolabs) and DNA sequencing (DNA Read service, Eurofins MWG Operon). Transformation of *E. coli* lysY/I^q produced the most colonies using 50 µL cells with 5 ng plasmid. Over-expression was confirmed using SDS-PAGE and NADH oxidase activity assays.

Cloning of 6xHis-NADOX

With the exception of the plasmid, forward primer, and the host strain (noted below), all procedures were carried out as performed for WT-NADOX. The NADOX gene was inserted downstream of polyhistidine (6xHis) and TEV coding regions in pET15TEV_NESG (54-56) to create the N-terminally His-tagged NADOX (6xHis-NADOX) plasmid pAFJ2HIS (**Table 3.1**). The forward primer was designed to introduce a NdeI restriction site and a Gly (GGC) Ser (AGC) linker: 5'- TTT TTT CAT ATG GGC AGC GAA GCG ACC CTT CCC GTT TTG-3'. The resulting plasmid was transformed into *E. coli* host strain T7 Express LysY (#C3010, New England Biolabs).

Over-expression and purification of wild-type NADOX

Terrific broth (TB) culture media (per liter: 12 g tryptone, 24 g yeast extract, 4 mL glycerol, pH 7.5) was supplemented with 100 µg mL^{-1} ampicillin (final concentration). Inoculation of 2 L TB media with 100 mL of an optical

density of 3 (OD_{600} = 3) produced ample cell density for Isopropyl β-D-1-thiogalactopyranoside (IPTG) induction within 3 hours (OD_{600} = 2.5) of shaking at 37ºC at 220 rpm. Following 3 hours after inoculation, IPTG addition to a final concentration of 0.5 mM was accompanied by a second addition of 100 µg mL^{-1} ampicillin. Overexpression was allowed to continue for an additional 2.5 hrs before harvesting ~11 g of wet cell paste by centrifugation. Cells were washed two times and lysed in 40 mL of lysis buffer: 50 mM tris, 5mM EDTA, 1mM β-mercaptoethanol (BME), 100 µM 4-(2-Aminoethyl)benzenesulfonyl fluoride (AEBSP), 1% glycerol, 1 mM FMN, pH 7.5. Cell lysis was initiated with 3.6 mg lysozyme (20 min) followed by the addition of $MgSO_4$ (25 µM final concentration) and 2.4 mg DNAase. After an additional 20 min, the resulting mixture was sonicated for 10 min using 15 second pulses interspersed with 5 second delays. The lysate was cleared by centrifugation (10,350 rpm, 2 hrs, 4ºC).

Heat denaturation of cleared lysate was performed at 70ºC for 1 hr and was followed by centrifugation. The resulting supernatant (the heat cut) was concentrated to 5 mL using an ultrafiltration membrane (10 kDa ultrafiltration disc #13622, EMD Millipore). Anion exchange chromatography was performed using DEAE-cellulose (#D3764, Sigma-Aldrich) in a low salt buffer: 50 mM tris, 10mM $MgCl_2$, 1mM BME, 5% glycerol, 0.02% NaN_3, pH 7.5. The heat-denatured supernatant was loaded onto a pre-equilibrated 2.5-cm x 20-cm column and eluted at a flow rate of 1 mL min^{-1}. Within an hour, yellow holoenzyme NADOX was eluted and concentrated to 7 mL using an ultrafiltration membrane.

The purified material was subjected to a second round of column chromatography using the gel filtration matrix Sephacryl S-200 HR (#17-0584-10, GE Healthcare Lifesciences). The concentrated anion exchange fractions were loaded onto a 2.5-cm x 30-cm column pre-equilibrated in gel filtration buffer (50 mM tris, 0.2 mM EDTA, 50 mM NaCl, 1mM BME, 0.02% NaN_3, pH 7.5) and eluted under gravity at a flow rate of 0.4 to 0.5 mL. Within 6.5 hrs, yellow

holoenzyme NADOX was eluted and concentrated. Protein concentration was estimated using the Bradford assay (#B6916, Sigma-Aldrich) and ε_{450} = 17.61 × 10^3 $M^{-1}cm^{-1}$ (57). Purity was assessed by SDS-PAGE and assays of NADH oxidase activity.

Over-expression and purification of 6xHis-NADOX

Over-expression and purification were carried out similarly to that of WT-NADOX. In place of anion exchange chromatography, Ni-affinity chromatography was used. Without concentration, 30 mL of the heat cut supernatant was directly loaded onto a 2.5-cm x 5-cm column of Ni-NTA agarose (#30210, Qiagen) pre-equilibrated in lysis buffer supplemented with NaCl (300 mM), and imidazole (20 mM). Under gravity flow, the eluent was collected and reloaded onto the column three times. Once 6xHis-NADOX was bound, contaminating proteins were eluted with 120 mL of the supplemented lysis buffer (above). Purified 6xHis-NADOX was eluted with 50 mL the same buffer but at 250 mM imidazole. Imidazole was removed by dialysis against 500 mL of the gel filtration buffer refreshed twice over the course of 15 hours.

Kinetic Assays

Specific Activity- NADH oxidase activity was evaluated by first incubating 0.7 to 5 ng enzyme in 50 µL of 1.2 mM FMN, 50 mM potassium phosphate, pH 7.5 at 25 º C for 5 min. The mixture was added to a cuvette containing 900 µL 50 mM potassium phosphate, pH 7.5 pre-equilibrated at 25ºC in the ultraviolet-visible (UV-Vis) spectrophotometer (Cary 300, Agilent Technologies). The reaction mixture was brought up to 1 mL by the addition of buffer and NADH to a final concentration of 100 µM and the initial velocity of NADH consumption was recorded at 370 nm, which is an absorption maximum for NADH but not NAD^+ (ε_{370} = 2,660 $M^{-1}cm^{-1}$) (58).

The secondary substrates 2,4-dinitrotoluene (2,4-DNT) and FMN were assessed on the basis of their ability to support increased NADH oxidation rates. For the secondary substrates ferricyanide and cytochrome c, direct observation of secondary substrate reduction was assessed by monitoring the loss of the oxidized optical signature. In the NADOX assay above for NADH oxidase activity, the secondary substrate is O_2 present in buffers at equilibrium with air. Secondary substrates were added to the cuvette prior to NADH addition, which initiated the reaction. The reduction of ferricyanide [$K_3Fe(CN)_6$] was monitored via the disappearance of absorbance at 410 nm (ε_{410} = 1000 $M^{-1}cm^{-1}$) (59). The reduction of cytochrome c was monitored via the increase of absorbance at 550 nm (ε_{550} = 18,500 $M^{-1}cm^{-1}$) (60). The possible intermediacy of superoxide was assessed via the effect of inclusion of MnSOD in an assay measuring the rate of reduction of cytochrome c: MnSOD at room temperature (~22 °C) was added (<10 µL) just prior to the start of the reaction (initiated upon the addition of NADH).

Response to FMN- Initial velocities for FMN reduction were measured similarly to those for the specific activities but the concentration of added FMN was varied from 0.05 to 200 µM and did not include the FMN incubation step.

Initial rates -were fit to the Michaelis–Menten model using OriginPro 9.0 software (Levenberg Marquardt algorithm):

$$v = \frac{V_{\max}\,[\mathrm{S}]}{K\mathrm{m} + [\mathrm{S}]} \tag{3.1}$$

Assays of Anaerobic Reduction of WT-NADOX

The procedures including the modified cuvette described by Massey were used with only slight changes (61). An anaerobic cuvette (3mL, 1cm-path length) was equilibrated in the glove-box ([O_2] ≤ 10 ppm) overnight. The analysis

mixture was prepared in a 15 mL Wheaton vial with 18 µM NADOX, 2 µM benzyl viologen, and 400 µM xanthine with 50 mM potassium phosphate, pH 7.5 (2.982 mL total volume). Xanthine oxidase (6 ng, 18 µL) was placed in a 1.5 mL standard centrifuge tube. Both the analysis mixture and the xanthine oxidase were rendered anaerobic by 5-10 pump-purge cycles of ~30 seconds in the glovebox antechamber followed by equilibration in the glovebox for at least 1 hour but not longer than 2 hours. The solution containing NADOX was placed in the cuvette along with a small magnetic stir bar. Xanthine oxidase was placed in the side arm of the cuvette where it remained separated from the rest of the analysis mixture. After removing the sealed cuvette from the glovebox, the solution was allowed to equilibrate at 25 ºC in the spectrometer for 15 min. Initial scans were stable and showed the expected trace for fully oxidized NADOX. The reaction was initiated by tipping the cuvette to mix the xanthine solution from the sidearm into the NADOX solution in the cuvette.

3.3 Results

Two over-expression vectors were prepared and purification procedures were developed for the resulting WT-NADOX and 6xHis-NADOX proteins. Prior attempts to prepare large quantities of WT-NADOX using the plasmid and similar procedures to those described by Park et al. had failed to yield >10 mg pure protein from 10 L cultures (49,62). Multiple rounds of this culture preparation became time-consuming and produced varied yields. In contrast, the new expression vectors yielded 6 or 12 mg of purified protein starting from 2 or 3 L cultures for WT-NADOX or 6xHis-NADOX, respectively.

The purified proteins displayed the expected NADH oxidase activity but the WT-NADOX was more active (13.1 units mg^{-1}) compared to the preparation reported by Park et al. (5.2 units mg^{-1}) (49).

Cloning and expression

Conditions were optimized for a high annealing temperature protocol for TD-PCR. The use of TD-PCR was prompted by failed attempts to ligate PCR products obtained from standard PCR protocols. The PCR products following TD-PCR were clean and permitted ligation for both WT-NADOX and 6xHis-NADOX (**Figure 3.1**, only shown for 6xHis-NADOX). The WT-NADOX gene was sub-cloned into pET-21 a (+), while the 6xHis-NADOX cloned gene was sub-cloned into pET15TEV_NESG. The constructs displayed the expected digestion patterns and were used to transform *E. coli* T7 Express host cells. Protein overexpression was achieved for both WT-NADOX and 6xHis-NADOX. A sequence reading error at position 195 is likely to blame for the discrepancy between the Ala identity of the residue reported in Siebner's dissertation (57) for their plasmid sequence versus the Arg reported by Hecht et al. (63) for the crystal structure. Sequencing results for our WT-NADOX and 6xHis-NADOX plasmids revealed an Arg at position 195.

For WT-NADOX, modification of previously reported purification schemes (49,62) afforded a simplified three-step purification protocol by eliminating the need for affinity and cation exchange chromatographic steps (**Figure 3.2**). The new three-step purification yielded WT-NADOX holoenzyme with final specific activity of 13.1 units mg^{-1} (**Table 3.2**).

For 6xHis-NADOX, heat denaturation of crude lysate and Ni-column purification yielded pure protein (**Figure 3.3**) with a final specific activity of 7.2 ± 1.5 units mg^{-1} (**Table 3.3**). Efforts to improve the specific activity following the precipitation of contaminating proteins by heat were not successful. Future efforts should including the testing of temperature ranges and duration during the heat denaturation step.

Enzyme Kinetics

In the development of a new specific activity assay, a response to FMN concentration was observed even for holoenzyme (**Figure 3.4)**. Thus, although as isolated NADOX holoenzyme contains near stoichiometric FMN (~2 FMN per

dimer) in the active site, as demonstrated by its optical spectrum and reported extinction coefficients (57), provision of additional FMN was required for NADH oxidation activity. This observation prompted experiments to determine the k_{cat} and K_M for FMN. FMN is a substrate for NR, so it is not unexpected that NADOX is also able to reduce FMN.

Nitroreductase activity was observed for both WT-NADOX and 6xHis-NADOX (**Table 3.5**). Reduction of 2,4-DNT could not be detected without the addition of excess FMN. Rates for 2,4-DNT reduction by WT-NADOX and 6xHis-NADOX were 24 ± 4 units mg^{-1} and 27 ± 3 units mg^{-1}, respectively. In the absence of 2,4-DNT, the rate of NADH oxidation tended to be only slightly smaller (WT-NADOX: 17 units mg^{-1}; 6xHis-NADOX: 21 units mg^{-1}). By contrast, NR displayed very low NADH oxidase activity in the absence of the secondary substrate 2,4-DNT (2 units mg^{-1}). To substantiate nitroreductase activity by NADOX, continued effort is needed to directly measure the reduction of a nitroaromatic substrate rather than the measurement of NADH oxidation we have observed and report herein. An exciting next step should include modified use of the new and improved assay detailed in Chapter 2.

One-electron reductase activity against ferricyanide and cytochrome c was observed for WT-NADOX (**Table 3.6**). (The corresponding tests have yet to be done for 6xHis-NADOX). For WT-NADOX, ferricyanide was the fastest secondary substrate tested, undergoing reduction at a rate of 59 ± 12 units mg^{-1} without excess FMN and 107 ± 7 units mg^{-1} in the presence of 60 µM FMN. Rates were much slower for cytochrome c (5.7 ± 0.3 units mg^{-1}). A superoxide intermediate was ruled out on the basis of the lack of inhibition of cytochrome c reduction by MnSOD. Thus, our NADOX has activity comparable to reported values (49,50,62). Similarities with the activity of NR were observed (e.g. - 2,4-DNT reduction), but important differences were also observed (e.g. – O_2 reduction). Whereas NR does not reduce cytochrome c or ferricyanide at significant rates, NADOX does. This suggests that NADOX can access a flavin SQ state more readily than NR does.

Anaerobic Reduction of WT-NADOX

To seek evidence for stabilization of SQ, an anaerobic redox titration was performed using the method of Massey et al. (61). The presence of an SQ intermediate could not be detected for WT-NADOX even though both protonation states of flavin SQ have strong optical signatures that are distinct from that of the oxidized flavin. The single isosbestic point at 342 nm and a linear decrease in 450 nm absorbance support the participation of only two flavin cofactor states: the oxidized and hydroquinone (HQ) states (**Figure 3.5**). We observed no increase followed by a decrease in absorbance in the region of 500-600 nm that is characteristic of neutral flavin SQ (**Figure 1.2**).

The anionic flavin SQ is difficult to detect due to its low absorbance at wavelengths >530 nm (which is lower in energy) and spectral overlap in the region of 370 nm that is characteristic of anionic flavin SQ (64). Following full reduction of WT-NADOX, reduction of the benzyl viologen mediator produces a sharp peak at 400 nm and broad absorbance at wavelengths greater than 500 nm. The spectral features of reduced benzyl viologen serve as an internal indicator of achieving a solution potential below the reduction potentials typical for flavins (i.e., $E^{\circ\prime} = < -374$ mV).

3.4 Discussion

Little research has been conducted on NADOX to better understand its substrate preference or reductase mechanism. The kinetic mechanism of NADOX is not known but has been suggested to be a double-displacement ("ping-pong") reaction (52). Many studies perform steady-state kinetic assays where FMN is used in excess (52,57,62,65). Reductase activity may be in part due to weakly bound reduced FMN which diffuses freely into solution to then reduce secondary substrates. We observe that excess FMN is required for 2,4-DNT reduction and, nearly doubles the rate of ferricyanide reduction (**Table 3.6**).

In the absence of excess FMN, the reduction of ferricyanide and cytochrome c was observed by directly monitoring the loss of oxidized secondary substrate rather than NADH (**Table 3.6**). These one-electron reductions observed under the aerobic conditions of the kinetic assays are interesting given that SQ was not detected in the anaerobic reduction (**Figure 3.5**).

Excess FMN in the presence of O_2 could be involved in non-enzymatic substrate reduction. If reduced FMN acts as a shuttle by freely diffusing into solution, we expect an FMN concentration-dependence for the rate of secondary substrate reduction as shown in **Figure 3.4**. Thus, we interpret the results shown in **Figure 3.4** to be the result of excess FMN acting as a secondary substrate. The FMN concentration-dependence should also be affected by O_2 concentration. Flavoenzyme-specific methods are available for testing the effect of O_2 concentration and such experimentation should be part of future work (66,67).

The current literature has framed NADOX as an extremely stable NADH oxidase and much attention has been focused on oxidase activity under extreme conditions of pH, heat, and high chaotropic agent concentrations (50,52). To our knowledge, only one other report of nitroreductase activity by NADOX has been published (57). Our observations of nitroreductase activity by NADOX (**Table 3.5**) are encouraging given the many tools developed by our lab for the study of NR. However attempts to study NR by mutation of proposed key residues have yielded limited success because many of the resulting proteins fail to express, fold, or bind FMN (personal communication with Xiaonan Mei, M.Sc.). Nitroreductase seems to be intolerant of mutation or even tagging with polyhistidine. For NADOX however, activities of WT and 6xHis proteins were similar (**Table 3.5**) and suggest a higher degree of tolerance to mutation compared to NR. Published reports of W47, W52, and W132 mutants demonstrate that even residues near the active site can be changed without great loss of protein activity (68).

3.5 Conclusion

The initial characterization suggests NADOX to be tolerant of a polyhistidine tag with regards to NADH oxidase and nitroreductase activity. Ideally, a library of 6xHis-NADOX mutants can be generated without the complications encountered for NR. Specific activity for NADH oxidation depends on excess FMN for the canonical secondary substrate 2,4-DNT. Future work should follow up our observation that excess FMN is not required for the non-canonical one-electron secondary substrates ferricyanide and cytochrome c.

3.6 Abbreviations

[1]: ANOVA, analysis of variance; 2,4-DNT, 2,4-dinitrotoluene; MBTH, 3-methyl-2-benzothiazolinone hydrazone; NADOX, NADH oxidase; NR, nitroreductase; *p*-ABA, para-aminobenzoic acid; *p*-HABA, para-hydroxylaminobenzoic acid; *p*-NBA, para-nitrobenzoic acid; *p*-NOBA, para-nitrosobenzoic acid; TNT, trinitrotoluene; WT, wild-type.

Table 3.1: PCR primers

Construct	Primer	Sequence 5'-3'	Restriction Site
p234NADOX	Forward	T TTT GAA TTC GA*A GGA GAT ATA* CAT ATG GAA GCg ACC CTT CCC GT[a]	*Eco*RI
	Reverse	TT TTT TAA GCT TTT AGC GCC AGA GGA CCA CC	*Hind*III
pAFJ2HIS	Forward	TTT TTT CAT ATG ggc agc GAA GCG ACC CTT CCC GTT TTG	*Nde*I
	Reverse	Same as p234NADOX	

[a] Restriction sites underlined with a solid line, ribosomal binding site italicized and underlined with a dashed line, and the silent mutations are shown in lowercase

Table 3.2: Purification of WT-NADOX.

Step	Protein (mg)	Specific activity [a] (Units * mg^{-1})	Total activity (Units)	Yield (%)
1. Crude	242	2.1	514	100
2. Heatcut	32	4.3	136	27
3. Anion exchange	9	12.8	120	23
4. Gel filtration	6	13.1	73	14

[a] Unit = 1 µmol NADH * min^{-1}

60 µM FMN (5 min incubation), 100 µM NADH, 25^0C

Table 3.3: Purification of 6xHis-NADOX.

Step	Protein (mg)	Specific activity [a] (Units * mg^{-1})	Total activity (Units)	Yield (%)
1. Crude	62	8.2 ± 6	506	100
2. Heatcut	34	11.8 ± 1.0	397	79
3. Ni-column	12	7.2 ± 1.5	89	18
4. Dialysis	12	5.4	68	13

[a] Unit = 1 µmol NADH * min^{-1}

60 µM FMN (5 min incubation), 100 µM NADH, 25^{0}C

Table 3.4: WT-NADOX response to exogenous FMN at 25°C as compared to the reported value at room temperature (r.t.) (49).

	Modified Purification	**Park et al. (49)**
NADH (uM)	100	90
k_{cat} (s^{-1})	42 ± 4	5.28
k_{cat}/K_M (s^{-1} μM^{-1})	0.88	0.15
K_M (µM)	48 ± 13	34.6
Temp	25^0C	r.t.

Table 3.5: Specific activity for wild-type NADOX in the presence and absence of 2,4-dinitrotoluene (2,4-DNT).

Sample	2,4-DNT [a] (150 µM)	Specific activity [b] (Units * mg^{-1})
NR	+	47 ± 4
	-	2
NADOX-His	+	27 ± 3
	-	21
NADOX	+	24 ± 4
	-	17

[a] Nitroreductase activity against the model substrate 2,4-dinitrotoluene (2,4-DNT) shown in "+" rows. The NADH oxidase activity in the absence of 2,4-DNT is shown in "-" rows

[b] Unit = 1 µmol NADH * min^{-1}

60 µM FMN (5 min incubation), 100 µM NADH, 25^{0}C

Table 3.6: Specific activity for wild-type NADOX for one-electron acceptors.

Substrate	Specific activity [a] (Units * mg^{-1})
150 µM $[Fe(CN)_6]^{3-}$	59 ± 12 [b]
+ 60 µM FMN	107 ± 7 [c]
30 µM Cytochrome c	5.7 ± 0.3 [b]
+ 10 nM MnSOD	4.7 ± 0.6 [d]
+ 50 nM MnSOD	4.8 ± 0.2 [d]

[a] Unit = 1 µmol NADH * min^{-1}, 100 µM NADH, 25^{0}C

[b] No FMN added

[c] Five min incubation with 60 µM FMN prior to the initiation of the reaction upon NADH addition

[d] MnSOD added immediately prior to the initiation of the reaction upon NADH addition

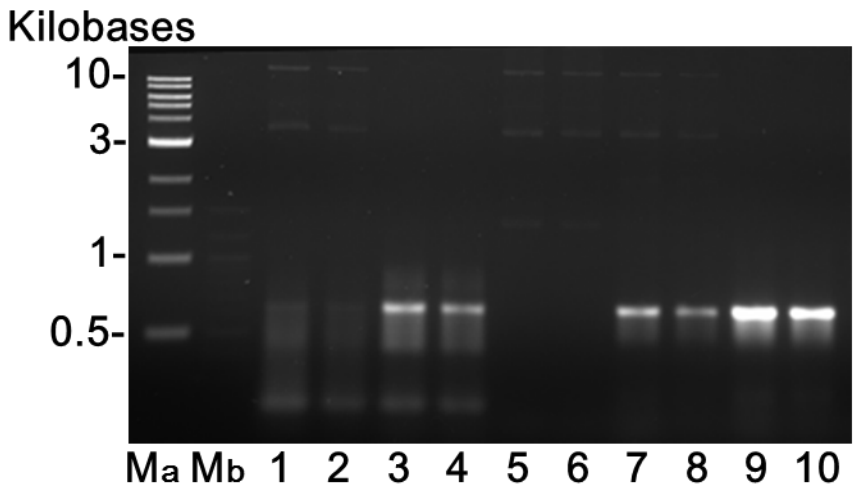

Figure 3.1: 6xHis-NADOX PCR products resulting from two different annealing temperatures(low temperature, low-T; high temperature, high-T). Samples were loaded in duplicate for the purpose of excising bands with limited UV light exposure. Lanes: Ma, 1 kb ladder; Mb, 100 bp ladder; 1-2, low-T with 9 ng template; 3-4, low-T with 1 ng template; 5-6, low-T control without C-terminal primer; 7-8, high-T with 95 ng template; 9-10, high-T with 1 ng template. Low -T program: 70^0C x20 cycles , 60^0C x10 cycles, and 50^0C x10 cycles High-T program: 72^0C x10 cycles , 67^0C x10 cycles, and 62^0C x10 cycles

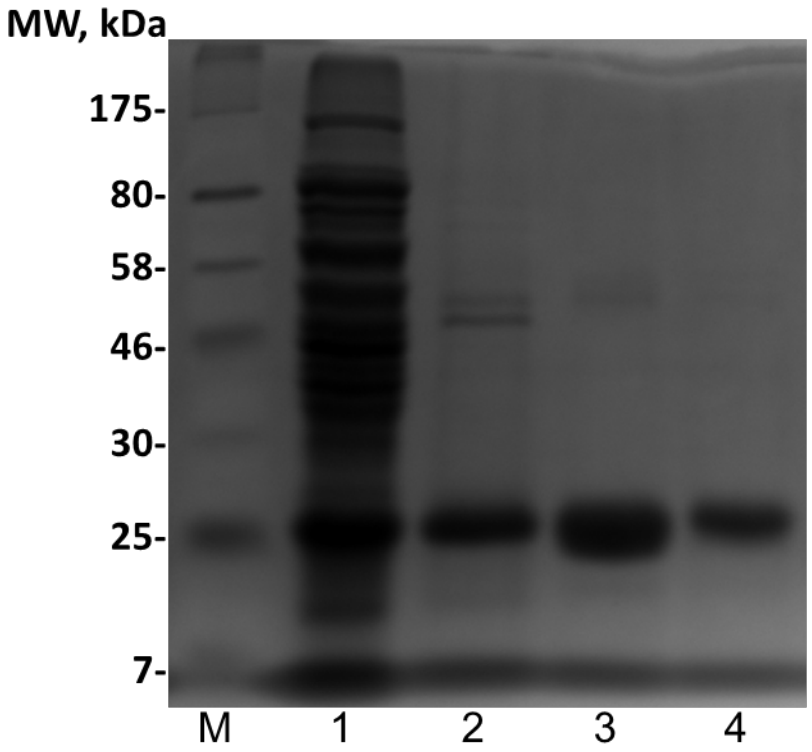

Figure 3.2: SDS/PAGE of WT-NADOX purification steps. Lanes: M, marker; 1, crude lysate; 2, heat denaturation supernatant; 3, anion exchange; 4, gel filtration.

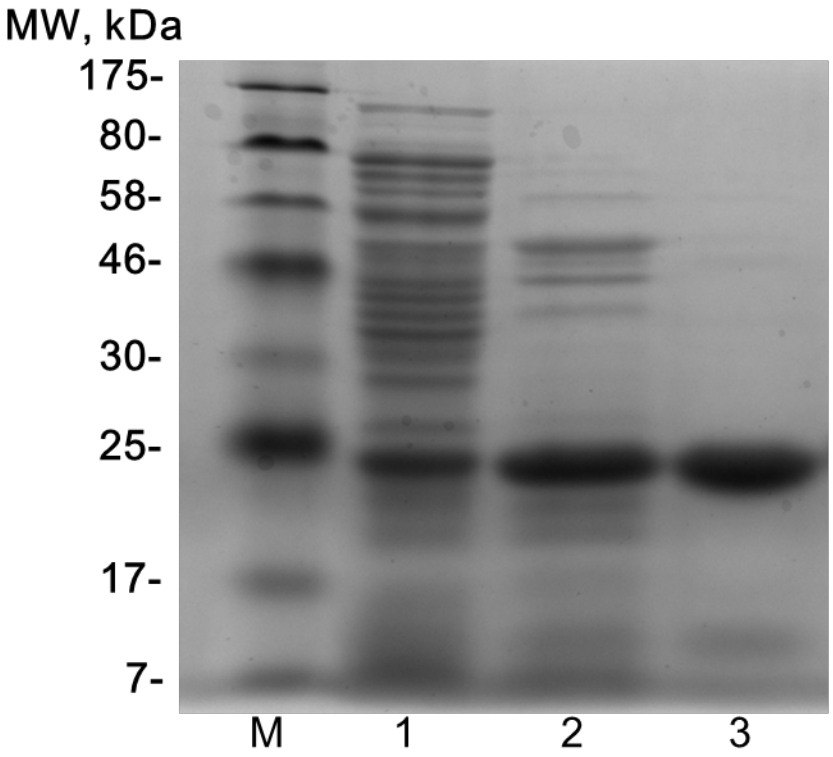

Figure 3.3: SDS/PAGE of 6xHis-NADOX purification steps. Lanes: M, marker; 1, crude lysate; 2, heat denaturation supernatant; 3, Ni-column.

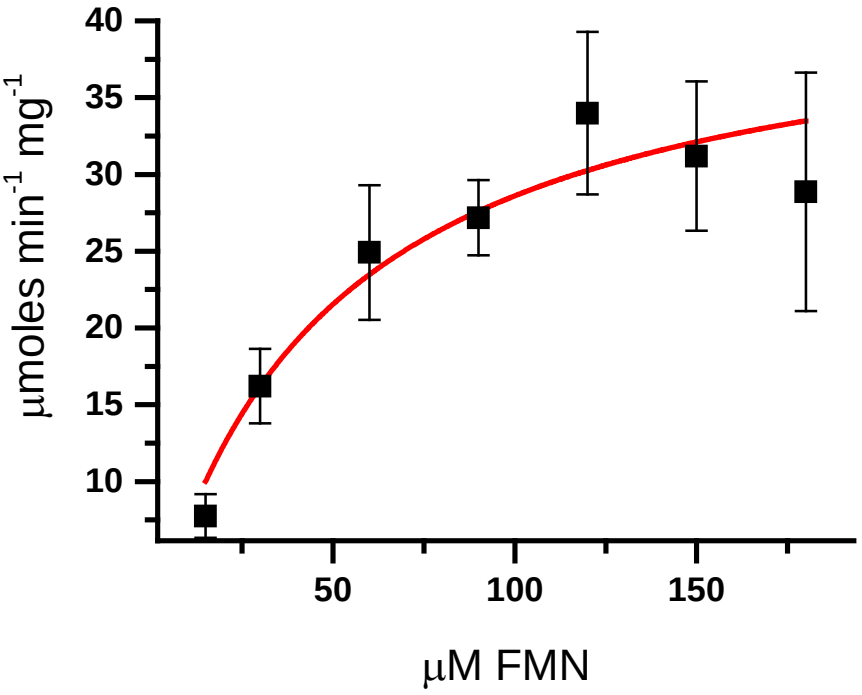

Figure 3.4: WT-NADOX response to FMN. Specific activity (µmoles min^{-1} mg^{-1}) for NADH oxidation was measured using 100 µM NADH at 25°C by monitoring the absorbance change at 370 nm. Initial rates were fit to the Michaelis–Menten model and resulted in a K_m for FMN of 48 ±13 µM.

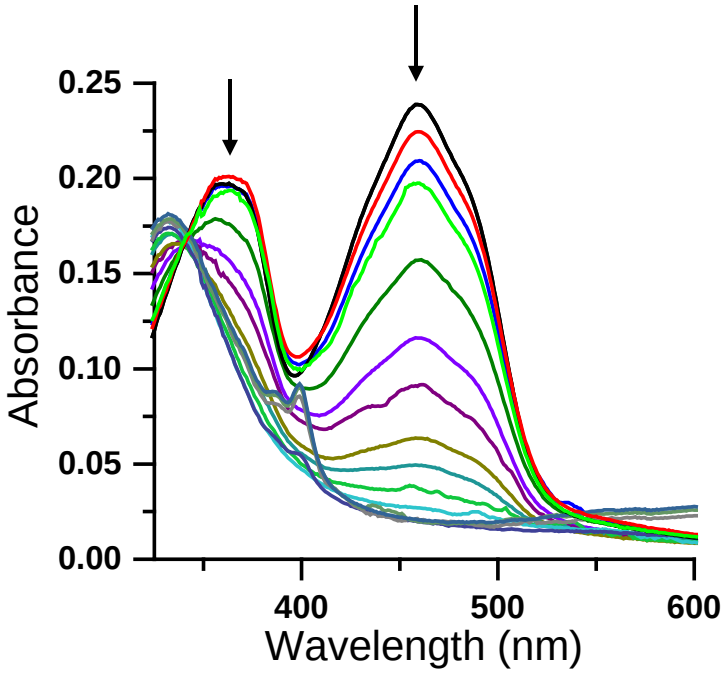

Figure 3.5: Anaerobic reduction of WT-NADOX using xanthine oxidase with xanthine to provide reducing equivalents. The titration was performed using benzyl viologen as a redox mediator but without a redox dye standard. Arrows denote the signal change during the course of reduction.

CHAPTER 4 EQUILIBRIUM AND ULTRAFAST KINETIC STUDIES MANIPULATING ELECTRON TRANSFER: A SHORT-LIVED FLAVIN SEMIQUINONE IS NOT SUFFICIENT FOR ELECTRON BIFURCATION

NOTE: This chapter is presented as a reformatted publication reprint in accordance with the policies set forth by the American Society for Biochemistry and Molecular Biology which allow reuse of any material published in its journals (the Journal of Biological Chemistry, Molecular & Cellular Proteomics and the Journal of Lipid Research):

Hoben, J. P., Lubner, C. E., Ratzloff, M. W., Schut, G. J., Nguyen, D. M. N., Hempel, K. W., Adams, M. W. W., King, P. W., and Miller, A. F. (2017) Equilibrium and ultrafast kinetic studies manipulating electron transfer: A short-lived flavin semiquinone is not sufficient for electron bifurcation. *J. Biol. Chem.* **292**, 14039-14049.

4.1 Introduction

Electron transfer bifurcation is emerging as third fundamental mechanism of energy conservation in biology (31,69). In this process a pair of electrons is acquired at intermediate reduction potential (intermediate reducing power), but the electrons are each passed to different acceptors as implied by the term 'bifurcation'. This process accomplishes a critical redistribution of energy between the two electrons. One passes to a high-potential acceptor whose reduction makes the reaction favorable overall despite passage of the other electron to an acceptor with a reduction midpoint potential lower than that of the initial donor. Thus one strongly-reducing carrier such as reduced ferredoxin is produced at the expense of two medium-potential electrons from NADH. Ability to produce more powerful reducing equivalents allows organisms to conduct reactions that would otherwise not be possible, such as cleavage of the triple bond of N_2, which removes a critical nutrient limitation and makes more environments habitable (34,70-72).

In both flavin- and quinone-based bifurcation (73), it is deemed crucial that the bifurcating cofactor be able to acquire electrons in pairs but that the radical semiquinone (SQ) state involved in one-electron chemistry be thermodynamically unstable (high energy) (31,74). Such a species would not accumulate in equilibrium titrations, but if formed transiently as part of a reaction it would be a potent reductant able to transfer an electron to a low-potential acceptor (31,69,74). By definition, such a species is difficult to observe and characterize. However, recent transient absorption spectroscopy (TAS) on NADH-dependent ferredoxin-$NADP^+$ oxidoreductase I from *Pyrococcus furiosus* (Nfn) succeeded in doing so by photoexciting active site flavin and using rapid time-resolved (100 fs to 5.1 ns) dual-beam spectroscopy to observe the resulting species (39). We were thus able to detect anionic flavin SQ and measure its lifetime (absorption decay at 366 nm, τ = 10 ps). Rapid re-oxidation of this species could be understood in terms of modest distances to nearby electron carrier cofactors, and permitted estimation of the midpoint potential associated with the flavin OX/ASQ redox couple. This is presumed to provide the driving force for electron transfer (ET) into an endergonic pathway. Thus, observation of a short-lived ASQ provided important conformation of the proposal for flavin-based electron bifurcation in this complex flavin and iron-sulfur cluster containing enzyme (32,74).

Although necessary, an unstable SQ may not suffice to produce bifurcating activity. Specifically, we have proposed that conservation of energy requires that the system include a mechanism allowing only one electron to pass down the exergonic path, thus constraining the other electron to pass along the endergonic path from the high-energy SQ (31). We additionally proposed that highly efficient ET would be a signature of bifurcating activity (39) as this could effectively propagate the high-energy electron to carriers distant from the low-energy (exergonic) carriers. Conformational change has also been invoked as a mechanism that could interrupt / disconnect a path for ET once one electron has taken that path,

thus preventing a second one from following (34,75). We note that in Nfn, this appears built-into the natures of the cofactors present. Thus the flavin proposed as the site of bifurcation is flanked on two sides by iron-sulfur clusters. An Fe_2S_2 cluster believed to have a high potential can readily accept one electron but not a second because of the very large energetic separation between successive oxidation states of such clusters (39). However the other cluster is only 7.5 Å away based on the crystal structures (39,75), and provides a highly competitive second path for electron escape from the flavin. Although the midpoint potential of this Fe_4S_4 cluster is very low, this is offset regarding ET efficiency by the short distance not only between it and the flavin but also in the direction of on-going electron propagation to a higher-potential Fe_4S_4 cluster that provides an exergonic step which increases the irreversibility of ET. Thus, existing data suggest that an unstable SQ state is essential in conjunction with efficient ET along two physically separate paths.

To elucidate the significance of efficient ET in conferring bifurcation activity on a flavin, we have compared the bifurcating flavoenzyme Nfn with two non-bifurcating flavoenzymes that nonetheless also thermodynamically suppress the SQ state. Nitroreductase from *Enterobacter cloacae* (NR, (19,23)) and NADH oxidase from *Thermus thermophilus* (NADOX, (49,63)) are structural homologues that are known or shown herein to lack a stable SQ state (22). Their comparison with Nfn thus holds constant the suppression of SQ so we can focus on other features that may contribute to NfnI's ability to bifurcate. As a control system with a very stable SQ we have also included flavodoxin from *Desulfovibrio vulgaris* (Fld) in our comparisons (76).

A critical concept is the distinction between thermodynamic and kinetic stability. Thermodynamic instability (suppression at equilibrium) is not necessarily accompanied by rapid reaction, although a correlation is common. A thermodynamically unstable species can persist if no efficient mechanism is

available for its reaction. Thus bifurcation is expected to require not only driving force based on favorable thermodynamics, but also mechanistic features that allow it to kinetically outcompete other potential fates for the high-energy species proposed.

To address this, we extended the TAS approach that was successful in Nfn to detect ASQ in each of our systems, and discovered ASQ lifetimes ranging over two orders of magnitude, demonstrating that short lifetime alone does not necessarily imply thermodynamic instability of the flavin ASQ *per-se*. Moreover the lifetime of NADOX's ASQ was comparable to that of Nfn's, showing that a short-lived ASQ is not a guarantee of bifurcating activity, although we maintain that it is necessary. We are able to understand the different ASQ lifetimes represented in our set of proteins in terms of the presence of ET relays able to mediate multiple ET steps and thereby separate the photogenerated hole and electron from one- another, versus the dominance of stand-alone electron donors that result in the photogenerated hole remaining close to the ASQ where it can rapidly recombine with the ASQ.

4.2 Experimental

Reagents

The exogenous electron donors/NR substrate analogs benzoic acid (99.5%; Catalog #242381), 2-aminobenzoic acid (98%; Catalog #A89855), and 2-(phenylamino)benzoic acid (%95%; Catalog #78153) were obtained and used directly from Sigma. The plasmid (pKK223-3) containing the WT-NADOX gene (TTHA0425) from *Thermus thermophilus* HB8 (ATCC 27634) was a gift from Professor Erdmann (Laboratorium fur Biochemie, Universitat Bayreuth, Germany). Primers were ordered from Integrated DNA Technologies (Coralville, IA; Rapid HPLC Oligo service).

Production of flavodoxin

His-tagged flavodoxin was produced from the *Desulfovibrio vulgaris* gene cloned into pET-32a(+) (EMD Biosciences, Darmstadt, Germany) to add a hexahistidine tag to the N terminus (77). The protein was purified from the BL21 (DE3) strain (Novagen, Madison, WI) by IMAC according to the vendor's instructions Qiagen, Hilden, Germany). The concentration of the protein was determined via absorbance at 272 and 445 nm (ε_{272} = 47,600 M^{-1} cm^{-1}, ε_{445} = 10,200 M^{-1} cm^{-1}) (78).

Nitroreductase production

Wild-type NR from *Enterobacter cloacae* was expressed and purified as described previously (19,45,46). The concentration of holo-NR was evaluated based on the extinction coefficient of the bound flavin, $\varepsilon_{454} = 14.3 \times 10^3$ $M^{-1}cm^{-1}$.

Production of wild-type NADOX

The gene for *T. thermophilus* NADOX was cloned into an over-expression vector as follows: The forward primer was designed to introduce an *Eco*RI restriction site, a ribosome binding site, and a silent mutation to convert a rare Ala codon to a more common Ala codon (Ala3, GCG) better able to support overexpression in *E. coli*: 5'-T TTT GAA TTC GAA GGA GAT ATA CAT ATG GAA GCG ACC CTT CCC GT-3'. The reverse primer was designed to introduce a *Hind*III restriction site and a silent mutation to introduce a stop codon that is more common for *E. coli* (TAA): 5'-TT TTT TAA GCT TTT AGC GCC AGA GGA CCA CC-3'. High fidelity DNA polymerase (Phusion #M0530, New England Biolabs) was used to amplify the gene for NADOX from pKK223-3 isolated from *E. coli* JM109 host cells, by PCR. Difficulties with the ligation reaction were

overcome by not exposing the DNA to UV light, and the use of 'touch down' PCR (TD-PCR) to obtain clean PCR products (53). The PCR product was gel purified and ligated into digested vector pET-21a(+) (Catalog #69740-3, EMD Biosciences). The gene sequence was confirmed by DNA sequencing.

NADOX was over-expressed from transformed *E. coli lysY/I*^{q} grown in Terrific Broth (per liter: 12 g tryptone, 24 g yeast extract, 4 mL glycerol, pH 7.5, supplemented with 100 µg mL^{-1} ampicillin). Induction of expression and protein purification was carried out as for NR (79). Protein concentration was estimated using the Bradford assay (Catalog #B6916, Sigma-Aldrich) and the flavin content was determined using $\varepsilon_{450} = 17.61 \times 10^{3}$ M^{-1}cm^{-1} (57).

Production of Nfn

Nfn from *Pyrococcus furiosus* was expressed and purified as detailed in Lubner *et al.* (39). Flavin content of purified proteins was determined aerobically using a standard fluorescence method (80). Briefly, flavin from the protein was released by denaturing in 0.02% SDS at 95-100C for 30 min and subjected to phosphodiesterase cleavage (Catalog #P5263, Abnova, Taipei City, Taiwan) prior to measuring fluorescence on a Lumina fluorescence spectrometer (Thermo Fisher Scientific, Waltham, Massachusetts, USA).

Redox titration of NADOX

The procedures and modified cuvette described by Massey were used with only slight changes (61). An anaerobic cuvette (3 mL, 1 cm-path length) was equilibrated in a glove-box overnight ($[O_2] \leq 10$ mg/L). Solutions of 18 µM NADOX, 2 µM benzyl viologen, 400 µM xanthine in 50 mM potassium phosphate, pH 7.5 (2.982 mL) and 6 ng of xanthine oxidase (18 µL) were rendered anaerobic

by 5-10 pump-purge cycles of ~30 seconds followed by equilibration in the glove-box for 1 hour. The solution containing NADOX was placed in the cuvette along with a small magnetic stir bar. Xanthine oxidase was placed in a side arm of the cuvette, separated from the rest of the reaction mixture. After removing the sealed cuvette from the glove-box, the solution was allowed to equilibrate at 25°C in the spectrometer for 15 min. Initial scans were stable and showed the expected trace for fully oxidized NADOX. The reaction was initiated by tipping the cuvette to mix the xanthine solution from the side arm into the NADOX solution in the cuvette.

Transient Absorption Spectroscopy

The ultrafast (100 fs to 5.1 ns) TAS spectrometer employed in this study uses an amplified 4W Ti:sapphire laser (Libra, Coherent, 800 nm, 1 kHz, 100 fs pulse width) to deliver excitatory pulses of light, and a Helios spectrometer (Ultrafast Systems, LLC) to probe the sample afterwards. A fraction of the 800 nm Libra output was frequency-doubled in β-barium borate to produce the desired pump wavelength (400 nm in the experiments described here) for sample excitation, which was then directed into the Helios. The pump pulses were passed through a depolarizer and chopped by a synchronized chopper to 500 Hz before reaching the sample. The pump pulse energy was 1.1 μJ per-pulse at the sample. Another fraction of the Libra output was guided directly into the Helios for generation of the probe. Within the spectrometer, a white light continuum of wavelengths including 340 – 800 nm was generated using a 2 mm thick CaF_2 crystal. This beam was split into a probe and a reference beam. The probe beam was focused into the sample where it was overlapped with the pump beam. The transmitted probe and reference beams were then focused into optical fibers

coupled to multichannel spectrometers with CMOS sensors with 1 kHz detection rates. The reference signal is used to correct the probe signal for pulse-to-pulse fluctuations in the white-light continuum.

For all transient absorption measurements, samples were transferred into 50 mM potassium phosphate pH 7.5, 50 mM KCl by diafiltration (10 kDa, Catalog #UFC501024, EMD Millipore, Billerica, Massachusetts, USA) to remove possible traces of free flavin, immediately prior to collection of spectra. NADOX samples were at pH 7.0. Manipulations were performed in an Mbraun glove-box (N_2 atmosphere). Each sample was sealed in a 2 mm quartz cuvette and stirred continuously to prevent photodegradation. Protein concentrations were approximately 250 µM for NR, NADOX and Fld while Nfn concentration was 200 µM. Samples with exogenous electron donors were prepared in 250 µM NR with the exception that the sample containing 25 µM PAB was 229 µM in NR. All experiments were conducted at room temperature.

Photoexcitation of flavin at 400 nm was used to initiate formation of ASQ by generating excited state (F*) which then abstracts an electron from a nearby donor. ASQ then relaxes by various pathways to return to the oxidized ground state. The change in absorbance signal (ΔA) was calculated from the absorbances measured by alternating probe pulses with and without prior pump pulse excitation. The time delay between the pump and probe pulses was controlled by a motorized delay stage. The data collection (350 pump shots per time point) was carried out four consecutive times and then averaged. The experiment was repeated 2-3 times for each protein to ensure similar results across different days and preparations. Data were corrected for spectral chirp using SurfaceXplorer (Ultrafast Systems). Additional time zero (t_0) correction was

performed by adding 1.99 ps for NR and subtracting 0.30 ps for Fld. Additional baseline correction was performed by subtracting the average ΔAbs from 790-800 for Nfn and from 780-800 for NADOX. Fitting for the determination of dynamic lifetimes was performed with slight adjustment to the instrument response function (IRF) and time zero (t_0) using Surface Xplorer (Ultrafast Systems). Similar results for lifetimes were obtained using Origin Pro 9 (Northampton, Massachusetts, USA).

Reduction Potentials of Exogenous Donors

Reduction potentials were determined by cyclic voltametry of 1 mM solutions of PAB, AB, and BA using a glassy carbon working electrode, Pt wire counter electrode, and Ag/AgCl reference electrode (Catalog: #CH104, #CHI115 and #CHI111 from CH Instruments Inc., Austin, Texas) in 5 mL of 500 mM potassium phosphate, 100 mM KCl, pH 7.0 (47). Saturated quinhydrone in the same buffer was also analyzed to calibrate the system at 84 ± 10 mV, 22 °C (81).

Steady-State Absorbance and Fluorescence

Measurements were carried out in 1 mL 50 mM potassium phosphate, 50 mM KCl, 5% ethanol, pH 7.0. Absorption spectra were recorded with a Hewlett-Packard (Palo Alto, CA, USA) 8452A diode array spectrophotometer and samples were held at 25°C in a water-jacketed cell holder. Fluorescence quenching of 5 μM NR was monitored at 10°C using 450 nm excitation with 5 nm slit widths in a Lumina spectrofluorometer (Thermo, Waltham, MA, USA) using a Peltier temperature controller. Fresh stocks of PAB, AB, and BA were made for titrations using ≤10 μL aliquots. The mechanism of quenching was probed by

fitting the data in Kaleidagraph (Synergy Software) to consider Stern Volmer vs. specific-bind*ing type behavio*r:

$F_o/F = c + K_{sv}[\text{Donor}]$ (Equation 4.1)

$F_o/F = c + K/(1+K_d/[\text{Donor}])$ (Equation 4.2)

$K=k_{ET} * \tau_0$ (Equation 4.3)

Where F_o/F is the fluorescence in the absence of electron donor divided by the fluorescence at a given concentration of donor, K_{sv} is the Stern Volmer constant for non-specific quenching, K is the electron transfer rate constant (k_{ET}) times the natural lifetime of the emissive state (τ_0), and K_d is the dissociation constant for specific binding (82).

4.3 Results

Transient absorption spectroscopy (TAS) as a function of time after a short pulse of irradiation at 400 nm was used to probe for possible formation of ASQ (**Figures 4.1** and **4.2**). Photochemical formation of ASQ is understood to be the result of photoexcited flavin (F*) abstracting an electron from a nearby residue such as Trp or Tyr (83,84), producing the radical form of the donor residue ($Trp^{\bullet+}$ or $Tyr^{\bullet+}$ **Figure 4.3,** (84-86)). In flavoproteins where the ASQ is thermodynamically unstable it is expected to react rapidly, reducing a nearby electron carrier or recombining with the donor radical to return to the oxidized state (OX). Thus the time-courses of ASQ absorbance (365 - 375 nm), and OX absorbance (454- 467 nm) are expected to reveal increased ASQ and decreased OX formed upon illumination, which eventually both return to pre- illumination levels.

We compared four different flavin sites using TAS. As reported previously (39), photoexcitation of Nfn produced increased absorbance at

365 nm compared to reference intensities (positive ΔA_{365} upon subtraction of the spectrum without prior illumination). NR and NADOX also yielded increased A_{375} or A_{370}, respectively, and spectral analysis described below confirms their attribution to ASQ. This is the first observation of SQ in NR and NADOX, wherein the SQ state is thermodynamically unstable (**Supplemental Figure 4.S1**, (22)). Absorbance at 370 nm was also produced in Fld but was too short-lived to provide quality spectra and definitive assignment of the species present (**Supplemental Figures 4.S2d** and **4.S3d**).

Our set of flavin environments produced flavin ASQ lifetimes spanning more than two orders of magnitude, indicating that decay kinetics are exquisitely responsive to the context of the flavin and potentially informative on the processes contributing to ASQ decay (**Figure 4.1**). In each case, absorbance diagnostic of OX recovered on a similar or slightly longer timescale, indicating recovery of the pre-illumination state of the system (85,87). NR had the longest-lived ASQ consistent with naive expectations for non- bifurcating systems where the ASQ need not be very strongly suppressed. However, the comparable lifetimes of ASQ in Nfn and NADOX suggest that capacity to bifurcate is not an automatic consequence of a short-lived unstable ASQ, and thus that short-lived ASQ cannot be interpreted alone as diagnostic of bifurcation activity. The most rapid ASQ decay in our set is that of Fld, which is only fleetingly observed at our time resolution, consistent with the studies of He *et al.* (88).

To understand the significance of the ASQ's lifetime it is necessary to examine the mechanism by which it decays, as comparison of rates is not meaningful if they correspond to different events. Thus, for the example of NR, the time courses at several diagnostic wavelengths were compared to reveal intervals dominated by distinct processes (**Figure 4.2a**). Phase 1 was chosen as the time in which negative intensity at 455 nm had already been established but in which negative intensity at 565 nm was still growing, as was

positive intensity at 375 nm. At later times (phase 2), intensity at 375, 455 and 565 nm had all stabilized but weaker intensity at 515 nm displayed continued growth. In phase 3, negative intensity at 565 nm had begun to return to zero as had positive intensity at 375 nm, whereas at the longest times (phase 4) we observed concerted decay at all wavelengths. To discern the identities of the species growing and decaying in each interval, difference spectra were generated by subtracting the spectrum at the beginning from the spectrum at the end, for each phase. In these difference spectra, the non-illuminated background is expected to cancel out and we can interpret the result as representing changes that occurred during that phase. The four phase-associated difference spectra (PADS) representing intervals 1-4 are shown in **Figure 4.2d**, accompanied by the individual spectra (photoexcited minus not photoexcited) collected at the beginning and end of each phase in **Figure 4.2b**. The approach was verified in part by observation of the expected neutral semiquinone (NSQ) signal in the Fld control (**Supplemental Figure 4.S3d**). The analogous analyses of NADOX and Nfn are provided in **Supplemental Figures 4.S2** and **4.S3**.

For NR in phase 1, the PADS in **Figure 4.2d** displays a well-formed signature of ASQ with a maximum at 377 nm accompanied by intensity from 480 to 520 nm that is also consistent with ASQ (compare with **Figure 4.2c** and (89)). Positive intensity between 510 and 530 nm has been interpreted as absorption by photoexcited flavin (F*) (85,90) as well as $Trp^{\bullet+}$ (86). Similarly, we attribute the strong broad negative feature at 565 nm to emission from F* based in literature precedent (85,90). This signal indicates that a significant population of F* decays by emission, instead of electron acquisition to become ASQ (**Figure 4.3a**). This is consistent with the absence of electron donating redox cofactors in this system and the relatively long distances to the nearest Trp side chains, which are the amino acids most amenable to oxidation by photoexcited flavin (83,84,91). The phase 3 PADS shows that some half of the F* decays in this interval (loss of emission at 565 nm yields positive

PADS signal) with some decay of ASQ (365-375nm), and recovery of OX (440-480 nm, **Figure 4.2d**). These processes are completed in phase 4, in which the last of the F* emission is lost along with loss of ASQ absorption at 367 and 515 nm and formation of OX at 440-480 nm. However the phase 2 PADS displays formation of a signal suggestive of ASQ based on relatively narrow difference absorbance at 360 nm and broader difference absorbance near 510 nm, but there is a loss of ASQ signal at 377 nm where absorbance appeared earlier, and an analogous apparent loss of absorbance from 430 - 470 nm. These changes are all in regions where ASQ absorbs strongly, and the gains in absorbance are roughly offset by losses nearby in both the short-wavelength region of 360- 390 nm, and the longer wavelength region of 430 - 560 nm. Therefore, we speculate that this could reflect a change in the environment of the ASQ that produces shifts in its absorption maxima (92, 93). The time-scale of this interval from 5-30 ps is compatible with reorientation of protein and water dipoles near the flavin (94,95).

Analogous logic and literature precedent were used to propose processes associated with the PADS of NADOX, Nfn and Fld, as detailed in **supplemental Figures 4.S2 and 4.S3**. NADOX is a structural homologue of NR and like NR does not stabilize a SQ (**Supplemental Figure 4.S1**). As in NR, photoexcitation results in formation of ASQ that is prominent near 380 nm as well as 480-520 nm in the PADS of phase 1 (**Supplemental Figure 4.S3b**). However the lifetime of this ASQ is some ten-fold shorter than that of NR (**Figure 4.1**). This is consistent with the lower fluorescence emission of NADOX than NR and possible quenching of F* by a Trp residue near the flavin that is replaced by Thr in the structure of NR (Figures 3b, S4, (63)). Thus, we hypothesized that the Trp distinguishing NADOX from NR serves as an electron donor in the production of ASQ but its proximity to the flavin permits relatively rapid charge recombination (CR) that rapidly returns the populations of $Trp^{\bullet+}$ and ASQ to zero (**Figure 4.3a**).

An extreme form of the same situation is found in the flavin-binding site

of Fld, which sandwiches the flavin between a Trp and a Tyr side chain (**Figure 4.3b**). As anticipated, flavin fluorescence is strongly quenched in Fld and this is consistent with onset of absorbance at 370 nm within the time resolution of our instrument (**Figure 4.S2d**), presumably due to electron abstraction from the nearby Trp to form ASQ (91). The Fld protein stabilizes SQ as the neutral form and the proton transfer required to generate NSQ from ASQ can be inferred from rapid formation of difference absorption from 510 to 660 nm consistent with the spectrum of NSQ shown in **Figure 4.2c** (**Supplemental Figure 4.S3d**). Growth of this species occurs during only a short interval, consistent with rapid disappearance of the ASQ from which NSQ is formed. The short lifetime of the ASQ is expected due to CR with the nearby oxidized $Trp^{\bullet+}$ formed by electron abstraction, in processes that have been described in detail (88). Even the NSQ is short-lived in this system, despite its well-known thermodynamic stability (76). This can be understood to be a consequence of the reactivity of the $Trp^{\bullet+}$ radical that is present along with photogenerated flavin NSQ, but absent from the Fld NSQ formed in normal biochemical contexts.

In the case of Nfn, phase 1 displays formation of ASQ at both 384 and 480-510 nm which decays in phase 2, accompanied by recovery of OX at λ_{max} = 455 nm (**Supplemental Figure 4.S3c**). However, there is no Trp or Tyr stacked against the active site flavin (**Figure 4.3b**), arguing against the mechanism of CR demonstrated for Fld and inferred in NADOX. Instead, rapid reoxidation of Nfn's ASQ has been argued to reflect highly efficient ET to Fe_4S_4 clusters that are only 7.5 Å away and display electronic coupling to the flavin (39). Thus, although we attribute the decay of ASQ to reoxidation in all four cases, we propose that it represents CR in NR, NADOX and Fld, as opposed to the ET into a chain of electron carrier cofactors that can propagate it further, that has been demonstrated in the case of Nfn (39). **Table 1** summarizes the species and their lifetimes obtained by fitting the time

dependence of absorption at their respective maxima, for each of the four proteins.

To test our hypothesis that the Nfn-like lifetime of NADOX's ASQ can represent CR, and that the comparative absence of this behavior in NR reflects absence of the active site Trp seen in NADOX, we employed aromatic substrate analogs in a 'chemical rescue' strategy to provide a Trp surrogate. The use of small-molecule electron donors instead of mutagenesis enabled us to vary both the reduction potential and the dissociation constant (K_d) of the donor (**Table 4.2**). We anticipated that if a long flavin-to-donor distance is responsible for the long lifetime of NR's ASQ, then provision of exogenous donors that bind close to the flavin should shorten this lifetime.

The addition of 2-phenylamino benzoic acid (PAB) or 2-amino benzoic acid (AB) results in rapid decay of ASQ and restoration of OX that occurs on a time scale comparable to formation of ASQ and thus greatly diminishes the extent to which ASQ accumulates (**Figure 4.4**). In both cases a small fraction of the sites appear to retain a comparatively long-lived ASQ despite the large concentration of donors used compared to their K_d values. We speculate that this could reflect an increase in the K_d upon flavin reduction, as has been demonstrated for benzoic acid (22). We note also that the use of a donor with a larger K_d results in attenuation of the effect even at the same donor concentration (benzoic acid, BA, **Figure 4.4**), as does use of a lower concentration of donor (**Supplemental Figure 4.S5**).

The donors also span a range of reduction midpoint potentials ($E°$; **Table 4.2**). The higher $E°$ of BA would be expected to make it a less favorable source of an electron for the photoactive flavin, yet it appears to have the highest yield of ASQ. Hence it appears that the photoactive flavin is a sufficiently strong oxidant that it can draw on any of the three donors. This is consistent with the fact that none of the donors is more difficult to oxidize than Trp and Tyr, that are known sources of an electron for

photoactivated flavin (83,84). Charge recombination of ASQ with oxidized donor is expected to be more favorable for the higher *E*° donor BA, yet this is the donor with the least impact on ASQ life time. Therefore it appears that driving force of ET is not the principal determinant of the variations of ASQ recombination rate in our time regime.

Efficient electron transfer is expected to reflect an effective mechanism as well as a short distance between partners. Consistent with this we find that PAB, which shortens the ASQ lifetime by two orders of magnitude, also efficiently quenches fluorescence (confirming rapid ET, **Figure 4.5b**) and displays a charge transfer (CT) band upon binding to NR (evidence for favorable orbital overlap and short distance (96-98); **Figure 4.5d**). Indeed, a CT band is also observed in the rapid-ET Y98W mutant of Fld (88,99). In contrast, **Figure 4.5** (*a* and *c*) shows that the least effective donor (BA) does *not* produce a CT band and is a much poorer quencher of the flavin fluorescence. Nonetheless, titration of NR with either donor demonstrates saturation and thus binding in a discrete site, which has been shown by crystallography to be directly over the *re* face of the flavin for BA (100).

Data adhered well to a model wherein binding of the donor produces partial quenching via introduction of additional ET that augments preexisting non-radiative decay and radiative decay (fluorescence) (see **supplemental materials**) (82). This analysis of fluorescence quenching yields a dissociation constant that is consistent with the one that emerges from analysis of the CT band amplitude *versus* [PAB], supporting the model. Thus, the fluorescence quenching achieved upon saturating NR with PAB indicates that radiative decay accounts for only 1% of photoexcited flavin, *versus* 4% for NR in the absence of exogenous donor, based on 25% for FMN in solution (101). In contrast, BA has only a very minor effect on the fluorescence quantum yield, which remains almost 4% even at saturating BA. This is consistent with BA's failure to produce a CT band indicating absence of good orbital overlap with the flavin (**Figure 4.5c**). Thus, we conclude that the rate of ET from BA to F*

is slow compared to the rate of radiative decay and infer that the rate of CR from flavin ASQ to BA is similarly slower than from ASQ to PAB. This provides an explanation for the discernible increase in ASQ yield observed in the presence of BA vs. PAB (**Figure 4.4**). We note that signatures of electronic coupling between cofactors were also observed in Nfn, consistent with the rapid rates of ET between them (39).

Thus, our experiments with exogenous donors demonstrate that increased CR can change the kinetics and ASQ amplitudes displayed by NR to behaviors more closely resembling those of NADOX and even Fld (**Figures 4.1, 4.4, 4.S2**). Therefore, the short lifetime of NADOX can be explained by CR. This is in contrast to Nfn where the short lifetimes have been explained in terms of ET (39).

4.4 Discussion

Electron bifurcation was first elucidated in the guise of the quinone-mediated Q-cycle in respiratory ET (73), and has more recently been recognized at the heart of a variety of enzyme complexes executing more reducing chemistry (31,69). In the latter it was proposed that the bifurcating step is mediated by a flavin (69), consistent with flavins' lower potentials and inherent tendency to undergo two-electron chemistry with only weak population of the SQ species corresponding to one-electron reduction. However there are numerous flavoenzymes that do two-electron chemistry but not electron bifurcation. Given bifurcation's recent recognition as a third fundamental mechanism for biological energy conservation, alongside substrate-level phosphorylation and chemiosmotic potential-based phosphorylation (102), it is important to identify factors required for a flavin site to execute bifurcation. Thermodynamic suppression of the SQ is deemed essential because this species would constitute a strongly reactive electron donor able to reduce low-potential acceptors such as ferredoxin and

semireduced flavodoxin. Generation of such a SQ is thought to be the result of oxidation of doubly-reduced flavin by a high potential electron acceptor, and this step is understood to provide the driving force for formation of the strongly reducing SQ. In the current studies we have dispensed with a high-potential one-electron acceptor by providing the driving force for this step via photoexcitation.

A strongly reducing SQ state does not suffice explain bifurcation, as there must be a mechanism requiring the SQ to transfer its electron to the low-potential acceptor rather than the high-potential acceptor. In Nfn, a combination of the distances between electron carriers, and their *E*° values was proposed to produce rates of ET that favor rapid separation of the two electrons derived from the bifurcating flavin along two different ET paths (39). Thus, the highly-reactive reducing equivalent is transferred quickly to Fe_4S_4 clusters distant from the high-potential acceptor that oxidizes the initial two-electron reduced flavin, and we have directly observed a short-lived ASQ state for the bifurcating flavin (39).

While the necessity of a high-energy short-lived SQ is on solid footing, the current work addresses its sufficiency. A short lifetime for a high-energy flavin SQ can reflect a variety of processes and mechanisms (**Figures 4.3a** and **4.6**). When oxidized flavin is photoexcited, it rapidly acquires an electron at the expense of residues nearby in a reaction that is driven by the high- energy of the photoexcited state (F*). However, F* can also return to the ground OX state by radiative decay in which excess energy is released as an emitted photon in fluorescence. Non- radiative decay can occur in competition, mediated by local motions that dissipate the excess energy. Additional pathways such as intersystem crossing have been documented (93) but are believed to be slower and thus less germane to bifurcation. Our TAS experiment is able to observe radiative decay via the emissive signal of F* as well as ET via the population of ASQ. Moreover we can also observe the sum of all restoring processes via the recovery of

OX which (like emission) appears as a negative signal. The fate of ASQ can be addressed via formation of the optical signature of NSQ in response to proton acquisition, or simple concurrent disappearance of ASQ and restoration of OX in the case of flavin reoxidation. In this connection, several seminal studies have succeeded in observing amino acid radicals that result from initial ET to the flavin, and documented ET back from ASQ to the oxidized donor $D^{\bullet+}$ as a mechanism for ASQ decay by CR (**Figure 4.6)** (86,88). While we detected optical signatures with properties consistent with amino acid radicals (see **Supplemental Figure 4.S3** for signals at 515 nm (NR), 518 nm (NADOX), 522 nm (Nfn) and 521 nm (Fld)), further studies such as time-resolved infrared spectroscopy are needed for a definitive assignment (103).

The several paths by which a high-energy ASQ can react provide ample justification for our finding that a short-lived ASQ does not suffice to predict or explain bifurcation activity. Not only does our non-bifurcating NADOX system display an ASQ lifetime comparable to that of bifurcating Nfn, but Fld has the shortest ASQ lifetime of all our systems, and it is known to stabilize a NSQ. Thus, we find that short-lived ASQ is not causative, but instead is a consequence of more fundamental properties necessary for bifurcation.

Table 4.1 compares the ASQ lifetimes in the several systems we have compared, and summarizes the different mechanisms that appear principally responsible for ASQ decay after photochemical production. The long ASQ lifetime in NR can be explained by the relatively long distances to the amino acid side chains that most likely served as donors in the photogeneration of ASQ. Electron transfer to NR's flavin is supported by the observed decrease in FMN fluorescence upon binding to the NR apoprotein. However, NR's active site lacks any ET path to other redox partners consistent with its ping pong mechanism that calls for retention of electrons on the flavin for transfer to substrates. The more rapid decay of ASQ in NADOX is consistent

with lower flavin fluorescence in this protein and the presence of Trp47 stacked 6.9 Å above the flavin in NADOX but replaced by Thr in NR (Figure 3b, S4). Fld's very rapid decay can be understood in the same framework as a consequence of rapid recombination of ASQ and the flanking $Trp^{\bullet+}$ that is produced upon photodriven ET (104). In this system we also detect transformation of ASQ to NSQ on the time scale of our experiment but even NSQ does not persist, likely because the nearby $Trp^{\bullet+}$ rapidly reoxidizes it. The breadth and strength of the NSQ signal prevented us from identifying spectral features we could attribute to $Trp^{\bullet+}$ or $Tyr^{\bullet+}$ to document this process, but these have been established in other work (88).

The active site of Nfn is distinct from those of NADOX and Fld in that the nearest Tyr/Trp residue is a Tyr that is in turn close to a Fe_2S_2 cluster which is thought to have a relatively high potential and therefore is most likely in its reduced state in our samples (39). This Fe_2S_2 cluster is therefore likely to rapidly rereduce $Tyr^{\bullet+}$ generated by ET to photoexcited flavin. The next closest redox-active group to the flavin is a Fe_4S_4 cluster whose low reduction midpoint potential suggests that it is in its oxidized state in our samples and therefore able to accept an electron from ASQ. Moreover this cluster is in turn coupled to another, which is expected to reoxidize it, in effect propagating the photochemically produced electron away from the flavin. We propose that this ET relay specific to Nfn can explain its longer ASQ lifetime than that of Fld.

We cannot build ET pathways into NR to test the significance of this proposed mechanism, but we were able to manipulate the balance between charge propagation *versus* CR by accelerating the latter via provision of exogenous donors. Indeed, upon addition of high concentrations of donors, CR appears to occur on a timescale competitive with ASQ formation and thereby prevent its accumulation. Thus, we propose that the relatively rapid decay of NADOX' ASQ represents CR with a donor radical, in this case the Trp

residue near the flavin (**Figure 4.6**). In this model, we propose that the similar ASQ lifetimes of NADOX and Nfn stem from different dominant mechanisms of ASQ decay (**Table 4.1**). We propose that the bifurcating activity specific to NfnI stems from its efficient ET chains, one of which can rereduce the donor oxidized by the photoexcited flavin, and the other of which can accept an electron from ASQ, mediating its decay. Together these two paths can separate the photogenerated hole from the electron, forestalling rapid CR, and mediating bifurcation *in vivo*.

4.5 Conclusion

In conclusion, our comparison of a set of complementary flavoproteins shows that while a short-lived ASQ may be an expected consequence of the high-energy SQ held to be necessary for bifurcation, it is not sufficient. By comparing and manipulating different mechanisms of ASQ reoxidation we show that rapid CR can shorten the lifetime of a photochemically generated ASQ as much as, and even more than, the efficient ET documented previously for Nfn. The necessity for ET along two separate paths is not in doubt, but our work cautions that neither thermodynamic suppression of a SQ state, nor a short-lived SQ state once formed, suffice to diagnose a system as bifurcating. Transient absorption spectroscopy is demonstrated to be an invaluable method of elucidating the steps by which a photochemical system evolves, and electrons may move within a system.

Table 4.1. Processes and lifetimes in proteins[a]

	NR	NADOX	Nfn	Fld
			Lifetimes (ps)	
ASQ (decay)	426±27	29±3	14±1	0.7±0.3
Mechanism	CR	CR	ET	CR
OX (recovery)	513±34	60±6	17±2	0.5±0.1 (24 %)[b] 2±0.5 (76 %)
F* Abs[c]	443±15	40±2	2.3±0.1 (72%)[b] 166±14 (28%)	3.7±0.3
F* Emit	337±17	16.6±0.4	8±1	---

[a] Wavelengths used are provided in captions of **Figure 4.1** (NR) and in **Supplemental Figure 4.S2** (NADOX, Fld, Nfn).
[b] Lifetime fit to a biphasic exponential process.
[c] Contribution from oxidized amino acid radical is also possible in this spectral region.

Table 4.2. Effects of exogenous donors on NR ASQ decay and OX recovery[a]

Donor[b]	Reduction Potential[c]	K_d[d]	Donor Concentration	365 nm	450 nm
	(mV)	µM	µM	t, ps	t, ps
None			0	436±20	533±63
PAB	743	47 ± 5	25	336±68	420±79
			2500	0.6±0.3	4.4±1.5
AB	977	32 ± 2	2500	237±106	1.4±0.2 (97%)[e] 643±82 (3%)
BA	>1405	420 ± 60	2500	380±17	370±24

[a] Lifetimes for anionic semiquinone Decay (365 nm) and oxidized flavin recovery (450 nm) for nitroreductase (NR) in the presence of 2-(phenylamino)benzoic acid (PAB), 2-aminobenzoic acid (AB), or benzoic acid (BA). Exogenous electron donors were prepared in 250 µM NR with the exception of the 25 µM PAB concentration ran at 229 µM NR.
[b] Structures of the donors are provided in Supplemental Figure 4.S6.
[c] All values are ± 10 mV, for literature values see (105-108)
[d] Determined via fluorescence-monitored titrations performed at 10 °C in 50 mM phosphate and 50 mM KCl with 5% ethanol at pH 7.0. Absorbance-monitored titration at 25 °C yielded somewhat smaller values: 27 ± 2.
[e] Lifetime fit to a biphasic exponential process, monophasic fits failed to converge in this case.

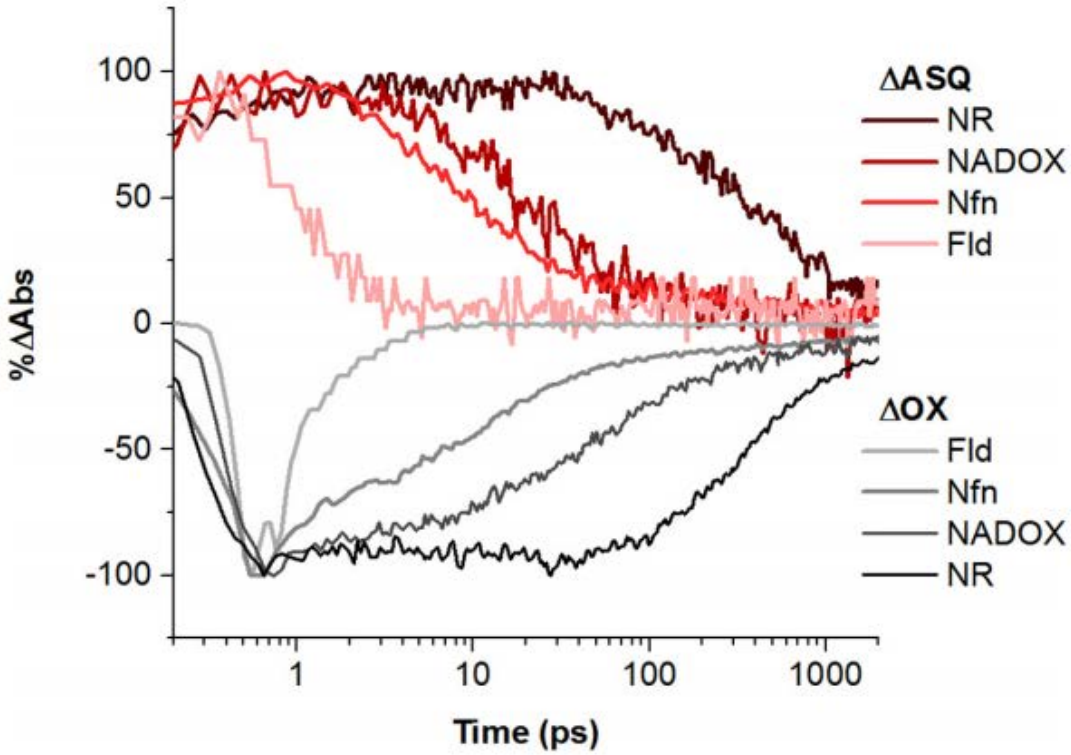

Figure 4.1. Recovery of oxidized flavin (454 to 467 nm) correlates with the decay of anionic semiquinone (ASQ, 365 to 375 nm) over 2 orders of magnitude. Data were normalized to the maximum absorbance change (ΔA) in each trace. Positive traces in *shades* of *red-pink* correspond to the amplitude of signal attributed to ASQ and were collected at the λ_{max} for each system: NR at 375 nm, NADOX at 370 nm, Nfn at 365 nm and Fld at 370 nm. Negative traces in *shades* of *black-grey* correspond to the amplitude of bleach of oxidized flavin and were collected at each system's λ_{max}: 455 nm for NR and NADOX, 454 nm for Nfn and 467 nm for Fld. Time zero was adjusted for NR (+1.99 ps) and Fld (-0.30 ps). While the same bands were monitored in all cases (**Figures 4.2** and **4.S3**), optimal wavelengths varied from protein to protein.

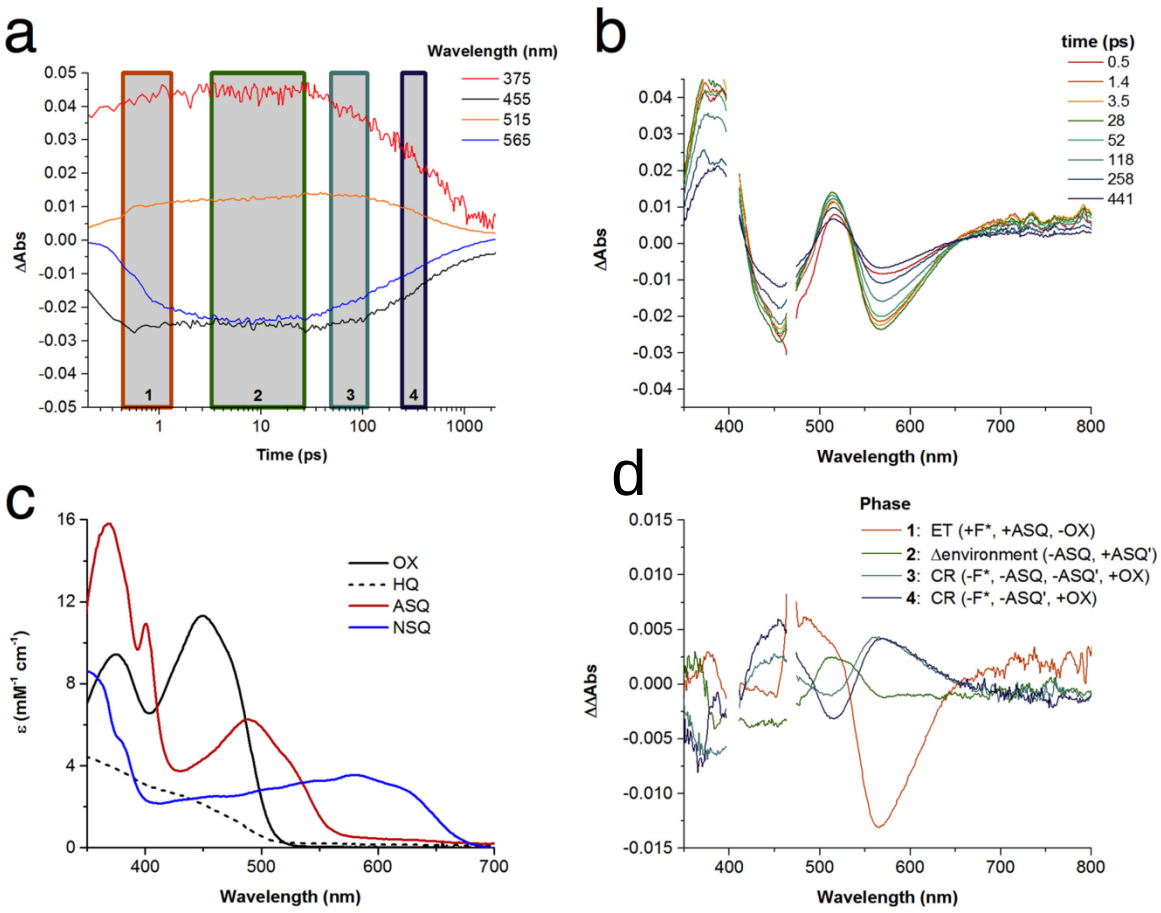

Figure 4.2. Transient absorption spectroscopy (TAS) of NR reveals long lifetimes for multiple dynamic components and permits observation of events that are difficult to observe in the other more rapidly evolving systems studied. *a*, Select phases (boxes) and transients (traces) used in the identification of species and dominant dynamics, respectively. Time zero was adjusted by +1.99 ps. *b*, Transient spectra at times corresponding to the start and end of each phase. *c*, Sample equilibrium spectra for the four flavin redox states: oxidized (OX), hydroquinone (HQ), anionic semiquinone (ASQ), and neutral semiquinone (NSQ). *d*, Phase associated difference spectra (PADS) corresponding to non-equilibrium ET events following photoexcitation. The *colors* identifying the different phases (*a*) have been applied to the PADS' associated with them (*d*), as well as the events depicted in **Figure 4.3a**.

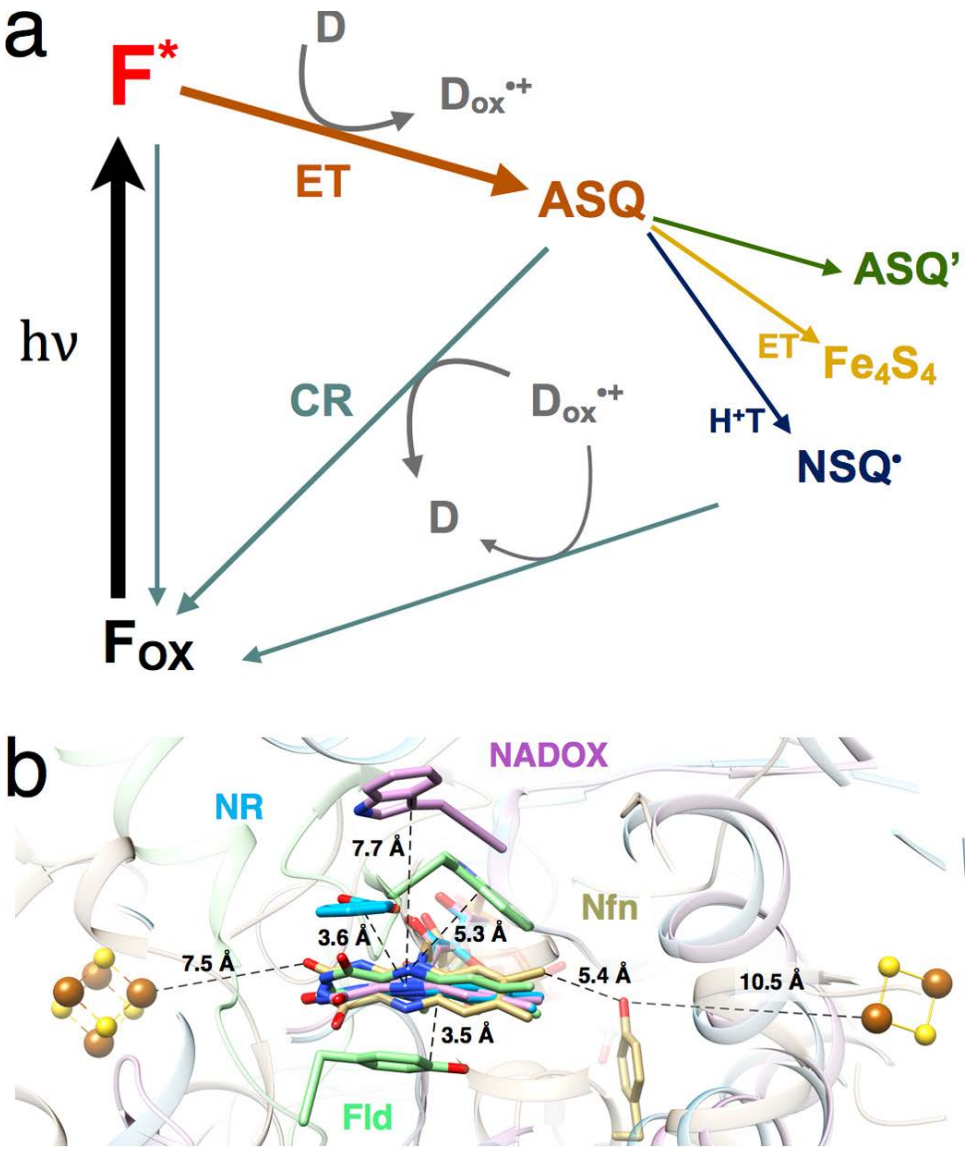

Figure 4.3. Electron transfer (ET) processes and overlay of the flavin sites. *a*, Simplified scheme for ET processes resulting from photoexcitation (*hv*) and varying depending on the flavin environment and context in each system. Processes (arrows) and resulting species are *colored* according to the phases in which they are most prominent (**Figure 4.2a**) and the PADS in which their spectral signatures appear (*dark orange*, ET; *green*, change in the flavin environment; *seafoam grey*, CR). *b*, overlay of the flavin sites (*magenta,* NADOX; *green,* Fld; *tan*, Nfn; *blue*, NR with BA bound). Panel *b* was generated using Chimera (109) and the pdb coordinate files 1NOX.pdb (63), 1KQC.pdb (100), 5JFC.pdb (39), and 1J8Q.pdb (104) for NADOX, NR, Nfn and Fld, respectively. Distances between cofactors in Nfn are provided in Å. The active site flavins of the four proteins were overlaid, using the L-FAD of Nfn since it is the one believed to bifurcate.

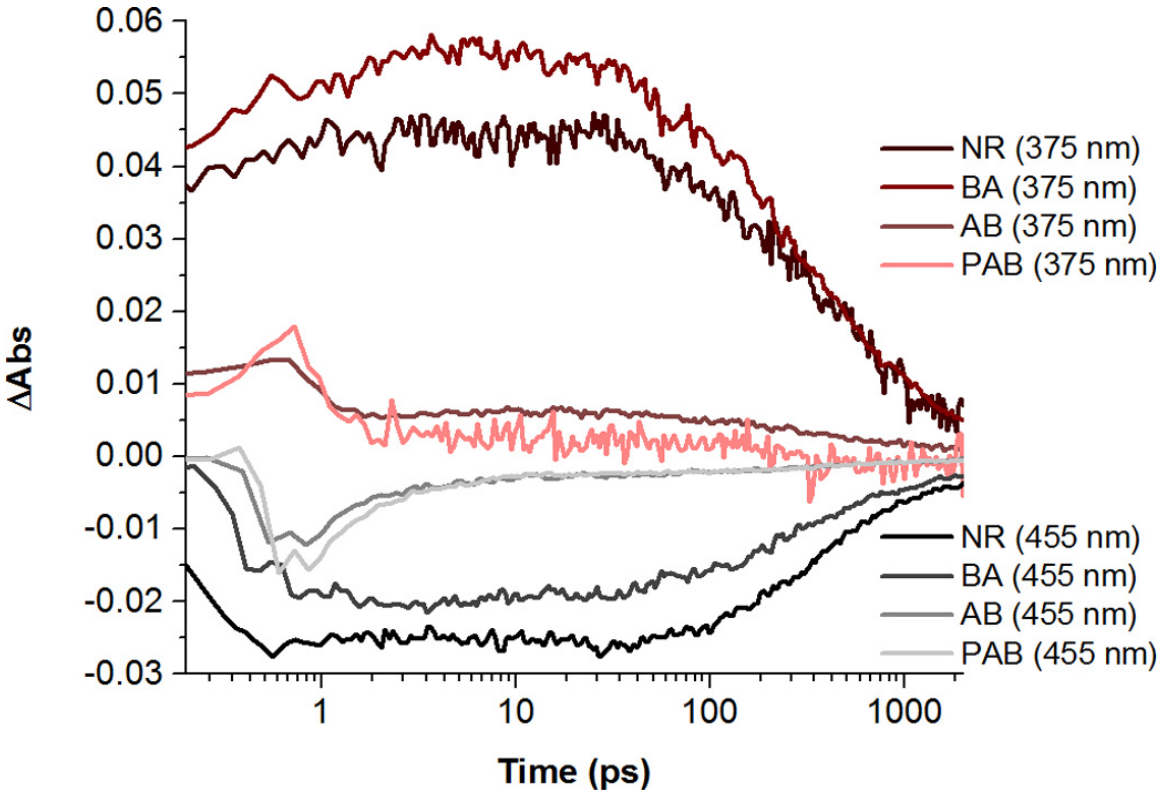

Figure 4.4. Recovery of oxidized flavin for NR (455 nm; *black-gray*) and decay of ASQ (375 nm; *red-pink*) in the presence of exogenous electron donors at 2.5mM: BA, AB, and PAB. The donors produced altered dynamics following photoexcitation of flavin, as evidenced by amplitude trends for the kinetic transients as well as overall shortened dynamics. Time zero was adjusted by +1.99 ps for the protein-only control (NR). *ΔAbs*, difference absorbance (photoexcited minus not photoexcited).

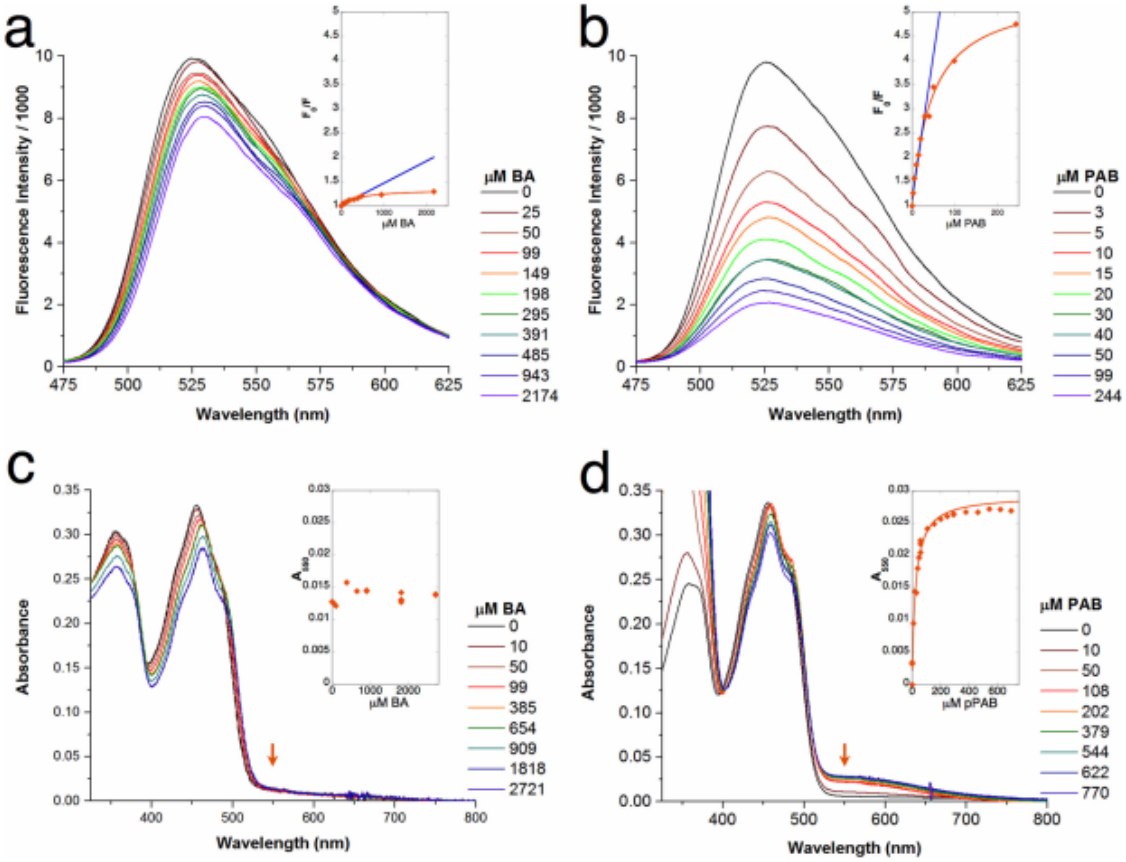

Figure 4.5. Fluorescence quenching (a and b) and formation of a charge transfer band near 550 nm (c and d) upon binding of the exogenous donors BA (a and c) or PAB (b and d) to NR. *Panel b* shows that flavin fluorescence is substantially quenched by the substrate analog PAB with saturation behavior diagnostic of specific binding (*orange curve* in *inset* of *panel b*) as opposed to Stern-Volmer type quenching (*blue line* in *inset*). *Panel a* shows that quenching of fluorescence upon addition of BA is also best described by specific binding but with a ten-fold smaller electron transfer rate (same *color convention* in *inset* of *panel a*). Temperatures of 10 °C (fluorescence) and 25 °C (absorbance) are compared. For fluorescence quenching by BA, the fit to the Stern-Volmer equation (Equation 1) neglecting the data at the four highest donor concentrations yielded y=1.016 + 0.00046x, and the fit to specific binding (Equation 2) yielded an intercept of 1.004 ± 0.007, $k_{ET}\tau_0$ = 0.34 ± 0.02 and K_d = 420 ± 60 μM. For quenching of fluorescence by PAB, the Stern-Volmer fit neglecting the data at the four highest donor concentrations yielded y= 1.15 + 0.059x, and the fit to specific binding yielded an intercept of 1.06 ± 0.07, $k_{ET}\tau_0$ = 4.4 ± 0.2 and K_d = 47 ± 5 μM. For both models, the data adhere well to the intercept of 1.00 predicted by theory. In absorbance-monitored titrations, *panel c* shows that BA yielded an insignificant increase in absorbance near 550 nm

(*orange arrow* in *panel c* and *inset*), but *panel d* shows that the addition of PAB produced a CT band near 550 nm that displayed saturation behavior consistent with specific binding (*orange arrow* in *panel d* and *inset*), albeit not in excellent conformity of the simplest model for independent binding at two identical sites: $A = \Delta Abs \times [donor]/([donor] + K_d) + b$, where b is the background, ΔAbs is the maximal absorbance change upon binding, and K_d is the dissociation constant describing binding. Fit to the data yielded $K_d = 27 \pm 2$ μM, $\Delta A = 0.027 \pm 0.0007$, $b = 0.002 \pm 0.0006$. The slightly lower K_d observed at 25 °C is consistent with slightly greater fluorescence quenching and static quenching, albeit incomplete.

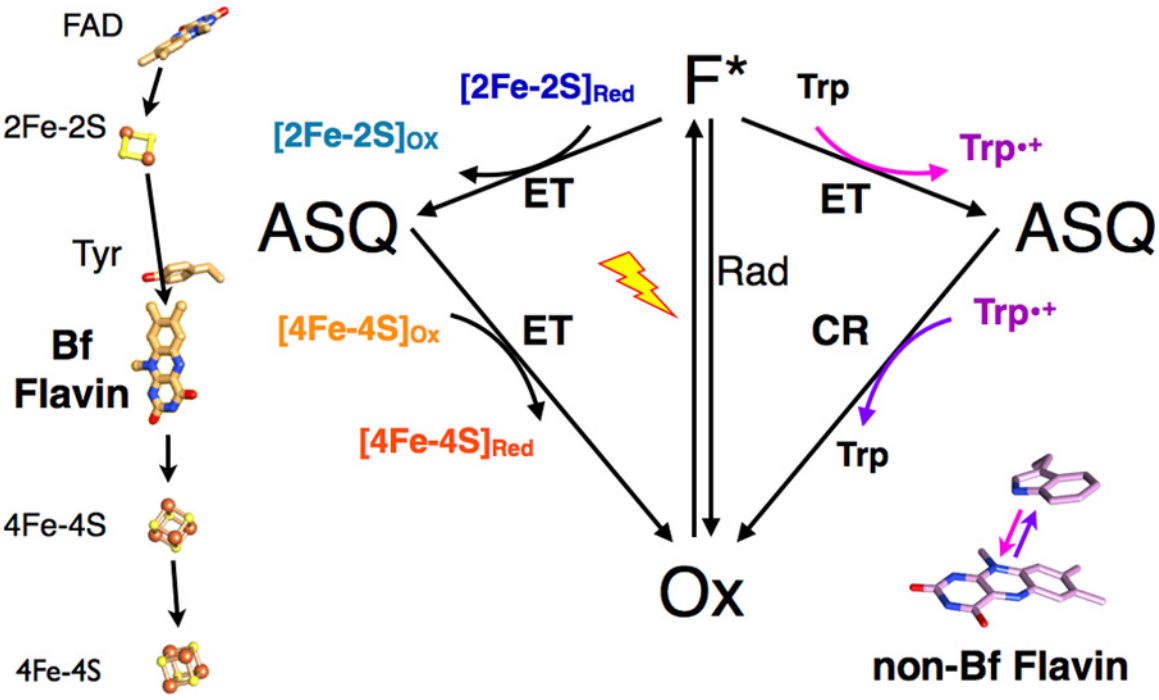

Figure 4.6. Structural mechanistic model. The electron transfer (ET) mechanism proposed for Nfn *versus* the charge recombination (CR) mechanism proposed for NADOX explains why bifurcation occurs in Nfn but not NR/NADOX despite a thermodynamically suppressed ASQ in all three systems. The diamond diagram in the center depicts the photoexcitation of OX to F* (*lightning bolt*) and some of the events that can then aid in restoring the system to its starting state, including radiative decay (*Rad*), ET, or CR. The *left half* of the diamond depicts events in Nfn, whereas the *right half* depicts events proposed to occur in NR and NADOX. The ET cofactors and proposed paths of ET in photoexcited Nfn are shown on the *left-hand side*, based on the crystal structure 5JFC.pdb (39). The distances between cofactors are as follows: Fe_4S_4–Fe_4S_4 = 9.4 Å, flavin–Fe_4S_4 = 7.5 Å, flavin–Tyr = 5.4 Å, Tyr–Fe_2S_2 = 10.5 Å, and Fe_2S_2–FAD = 8.3 Å. Note however that in the course of enzymatic turnover the direction of electron transfer between the bifurcating flavin (*Bf Flavin*) and the FAD would occur in the opposite direction to that shown. This figure depicts ET proposed upon photoexcitation of the flavin. The active-site FMN and Trp side chain of NADOX are shown to the *right* of the diamond diagram (*non-Bf Flavin*), based on the crystal structure 1NOX.pdb, and the closest distance between the Trp and the flavin is 6.9 Å (63).

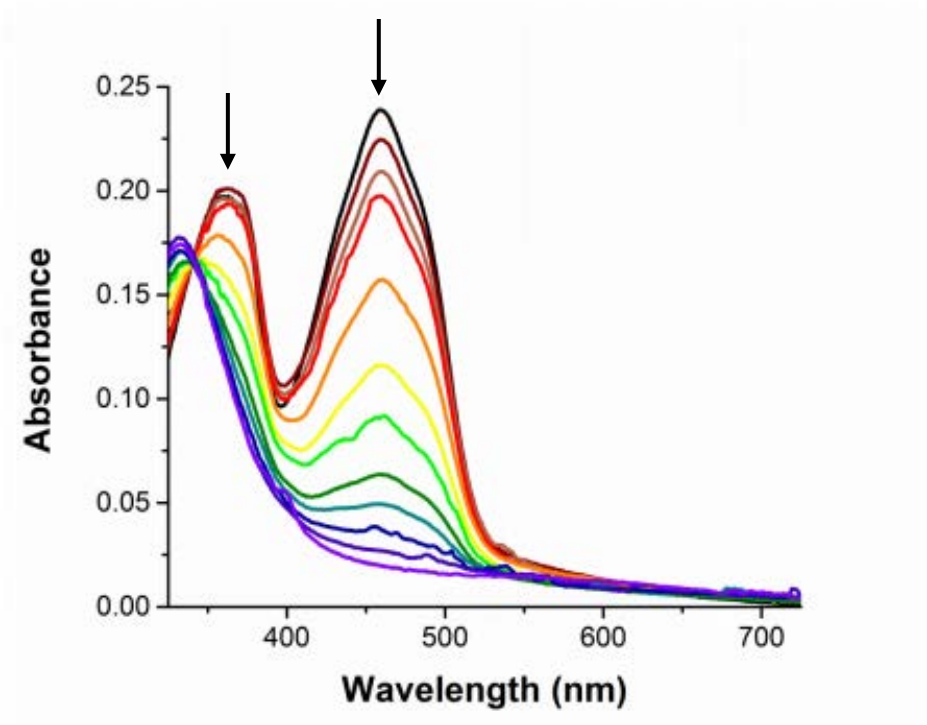

Figure 4.S1. Anaerobic reduction of WT-NADOX using xanthine oxidase with xanthine to provide reducing equivalents. The titration was performed using benzyl viologen as a redox mediator but without a redox dye standard. A clear isosbestic was observed near 340 nm and no signal from ASQ or NSQ was observed, indicating a single two-electron reduction of OX (*black spectrum*) to reduced flavin (*purple spectrum*), without formation of a stable SQ intermediate. *Arrows* denote the signal change during the course of reduction.

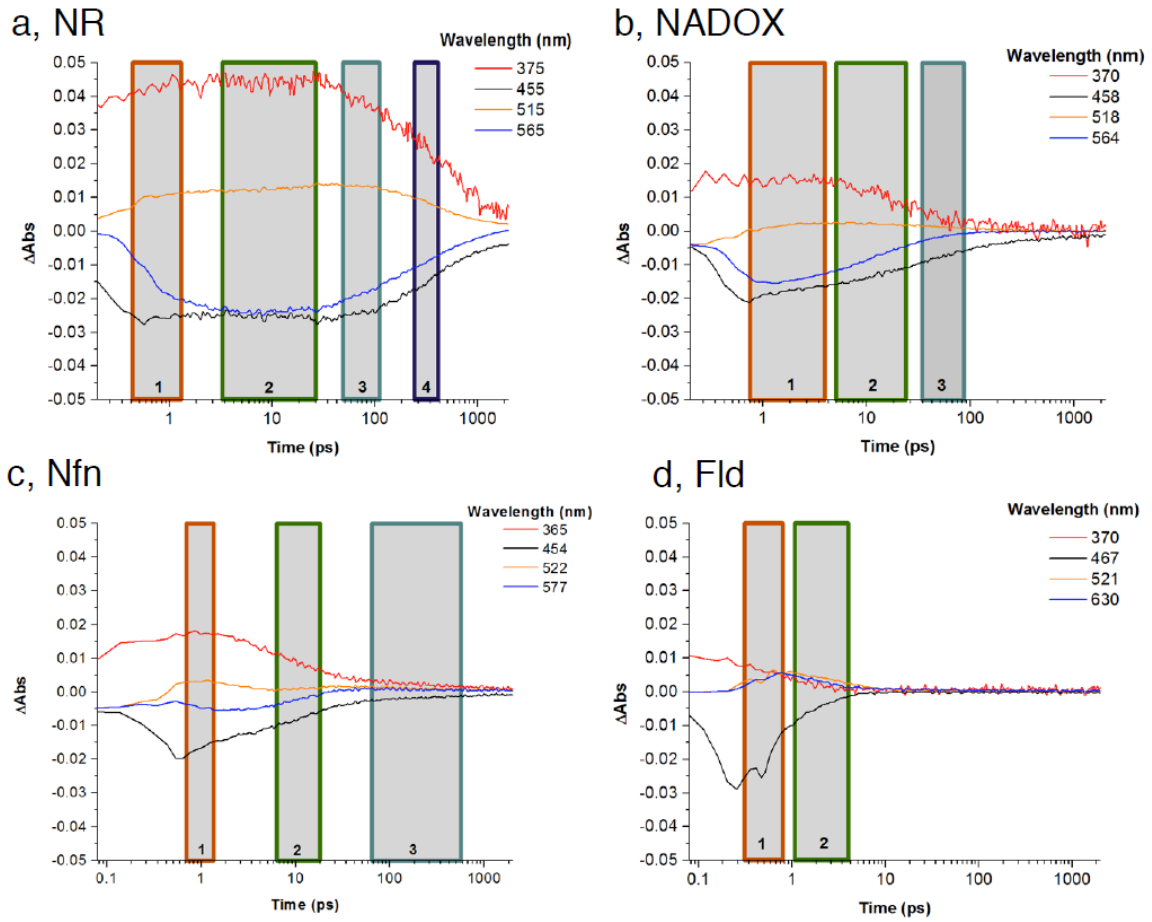

Figure 4.S2. Select absorbance transients for the identification of distinct dynamic phases following photoexcitation of nitroreductase (NR, *a*), NADOX (*b*), Nfn (*c*), and flavodoxin (Fld, *d*). Time zero was adjusted for NR (+1.99 ps) and Fld (-0.30 ps).

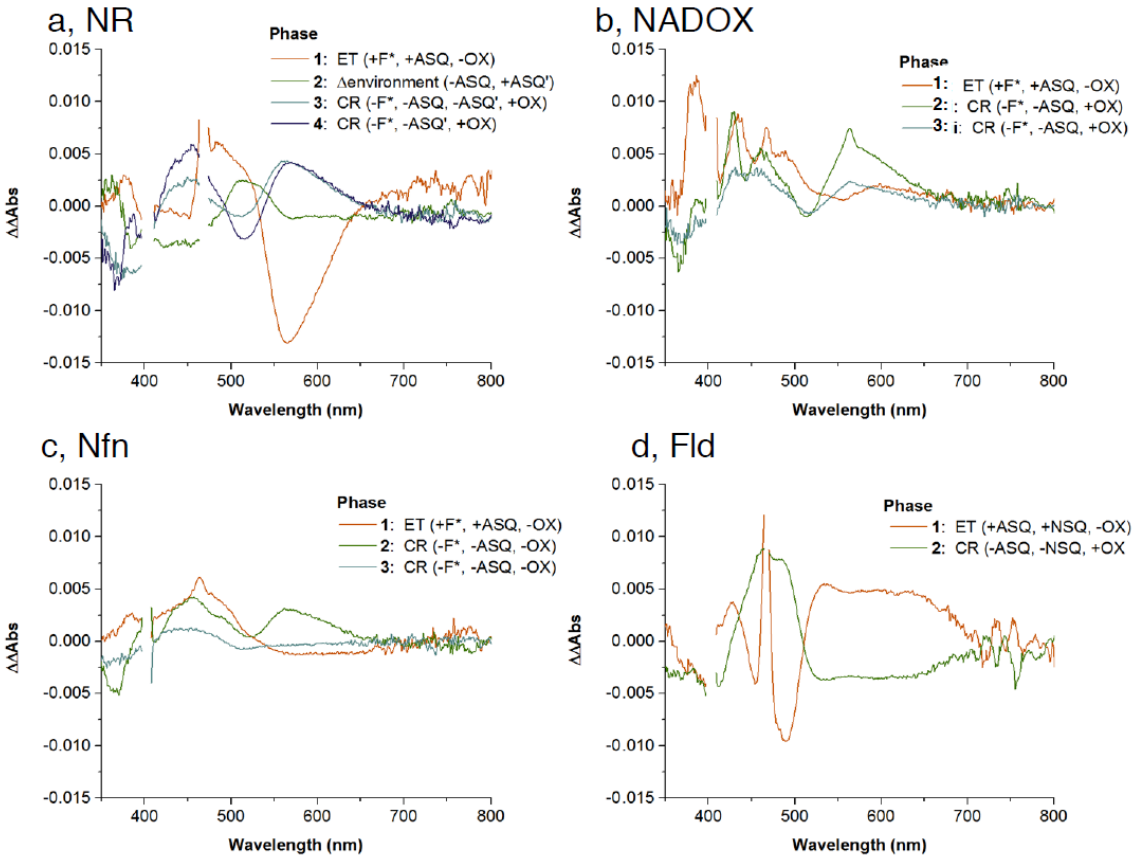

Figure 4.S3. Phase-associated difference spectra (PADS) corresponding to photogenerated species and outcomes of electron transfer and charge recombination events following photoexcitation of NR (*a*), NADOX (*b*), Nfn (*c*), and Fld (*d*). Time zero was adjusted for NR (+1.99 ps) and Fld (-0.30 ps).

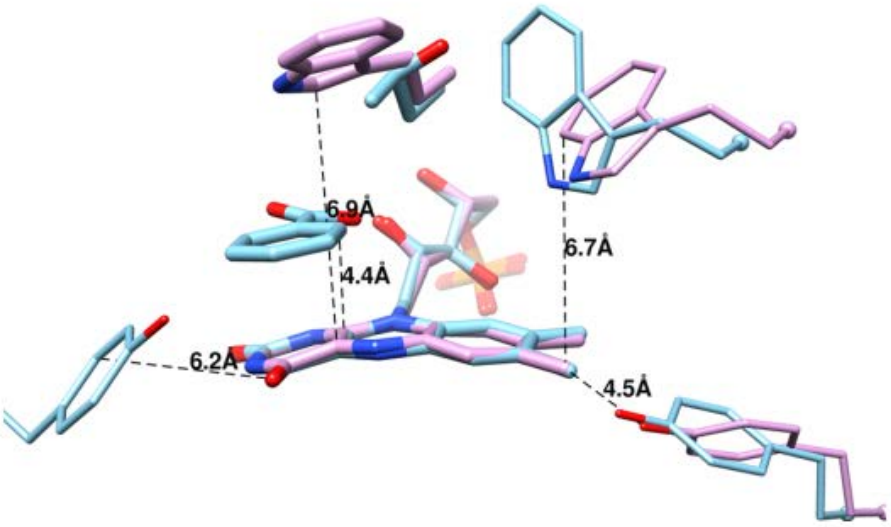

Figure 4.S4. Overlay of the active sites of NADOX (*magenta*) and NR with benzoic acid bound (*blue*). All aromatic side chains within 7 Å of the flavin are shown. Stacked above the flavin is NADOX' Trp47 which is replaced by Thr in NR. Exogenous donors mimic Trp47 by binding stacked against the flavin, but closer than the native amino acid side chain. The figure was generated from pdb coordinate files 1NOX.pdb (63) and 1KQC.pdb (100), for NADOX and NR, respectively.

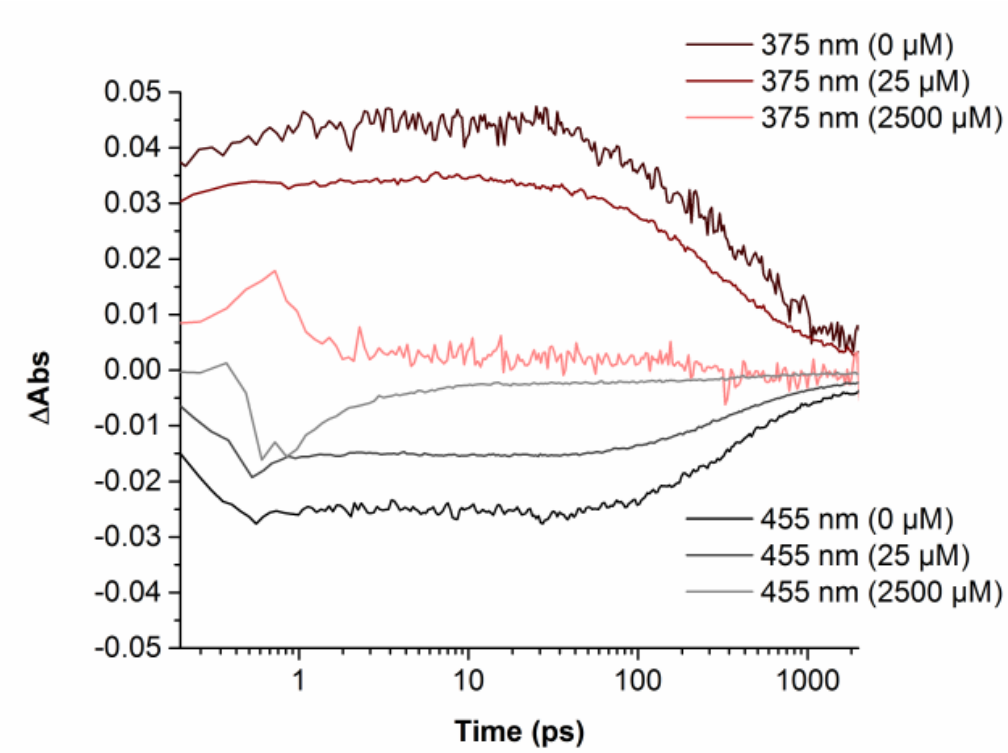

Figure 4.S5. Recovery of oxidized flavin (455 nm, *black-grey*) and decay of anionic semiquinone (375 nm, *red-pink*) for nitroreductase (NR) in the presence of 25 or 2500 µM 2-(phenylamino)benzoic acid (PAB). Time zero was adjusted for NR (+1.99 ps).

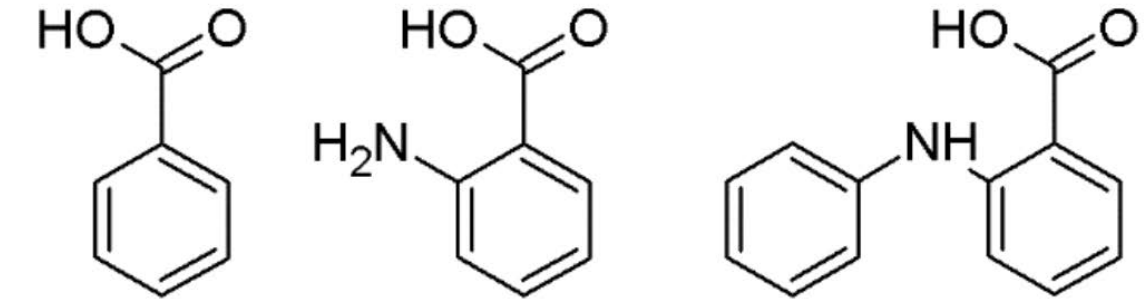

Figure 4.S6. Structures of the exogenous donors used. *a*, Benzoic acid, BA. *b*, 2-aminobenzoic acid, AB. *c*, 2-(phenylamino)benzoic acid, PAB.

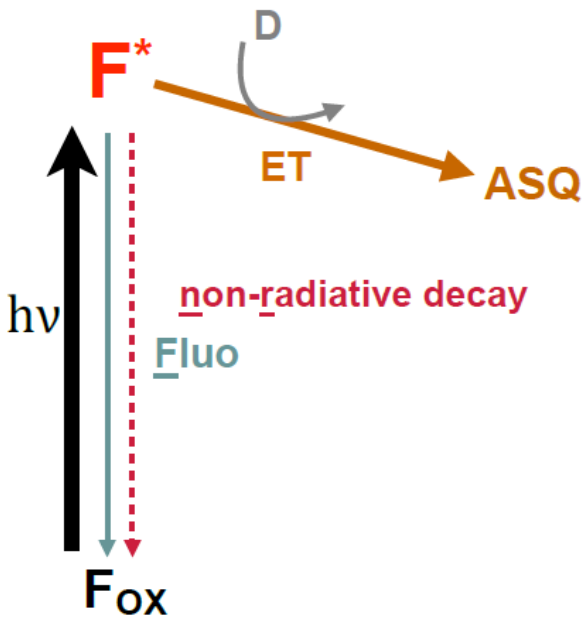

$\varphi_{F,0}$, is the fluorescence quantum yield at [donor] = 0

$\varphi_{F,0} = k_F/(k_F + k_{nr})$ where k_F is the rate of radiative decay via fluorescence, k_{nr} is the rate of non-radiative decay and intersystem crossing to form triplet can be neglected.

$1/(k_F + k_{nr}) = \tau_0$ is the natural lifetime, so

$\varphi_{F,0} = k_F\,\tau_0$

$\varphi_{F,d}$, is the fluorescence quantum yield in the presence of donor, D.

$\varphi_{F,d} = k_F/\left(k_F + k_{nr} + \dfrac{k_{ET}}{(1+ K_d/[D])}\right)$ where k_{ET} is the rate of quenching by electron transfer and $1/(1+ K_d/[D])$ is the fraction of sites in which donor (D) is bound, with binding described by the dissociation constant K_d .

$F/F_0 = \varphi_{F,d} / \varphi_{F,0}$ is the fraction of fluorescence that survives quenching.

$F_0/F = \left(k_F + k_{nr} + k_{ET}/(1+ K_d/[D]) \right) / (k_F + k_{nr})$

$F_0/F = 1 + k_{ET}\tau_0/(1+ K_d/[D])$

Figure 4.S7. Derivation of equation describing fluorescence quenching.

CHAPTER 5 INITIAL CHARACTERIZATION OF THE REDOX PROPERTIES OF *PYROBACULUM AEROPHILUM* ELECTRON-TRANSFERRING FLAVOPROTEIN

5.1 Introduction

Microbes employ an array of life strategies evolved to meet the bioenergetic demands of their environment (110,111). However, only two general mechanisms for energy conservation in biological systems have been widely studied (i.e.- substrate-level phosphorylation and electron transport-linked phosphorylation). Within the past decade, a third mechanism of biological energy conservation (electron bifurcation) has been discovered (30). Electron bifurcation couples favorable (exergonic) electron transfer with unfavorable (endergonic) electron transfer, essentially splitting electron pairs of intermediate-potential to generate both low- and high-potential electrons (**Scheme 5.1**) (112). Long before empirical confirmation of electron bifurcation in a biological system by Herrmann et al. in 2008 (30), Mitchell proposed in 1975 (73) that the process was operative in generating the proton gradient across the lipid bilayer of mitochondria. Specifically, the quinone (Q) cycle was proposed to explain how coenzyme Q–cytochrome c reductase (Complex III) catalyzes sequential oxidation and reduction that essentially bifurcates ubiquinone electron pairs and results in a proton and electron gradient. The Q-cycle is an example of quinone-based bifurcation.

Understanding of electron bifurcation is due in large part to discoveries made in the bifurcating members of the electron transfer flavoprotein (Etf) superfamily (34,36,37,113,114). In these systems, electron bifurcation occurs by way of protein bound flavin cofactors rather than diffusible quinones. The process is known as flavin-based bifurcation (FBEB) and appears to be particularly important in anaerobic metabolism for the generation of the low potential reduced ferredoxin and reduced flavodoxin (32). These low potential products of FBEB are used by anaerobic microbes to perform energetically demanding reactions such as protons to hydrogen and CO_2 to CO (32,69). The process of FBEB is likely essential to many anaerobic microbes (115,116). However, the recent discovery of electron bifurcation in the aerobe *Azotobacter vinelandii* suggests the process may be a general feature of microbial energy conservation regardless of extracellular oxygen concentrations (37).

While *Azotobacter vinelandii* is a strict aerobe, *Pyrobaculum aerophilum (Pae)* is capable of both aerobic and anaerobic respiration. The metabolic flexibility of *Pae* is intriguing in the context of FBEB and its Etf was selected for this study.

To assess the bifurcating capacity of EtfAB from the hyperthermophilic archaeon *Pyrobaculum aerophilum (Pae)*, initial biochemical characterization was carried out. The early results described herein include biochemical properties found in bifurcating systems and support the hypothesis that the heterodimer alone can support bifurcation. Such findings have yet to be reported for a thermophile or an archaeum.

5.2 Experimental Procedures

Materials

Pae EtfAB (~12 mg) was a gift from our collaborators in The Adams Lab.: Gerrit J. Schut, Diep M. Nguyen, Gina L. Lipscomb, and Michael W.W. Adams (Department of Biochemistry and Molecular Biology, University of Georgia, Athens, GA 30602). Briefly, the recombinant material was prepared by over-expression in the genetically tractable archaeon *Pyrococcus furiosus* at 95°C and purified as previously described (117,118). Fermentation, purification, and shipping of material were performed under strict anaerobic conditions. Strict anaerobic conditions were maintained out of the glovebox by placing purified protein in a standard 1 mL screw cap gas chromatography vial which was then placed into a 5 mL Wheaton vial (Item# 223685) containing 1 mL of a reducing solution which contained a redox indicator standard (~50 mM sodium dithionite (dithionite) and ~50 µM phenosafranin in 20 mM potassium hydroxide). Standard caps and rubber stoppers were used along with black vinyl tape to ensure an airtight seal out of the glovebox.

Buffer Exchange and Removal of Excess Flavin for As Isolated Samples and Following Flavin Reconstitution

As isolated protein samples and samples reduced with dithionite and/or NADH were reconstituted with flavin adenine dinucleotide (FAD) in a manner similar to that described by Koder et al. (22). Briefly, 100 to 400 uL of 15-30 µM *Pae* EtfAB was mixed with an equivalent volume of 10 mM FAD in 25 mM Bis-tris propane, 200 mM NaCl, pH 7 at 4°C overnight. Free flavin was removed by diafiltration (10K, Amicon Ultra-0.5 mL, Millipore, Darmstadt, Germany) by 4 to 5 spin cycles. Each spin cycle was followed by the addition of buffer (25 mM Bis-

tris propane, 200 mM NaCl, pH 7). Results for as isolated protein samples are those following diafiltration. Buffer exchange into 25 mM Bis-tris propane, 200 mM NaCl, pH 7 and removal of excess flavin was performed for all samples prior to experimentation.

Flavin Occupancy

The flavin identity and content of *Pae* EtfAB was determined aerobically by releasing the flavin with 0.02% SDS at 95-100°C for 30 min followed by centrifugation (10,000 x*g*, 4 C, 5 min) and observing flavin fluorescence (Thermo Scientific Lumina Fluorescence Spectrometer, Waltham, MA) of the supernatant before and after the addition of phosphodiesterase I from *Clostridium adamanteus* (Abnova, Taipei, Taiwan) as described by Aliverti et al. (5). Hydrolysis of unbound FAD by phosphodiesterase I was monitored by fluorescence for 20 min at which point the maximum increase in emission (554 nm) occurred.

Redox Titrations

Anaerobic conditions were established and maintained within a glovebox (Belle Technology UK Ltd., Waymouth, United Kingdom). Absorbance measurements were made using a diode-array spectrophotometer (Olis HP 8452A, Athens, GA) placed inside the glovebox. Stock solutions (0.5 to 1 mM) of dithionite or NADH were used as reductants and used within three hours. Stock solutions of dithionite also contained 20 mM potassium hydroxide. To test the ability of NAD^+ to bind to bound flavin in the hydroquinone (HQ) state, protein samples reduced with dithionite were titrated with NAD^+ stock solutions. Binding

of NAD^+ to HQ was considered on the basis of the formation of a charge transfer complex upon HAD^+ addition to samples reduced with dithionite (119).

Spectroelectrochemical titrations for the determination of reduction potentials were performed similar to procedures described by Massey (61) with dithionite as the reductant or xanthine/xanthine oxidase as the reducing system. Prior to the addition of a redox standard or initiation of the reduction, initial absorbance scans of protein solutions in a 1 mL 1 cm pathlength cuvette were stable and showed the expected trace for fully oxidized (OX) EtfAB (Etf-$A_{ox}B_{ox}$). To the protein solution, near equimolar concentrations of a redox standard and 0.5 µM methyl viologen were added with scans taken after each addition following 5 to 10 min equilibration. The redox standards thionin (E_m = +64 mV vs SHE, pH 7, n=2 (25)) and phenosafranin (E_m = -252 mV vs SHE, pH 7, n=2 (120)) were selected based on the expected reduction midpoint potentials for the OX/ASQ and OX/HQ in question. Because these are electron uptake reactions, the energies are customarily discussed as energy/electron = $E°'$. Reduction was achieved with 1-2 µL additions of a fresh 500 or 1 mM µM dithionite stock over the course of 75 min at 20-23 °C. For the xanthine/xanthine oxidase reducing system, reduction was initiated by the addition of ~3 ng of xanthine oxidase to 500 to 800 µL protein solutions containing 400 µM xanthine and monitored for at least 75 min at 20-23 °C. Linear regression was performed in OriginPro 9.0 (Northampton, Massachusetts) for the purpose of determining midpoint potentials using standard analysis (36,61,121):

$$\ln\left(\frac{\mathrm{E_{ox}}}{\mathrm{E}red}\right) = \frac{n_{\mathrm{E}}}{n_{\mathrm{S}}}\ln\left(\frac{S_{ox}}{Sred}\right) + b \qquad (5.1)$$

where $\frac{\mathrm{E_{ox}}}{\mathrm{E}red}$ is the ratio of oxidized to reduced bound flavin, $\frac{S_{ox}}{Sred}$ is the ratio of oxidized to reduced redox standard, n_{E} is the number of electrons acquired by the enzyme, n_{S} is the number of electrons acquired by the redox standard, and *b* is the intercept.

$$b = \left(\frac{F}{RT}\right) n_{\mathrm{E}} \left(E_{\mathrm{S}}^{\circ\prime} - E_{\mathrm{E}}^{\circ\prime}\right) \qquad (5.2)$$

where *F* is Faraday's constant, *R* is the ideal gas constant, *T* is the absolute temperature, $E_{\mathrm{S}}^{\circ\prime}$ is the midpoint potential for the redox standard, and $E_{\mathrm{E}}^{\circ\prime}$ is the midpoint potential of the enzyme.

The ratio of oxidized to reduced species (bound flavin and/or redox standard dye) was determined by the difference of the of the fully oxidized absorbance signal and the partially reduced absorbance signal for titration points during the course of the reduction:

$$\frac{OX}{Red} = \frac{i+1}{i-(i+1)} \qquad (5.3)$$

where *i* is the absorbance of the fully oxidized signal and *i*+1 is the absorbance of the first partially reduced titration point.

Calculation of a midpoint potential estimate was limited to those data for which both enzyme and the redox standard were partially reduced. For the thionin titration, the bound flavin was monitored at 450 nm and thionin was monitored at 600 nm. For the phenosafranin titration, the bound flavin was monitored at 408

nm (i.e., the isosbestic point of phenosafranin, **Figure 5.9**) and phensafranin was monitored at 520 nm.

Under more oxidizing conditions (≥ 0 mV vs SHE, pH 7), the solution reduction potential was monitored using an MI-800-410 combination Pt and $Ag/AgCl_2$ oxidation reduction potential (ORP) microelectrode (Microelectrodes Inc., Bedford, NH). Saturated quinhydrone in the same buffer was used for ORP microelectrode calibration (81).

Fluorescence

Fluorescence was monitored using 450 nm excitation with 5 nm slit widths in a Lumina spectrofluorometer (Thermo, Waltham, MA, USA) and a Peltier temperature controller at 25°C.

5.3 Results

Flavin Occupancy

Early observations revealed batch variability with regards to the flavin oxidation state endpoints following reductive titrations and raised concerns regarding bound flavin stoichiometry. The variability along with limited protein expression (~25 mg/15 L culture; gift from the Adams Lab, Department of Biochemistry and Molecular Biology, University of Georgia) made it difficult to reproduce results and draw conclusions early on in the project. Limited protein availability hampered early efforts and was in part overcome by the development of smaller volume assays (3 mL assay reduced to 1 mL or less).

We hypothesized flavin occupancy was affected by material handling and could be increased to the native stoichiometry (two flavins per heterodimer). Flavin occupancy was found to differ between samples isolated from cell lysate ('as isolated') *versus* those that underwent flavin reconstitution (**Table 5.1**). As isolated samples contained 0.96±0.23 (n=3) FAD per EtfAB dimer and hence were substoichiometric (i.e. samples contained only half the flavin content expected).

Based on visually detected protect precipitation, flavin reconstitution and protein stability was found to be optimal at protein concentrations ≤100 µM in 25 mM Bis-tris propane, 200 mM NaCl, pH 7. Removal of excess flavin by diafiltratration produced samples with the expected flavin:dimer stoichiometry of 2.12±0.17 (n=3) FAD per EtfAB dimer (**Table 5.1**). The resulting method proved suitable for the production of stable samples of expected flavin stoichiometry, which in turn allowed for more experiments within the research consortium. Results are presented for both as isolated and reconstituted samples.

Reductive Titrations and Redox States of the Individual Flavins

One vs. two electron reductants

While the two electron reductant NADH is the physiological substrate/electron source specific for the bifurcation site, we sought to probe the electron transfer FAD (ET-FAD) site using the one electron reductant dithionite. We hypothesized that reductive titrations using NADH (two electron source) or dithionite (one electron source) would produce bound flavin spectra with signatures specific to a given flavin site (bifurcation, Bf-FAD site versus ET-FAD site). The expectation for NADH reduction was that reduction would produce spectra which captured the OX to fully reduced hydroquinone (HQ) transition

typical of the Bf-FAD. For dithionite, the expectation was that reduction would produce both anionic semiquinone (ASQ) and HQ spectra typical of the ET-FAD site. Such expectations for *Pae* EtfAB were based on findings for the homologus EtfAB of *Megasphaera elsdenii* (122) and *Rhodopseudomonas palustris* (36).

As isolated samples were evaluated for the formation of semiquinone (SQ) and/or hydroquinone (HQ) upon reduction with either dithionite or NADH. The one electron reductant dithionite produced clearly identifiable spectral features known for anionic semiquinone (ASQ) (**Figure 5.2**). Interestingly, excess dithionite did not appear to fully reduce bound flavin to the point of HQ in as isolated samples.

Fully flavinated reconstituted samples were evaluated in a manner similar to that of the as isolated samples. Dithionite reductions resulted in an HQ endpoint with both the Bf and ET sites fully reduced (HQ-Bf-FAD, HQ-ET-FAD) (**Figure 5.3a**). Unlike the ASQ endpoint following reduction of the as isolated samples, the fully flavinated reconstituted samples displayed the expected redox behavior as observed in homologous systems (36,113,122). Altered redox behavior as a function of occupancy is an interesting result that highlights the interaction between the two flavin sites.

NADH: Two-electron Reductant

Reduction of as isolated samples using NADH produced more complex spectral features with regards to determining ASQ formation (**Figure 5.4**). The reduction does not appear to form the diagnostic shoulder (local λ_{max}= ~ 400 nm) known for ASQ (**Figure 1.3**). However, early steps in the titration (0 to 0.8 NADH equivalents) reveal much greater loss of the OX signal at ~450 nm without a

corresponding loss at ~375 nm. Considering the ~1.7x larger extinction of ASQ over OX at ~375 nm, the result indicates the possibility of an OX to ASQ transition. Following 0.8 equivalents NADH, the large magnitude of loss at both ~375 nm and ~450 nm is suggestive of ASQ to HQ and OX to HQ transitions for the ET-FAD and Bf-FAD sites, respectively. Later steps in the NADH reduction produced spectral features typical of charge transfer (CT) complexes. Specifically, the CT complex between NAD^+ and bound flavin in the fully reduced HQ state (119).

Following the observation of a CT band and a HQ endpoint upon NADH reduction, we hypothesized HQ-Bf-FAD to be in complex with NAD^+. To test if the CT band could be formed from the doubly reduced state (HQ for both Bf-FAD and ET-FAD), we performed NAD^+ titrations by addition of NAD^+ into prereduced reconstituted *Pae* EtfAB samples which had been reduced with dithionite. Starting from dithionite reduced *Pae* EtfAB (**Figure 5.3a**), the CT band was obtained upon NAD^+ addition (**Figure 5.3b**), thus, substantiating the hypothesis of a HQ-NAD^+ state. We assign the CT band to the Bf-FAD site, the known site of NADH binding (32,38).

Indeed the results shown in **Figure 5.3** help confirm the ability of nicotinamide (NAD^+) to bind to Bf-FAD even under reducing conditions where the HQ for Bf-FAD results from dithionite reduction (two-electron reduction mediated by methyl viologen) rather than the physiological reductant NADH (**Scheme 5.2**). Under reducing conditions in the presence of nicotinamide, we assign the flavin redox state endpoint of both flavins to be HQ with the bifurcation site in complex with NAD^+ (i.e.- HQ-NAD+ CT complex). Additionally, comparison of **Figure 5.3a**

and **Figure 5.3b** supports assignment of the long wavelength spectral features (λ_{max}= ~ 750 nm) to a CT complex as observed with NADH (**Figure 5.4**).

Assessment of the energies (E°') associated with reduction

Prior research by Sato *et al.* (122) and Duan *et al.* (36) indicated that homologous Etfs have 3 distinct reduction potentials, so we tested the hypotheses that *Pae* EtfAB will have two one-electron potentials in the range of +50 mV (ET-FAD: OX/ASQ) and -100 mV (ET-FAD: ASQ/HQ), and one two-electron potential in the range of -300 mV.

Early efforts with *Pae* EtfAB from multiple preparations produced extensive precipitation during extended reductive titrations (4 to 24 hours). Glycerol addition (5 to 10%) did not reduce precipitation. Limiting reductive titrations to ≤2 hours permitted absorbance and fluorescence measurements of reconstituted samples buffer exchanged the day of the experiment. Samples were exchanged into the final buffer used for analysis (25 mM Bis-tris propane, 200 mM NaCl, pH 7) in order to replace the buffer used for isolation and shipping (25 Tris-HCl, 300 mM NaCl, pH 8). The analysis buffer appeared to slow precipatation of samples in storage as compared to the isolation and shipping buffer. Further optimization was provided using 0.5 µM methyl viologen to mediate reduction in place of a mediator cocktail.

Reductions Monitored by an ORP Microelectrode

In more oxidizing conditions (≥ -120 mV vs SHE, pH 7), the solution potential could be monitored by an ORP microelectrode. Reduction potentials lower than -120 mV for 5-30 µM *Pae* EtfAB solutions in various conditions produced erratic and non-equilibrium electrode behavior typical of electrode

fouling by protein deposition and protein precipitation. Starting with a fully oxidized reconstituted sample (ET-FAD-OX; Bf-FAD-OX) prepared by ~5 min exposure to atmosphere, **Figure 5.5a** shows accumulation of ASQ for early steps in the dithionite titration as indicated by an increase in absorbance at 368 nm for potentials ≥ +55 mV. Loss of absorbance at 450 nm and gain in absorbance at 368 nm for titration steps down to -19 mV indicates a loss of oxidized flavin with the product as ASQ. Further titration results in spectra that are more difficult to interpret for the assignment of distinct redox states and their assignment to a specific site. However, analysis of spectra for the early titration steps provide a qualitative estimate for the more positive redox couple ($E_{OX/ASQ}$) we determined to be +133 ±10 mV and assign to the ET-FAD site.

The ORP microelectrode method for spectroelectrochemistry required lower protein concentrations and use of a micro volume cuvette. Using this method with *Pae* EtfAB resulted in limited absorbance signal, scatter from the microelectrode, and protein precipitation. Conventional analysis by linear fitting to the Nernst equation failed to provide reasonable y-intercept values for midpoint potentials. Alternatively, fluorescence quenching of flavin upon reduction was monitored in parallel with the absorbance measurements to help assign redox transitions to a given flavin site (**Figure 5.5b**). The first step in the titration results in a slight blue (hypsochromic) shift (518 to 515 nm) but retains features characteristic of vibronic structure (shoulder, $\lambda_{local\ max.}$ = 533 and 552 nm) (82). In homologus systems (36,122), the Bf-FAD site has been determined to have a more negative reduction midpoint potential as compared to either of those of the ET-FAD site. Thus, the OX of Bf-FAD site is more likely to contribute to the absorbance and fluorescence spectra of points early in the titration. We

interpret the spectral contributions remaining after partial reduction for the early titration points to be those from the Bf-FAD site. In addition to spectral assignment supported by the relative midpoint potentials of the Bf-FAD site versus the ET-FAD site, the BF-FAD site is less solvent exposed than the ET-FAD and more likely to possess the features of blue shifted fluorescence with vibronic structure. Crystal structures of the bifurcating Etf homolog from *Acidaminococcus fermentans* reveal the ET-FAD to be solvent exposed and less likely to produce either effect on the emission spectra as compared to the Bf-FAD (34). Thus, we assign early portions of the reductive titration to reflect changes arising from the ET-FAD site.

Considering the potentiometric titration potentials as qualitative data, it is reasonable to assume that ASQ and OX concentrations are near equal around +133 mV before significant loss of OX occurs at +55 mV (i.e., maximum ASQ formation around +55 mV) (**Figures 5.5** and **5.6**). Subsequent steps in the reductive titration reveal a loss of ASQ signal indicative of HQ formation at potentials expected for the ASQ/HQ couple near -120 mV. Thus, these data indicate a midpoint potential of +133 ±10 mV for the more positive couple, $E_{OX/ASQ}$ ($E°' = E_m$ when [OX] = [ASQ]) assigned to the ET-FAD site. The following redox transition observed in the titration is assigned to the ASQ to HQ couple at potentials much lower than the OX to ASQ couple ($E_{ASQ/HQ}$ << +133 mV) but outside of the range of the ORP microelectrode spectroelectrochemical method.

Reductions Monitored by Redox Standards

To probe the reduction potentials beyond the limits of the ORP microelectrode, redox standard dyes were used in a manner typical for

flavoproteins (61). Briefly, redox standard were selected to match the reduction potentials under characterization as estimated by values reported for homologous systems (36,122). Reductions were performed in the presence of the 0.5 µM methyl viologen (mediator) with enzyme and the redox standard at equimolar concentrations.

Thionine (+64 mV) was selected as a redox standard to test the hypothesis that the ET-FAD ASQ/HQ couple is at a potential much greater than NADH (-320 mV) but less than that estimated for the ET-FAD OX/ASQ couple (+133 mV). Direct monitoring of *Pae* EtfAB's FAD OX signal (450 nm) was achieved without significant contribution from thionine (**Figure 5.7**), which was monitored at longer wavelengths (600 nm) beyond the range of flavin. Reduced spectra for the co-reduction reveal a small feature in the diagnostic region for ASQ near 400 nm. The diagnostic feature is most prominent at 17 µM dithionite (**Figure 5.8a**). To aid identification of the flavin redox state transitions, difference spectra were analyzed for diagnostic features (**Figure 5.8b**). A given spectra (i) was subtracted by the spectra for the following step in the titration (i+i) (i.e., the spectrum at 5 µM was subtracted by the spectrum at 7 µM). The resulting difference spectra produce relative positive signal for absorbance lost and relative negative signal for absorbance gained.

The flavin redox transitions were best captured by difference spectra for titration steps from 5 to 7, 10 to 12, and 24 to 26 µM dithionite. Reduction occurring between titration steps 5 µM and 7 µM dithionite appears to be dominated by the loss of OX absorbance (**Figure 5.8**, λmax= 454 nm). The loss of absorbance at the OX maxima of 454 nm occurs without the loss of absorbance near 400 nm, the OX local minima for reconstituted Pae EtfAB

(**Figures 5.3a** and **5.5a**) and the expected ASQ local maxima (**Figure 1.3**). We interpret this result to be the loss of OX and formation of ASQ.

Similar analysis for the titration step from 10 to 12 µM reveals a difference spectrum with notable features for the loss of ASQ absorbance (relative positive signal, λmax= 384 nm and λlocal max= 398 nm). We assign this portion of the titration to the ASQ to HQ transition.

For the titration step from 24 to 26 µM dithionite the loss of OX absorbance relative positive signal, λ_{max}= 454 nm) dominates the resulting difference spectra and there are no features of ASQ. We assign this portion of the titration to the OX to HQ transition.

Transitions to HQ produced difference spectra similar to the starting species (i.e.- an ASQ-like spectrum for ASQ to HQ and an OX-like spectrum for OX to HQ) as is to be expected given the lack diagnostic features and lack of local maxima for HQ (**Figure 1.3**). Further confirmation for redox state transition assignments is provided by the crossing points for the three difference spectra. These wavelengths are characteristic of flavin isosbestic points for the conversion of OX to SQ (358 and 490 nm) and SQ to HQ (330, 370, and 436 nm) (61,78). The first two transitions (OX to ASQ and ASQ to HQ) are assigned to ET-FAD, while the last transition (OX to HQ) is assigned to that of Bf-FAD. The portion of data for the ASQ to HQ transition was analyzed for the purpose of providing an estimate of the reduction potential (**Figure 5.9**). Despite having only three data points where both reconstituted *Pae* EtfAB and thionine were undergoing reduction during the ASQ to HQ transition, the estimate of -100 ±28 mV for a one-electron process is comparable to those reported for homologous EtfAB systems which either bifurcate (*Megasphaera elsdenii,* -136 mV (122)) or

possess features of bifurcating systems (*Rhodopseudomonas palustris*, -83 mV (36)). We assign the estimate of -100 ±28 mV to the ASQ/HQ couple for the ET-FAD site.

Phenosafranin (-252 mV, pH 7) was selected as a redox standard to test the hypothesis that the Bf-FAD OX/HQ couple is at a potential greater than NADH (-320 mV) but less than that measured for the ET-FAD OX/ASQ couple (+133 mV). Direct monitoring of reconstituted *Pae* EtfAB's FAD OX signal (450 nm) was not possible due to contribution from phenosafranin (**Figure 5.10**). The FAD OX signal was instead monitored at an isosbestic point of phenosafranin (408 nm) while phenosafranin was monitored at 520 nm (max) without contribution from bound FAD. Reduction by xanthine/xanthine oxidase did not produce features in the diagnostic region for ASQ over the course of reduction (80 min) (**Figure 5.11a**). Difference spectra were again employed to help confirm the flavin redox state transition under observation hypothesized to be OX to HQ for the Bf-FAD site (**Figure 5.11b**). The difference spectra were dominated by the loss of phenosafranin oxidized absorbance (relative positive signal λ_{max}= 520 nm) as well as loss of OX absorbance (relative positive signal λ_{max}= 454 nm). No SQ was observed of either kind (anionic or neutral). From these data, the individual contributions of each flavin site are not clear and complicate deconvolution of ET-FAD absorbance from Bf-FAD absorbance. Regardless, we assign the flavin transition under observation to a OX to HQ transition with the understanding that one or more flavin sites may be participating in the reduction when phenosafranin is present. Although long wavelength absorbance for flavin was not detected upon the addition of

phenosafranin, the redox standard dye may be binding to one or more of the flavin sites. However, the lack of a red shift in flavin absorbance may be an indicator that phenosafranin is not tightly bound. Follow up fluorescence titrations could help determine the binding affinity of phenosafranin for *Pae* EtAB by monitoring the quenching of flavin fluorescence. The lack of ASQ, in the reductive titration points to the possibility of phenosafranin interacting with or otherwise bound to the ET-FAD site. We propose that most of the reduction under observation is that of Bf-FAD and assign the flavin redox change to a OX to HQ transition. The reduction potential of the OX to HQ transition was found to be -224 ±34 mV (intercept= -0.48) and occur as a two electron process (slope= 1.09) (**Figure 5.12a**). Calculation was limited to portions of the data where co-reduction was observed at 30 to 50 min (**Figure 5.12b**).

We conclude that the ET-FAD is reduced by two one electron events ($E_{OX/ASQ}$= +133 ±10 mV; $E_{ASQ/HQ}$= -100 ±28 mV) and that the Bf-FAD is reduced in a single two electron event ($E_{OX/HQ}$= -224 ±34 mV). The standard deviation for $E_{OX/ASQ}$ results from the calibration of the ORP probe. For $E_{ASQ/HQ}$ and $E_{OX/HQ}$, the standard deviation is from the linear best fit shown in **Figure 5.9** and **5.12**. The measured reduction potentials are within the range of those reported for other Etfs (36,122).

5.4 Discussion

We have observed endpoints of reduction and estimates for midpoint potentials for *Pae* EtfAB that are similar to reported observations and hypotheses regarding bifurcation. Our results support the hypothesis that *Pae* EtfAB can serve as the bifurcating center of the *Pae* EtfABCX complex. Consistent with known bifurcating systems, *Pae* EtfAB possesses an FAD site that suppresses SQ and uses NADH electron pairs.

We assign the FAD site performing NADH oxidation and formation of the observed CT complex to the EtfA subunit (Bf-FAD) **(Figure 5.1** and **5.13)**. The formation of ASQ was assigned to the EtfB subunit (ET-FAD) **(Figure 5.1** and **5.13)**. These assignments are based on our results in light of *Pae* EtfAB's sequence homology with other Etfs (38) and the results from studies on those systems (32,36,122).

The measured reduction potential of -224 ±34 mV for the OX/HQ couple is significantly more positive than that of NADH (E°'= -320 mV) and indicates favorable electron transfer as reported for homologous systems in *Rhodopseudomonas palustris* ($E_{OX/HQ}$= -223 mV, (36)) and *Megasphaera elsdenii* ($E_{OX/HQ}$= -279 mV, (122)). In our measurement of the OX/HQ couple using the redox standard phenosafranin, no ASQ was observed. Thus, these data require additional experiments with other redox standards to help determine why the ET-FAD site failed to form ASQ in the presence of phenosafranin. However, the measured value of -224 ±34 mV is similar to those previously reported for the

OX/HQ couple of Bf-FAD and suggests this value can be used as an estimate for *Pae's* EtfAB.

For the observed one-electron transitions, the two measured reduction potentials of +133 ±10 mV and -100 ±28 mV fall within the range of the reported values for the ET-FAD site of *Megasphaera elsdenii* ($E_{OX/ASQ}$= +81 mV, $E_{ASQ/HQ}$= -136 mV (122)). Because SQ suppression is expected only for the Bf-FAD, we assign the observed one-electron transitions (i.e., OX to ASQ and ASQ to HQ) to the ET-FAD site. Thus, reduction potentials measured as a result of the observed flavin redox state transitions are also assigned to the ET-FAD site of *Pae* EtfAB ($E_{OX/ASQ}$= +133 ±10 mV, $E_{ASQ/HQ}$= -100 ±28 mV). A summary of these results is provided in **Figure 5.13.**

Among Etfs which bind two FADs per AB dimer ((*Acidaminococcus fermentans* (34), *Megasphaera elsdenii* (122), *Rhodopseudomonas palustris (36)*)), *Pae*'s EtfAB appears to be the only one which forms a stable and strong CT band (λ_{max}= 724 nm). While other studies may have failed to report on longer wavelength absorbance and/or report on the observation of weak absorbance signal, we propose that the observed strong CT band is unique to *Pae* EtfAB. *Pyrobaculum aerophilum* (*Pae*) is a hyperthermophile with an optimum growth temperature of 80 °C. To our knowledge, this is the first study of an Etf from a hyperthermophile. The strong CT signal may be the result of the enhanced stability known for proteins from hyperthermophilic organisms. The intense nature of the CT band may be an indication of tight NAD^+ binding (lower K_d).

5.5 Conclusion

Using a series of reductive titrations to probe bounds for the reduction midpoint potentials of the two flavins, we argue that the heterodimer alone could participate in a bifurcation mechanism. Further experimentation is needed to ensure the midpoint potentials estimated herein can be duplicated using material from different preparations. Such experiments should also include the testing of a greater number of redox standard dyes. While low protein availability remains a limiting factor, reuse of material subjected to the flavin reconstitution conditions we developed may allow for a greater number of experiments and replicates.

Table 5.1: Flavin occupancy.

ID	UG#	Condition	Occupancy (FAD per dimer)	Average
jph-5-53	102	Reconstituted	1.79	
jph-5-79	116	Reconstituted	2.34	
jph-5-81	061	Reconstituted	2.23	2.12 ± 0.17 [a]
jph-5-81	102	As isolated	1.36	
jph-5-81	116	As isolated	0.95	
jph-5-81	138	As isolated	0.56	0.96 ± 0.23 [a]

[a] Standard error (n= 3, multiple preparations)

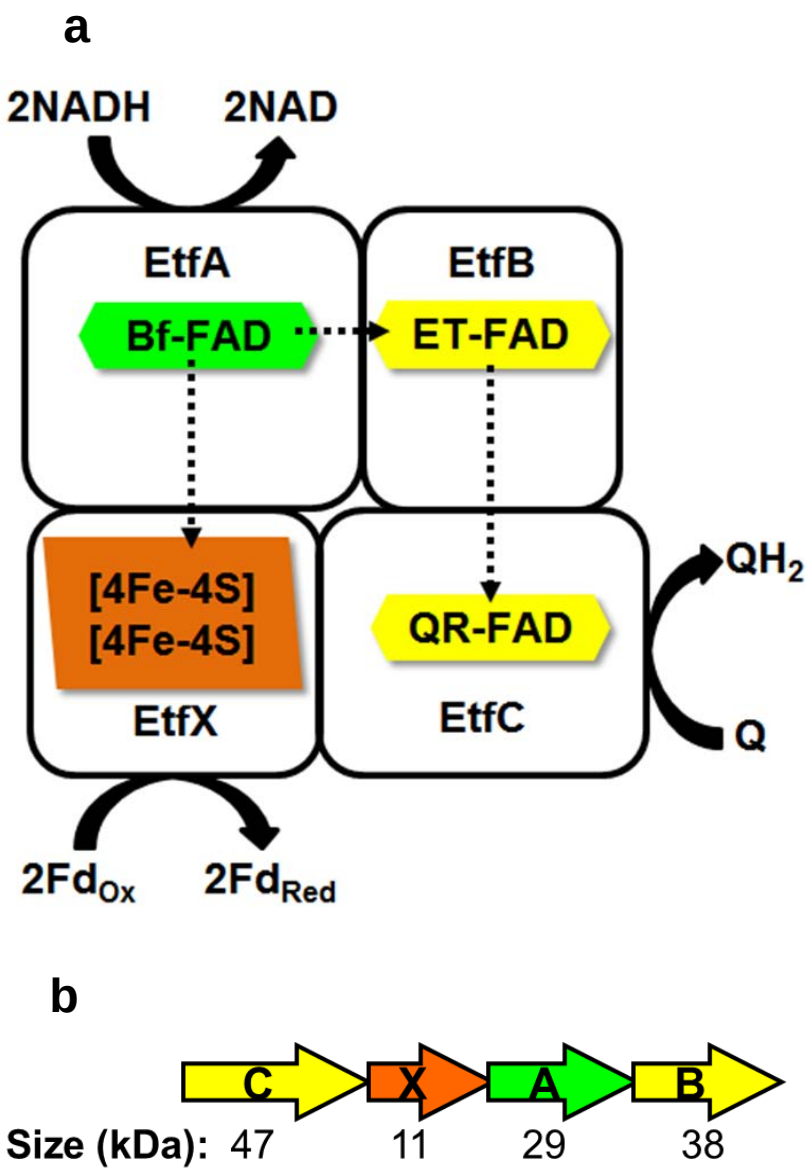

Figure 5.1: Electron flow in the proposed pathway for *Pae* EtfABCX (Credit: The figure has been modified from that of Gerrit J. Schut, Ph.D.) (**a**). Dashed arrows denote the direction of one electron flow between subunits. The gene order and protein sizes are shown for each of the Etf subunits (**b**).

Abbreviations: Bf--FAD, bifurcating flavin; ET--FAD, electron transfer flavin; QR--FAD, quinone reductase flavin; Q, quinone; QH2, reduced quinone; Fd_{ox}, oxidized ferredoxin; Fd_{red}, reduced ferredoxin.

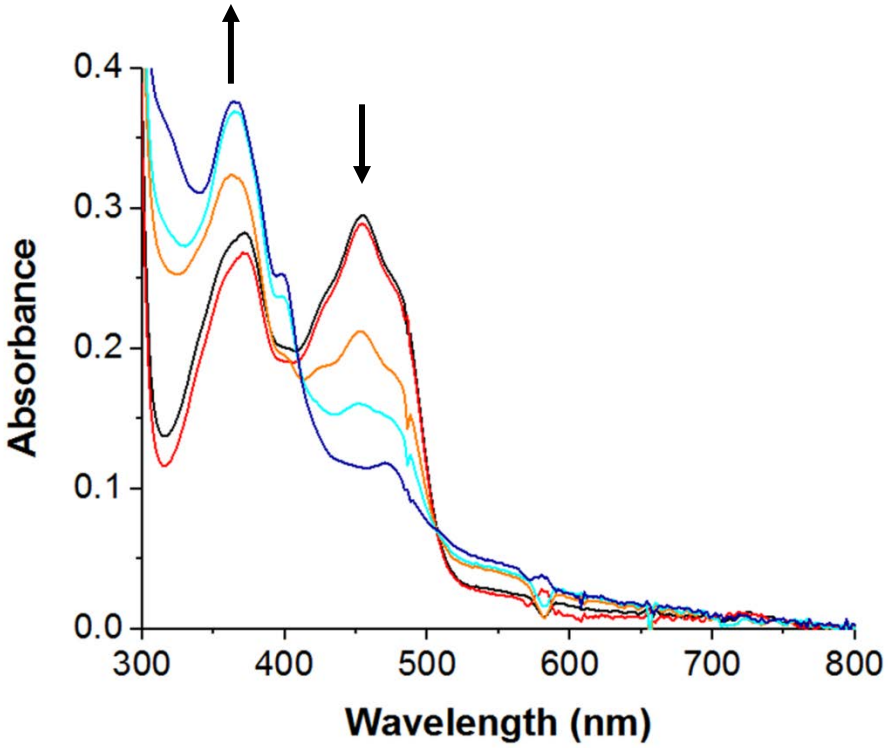

Figure 5.2: Reduction of 13 µM as isolated *Pae* EtfAB (jph-5-59; UG-116) with the one electron reductant dithionite. Arrows denote the signal change during the course of reduction (0, 2.5, 15, 17, 22 µM dithionite). The titration was conducted in 25 mM Bis-tris propane, 200 mM NaCl, pH 7 at 20-23 °C.

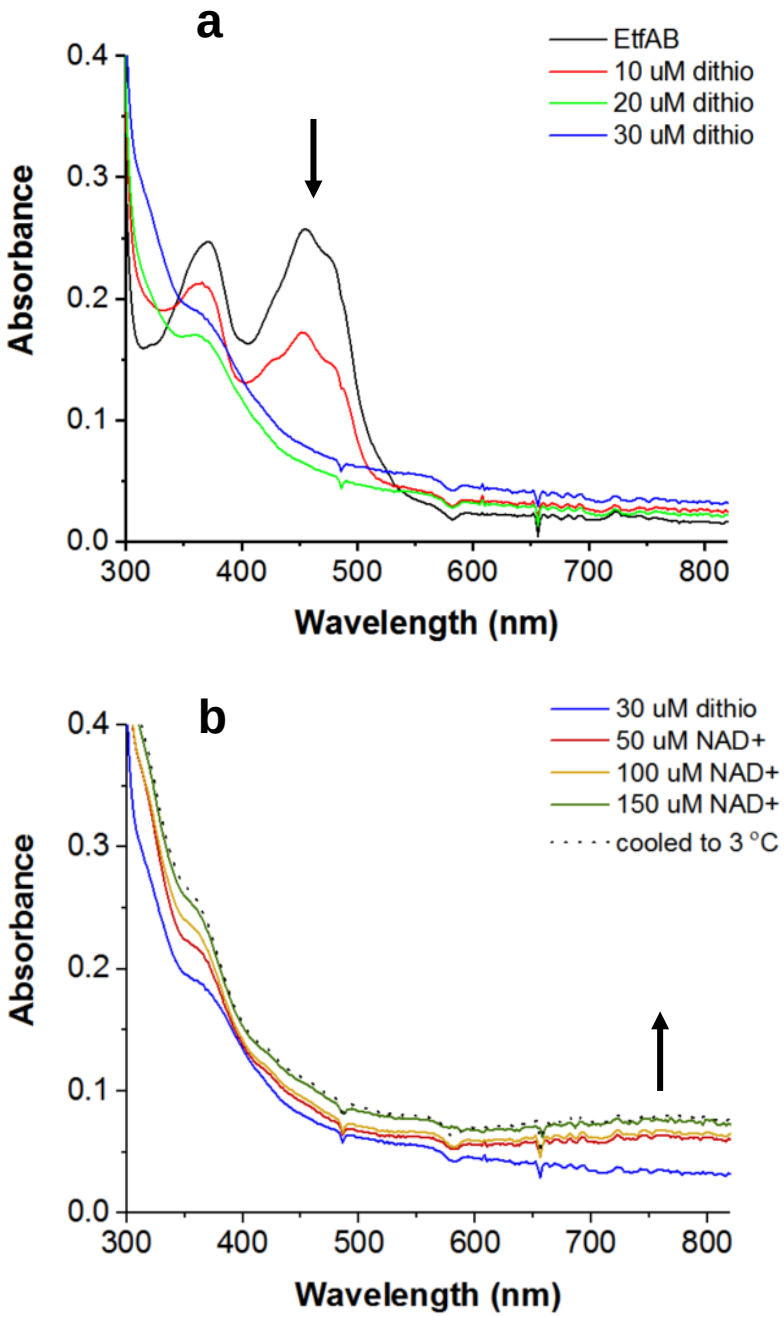

Figure 5.3: Dithionite reduction of 11 µM reconstituted *Pae* EtfAB (jph-5-78; UG-116) (**a**) followed by NAD^+ addition and then cooling to 3 °C for 1.5 hours (**b**). The titration was conducted in 25 mM Bis-tris propane, 200 mM NaCl, pH 7 at 20-23 °C.

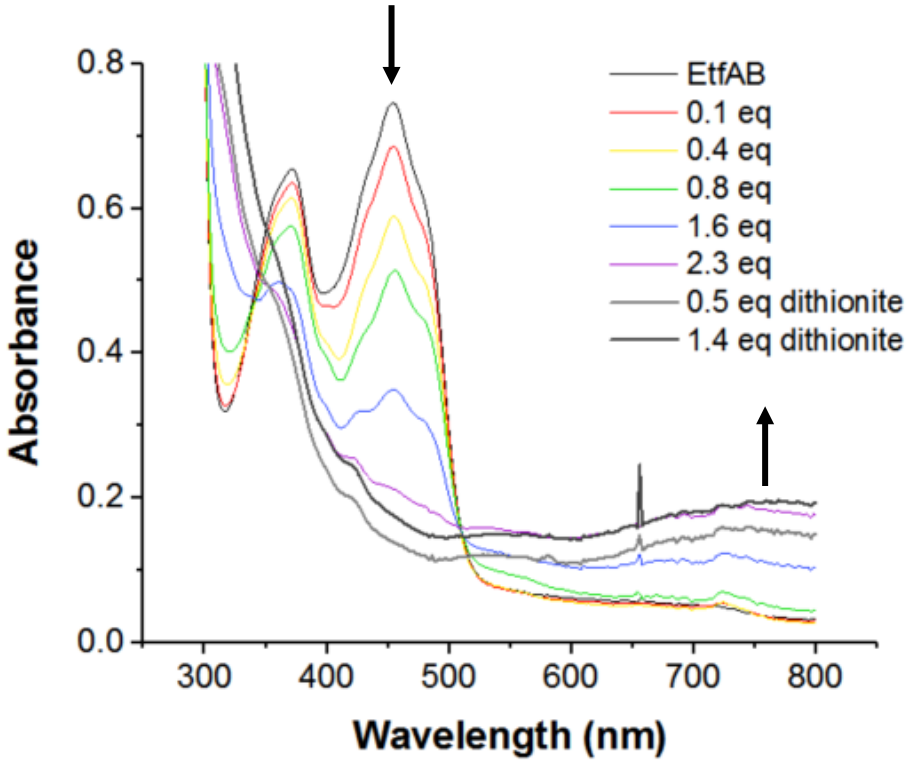

Figure 5.4: Reduction of 30 µM 'as isolated Pae EtfAB' (jph-5-60; UG-116) with the two electron reductant NADH. Following NADH addition (0.1 to 2.3 equivalents of NADH on an EtfAB basis), dithionite was added to ensure a low potential and, hence, a fully reducing environment was established. Arrows denote the direction of signal change during the course of the reaction. The titration was conducted in 25 mM Bis-tris propane, 200 mM NaCl, pH 7 at 20-23 °C.

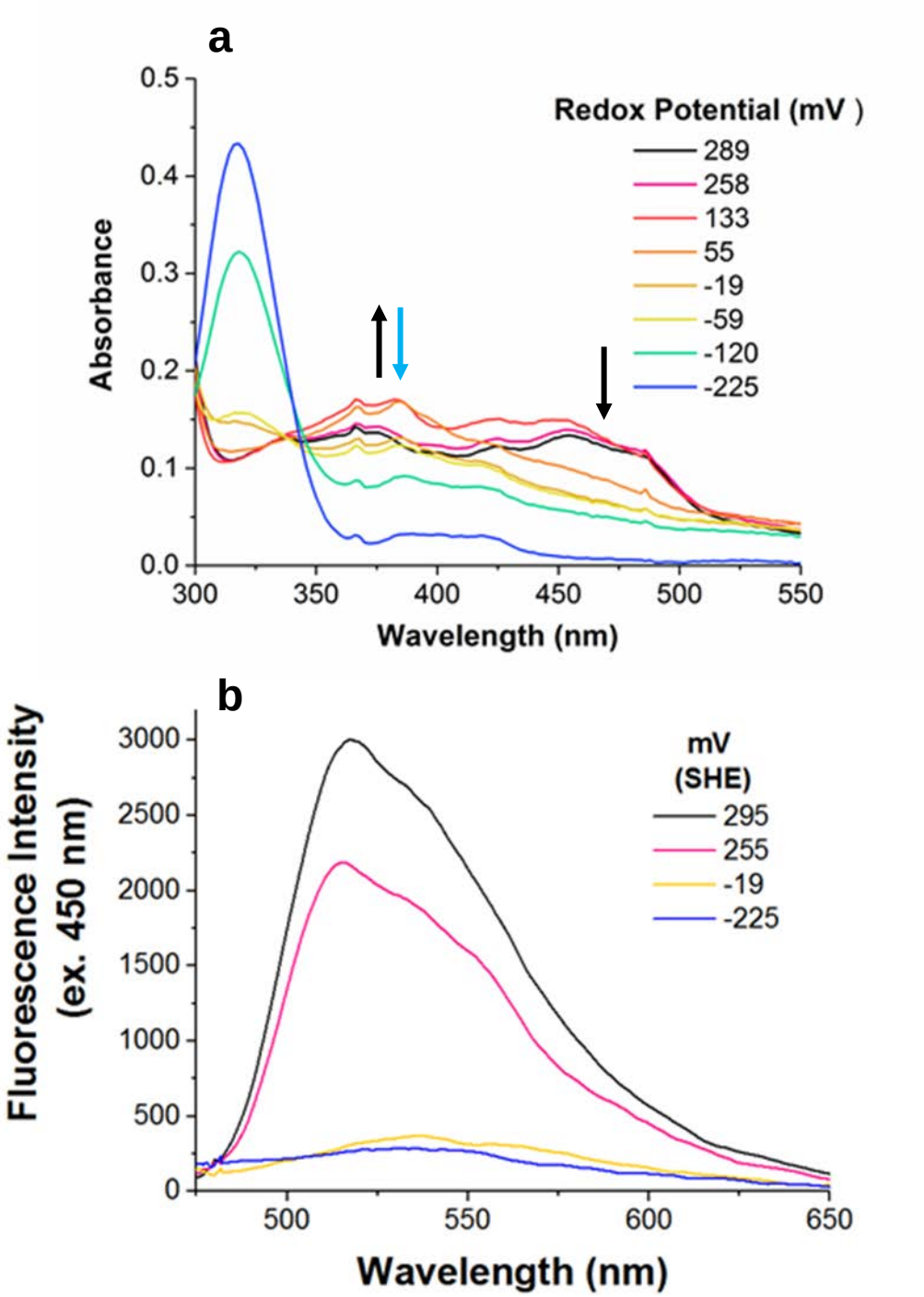

Figure 5.5: Potentiometric dithionite titration of reconstituted 6.5 µM *Pae* EtfAB (jph-5-37; UG-102) monitored by a combination Pt and $Ag/AgCl_2$ oxidation reduction potential (ORP) microelectrode using absorbance (**a**) and fluorescence (**b**) using the same sample. The arrows denote the direction of signal change during the reduction with the blue arrow indicating the direction for later steps in

the titration. The titration was conducted in 25 mM Bis-tris propane, 200 mM NaCl, 0.5 µM methyl viologen, pH 7 at 20-23 °C.

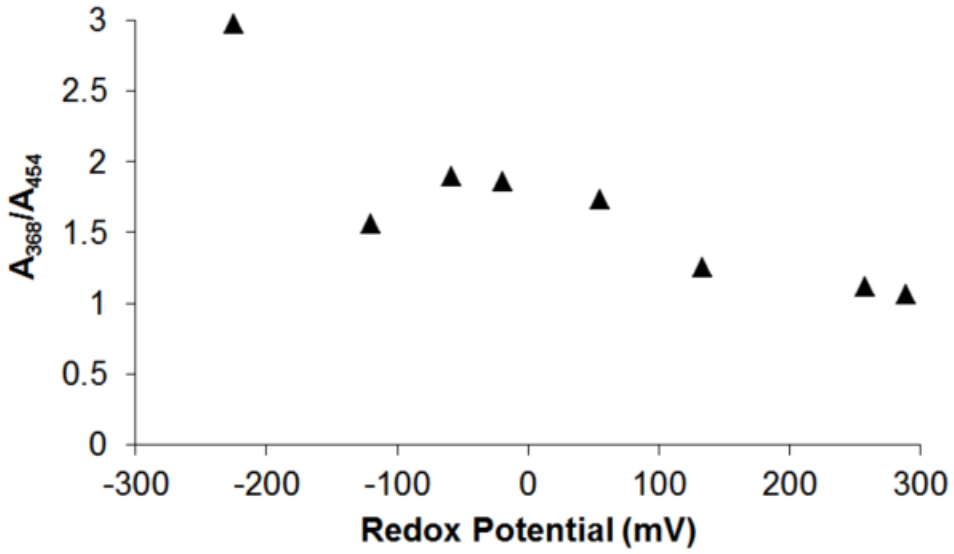

Figure 5.6: Plot of absorbance at 368 nm divided by absorbance at 454 nm (A_{368}/A_{454}) for the potentiometric dithionite titration of reconstituted 6.5 µM *Pae* EtfAB (jph-5-37; UG-102) monitored by a combination Pt and Ag/$AgCl_2$ oxidation reduction potential (ORP) probe. Data shown in **Figure 5.5** was used for plotting. The titration was conducted in 25 mM Bis-tris propane, 200 mM NaCl, 0.5 µM methyl viologen, pH 7 at 20-23 °C.

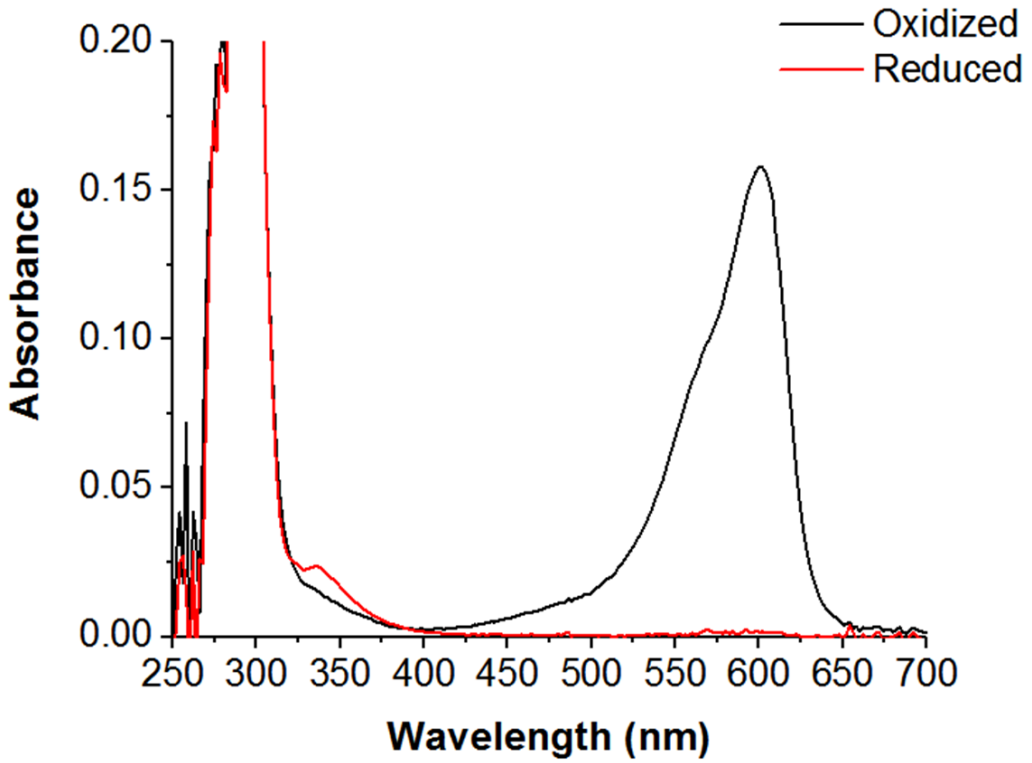

Figure 5.7: Thionine in the oxidized and reduced states. The titration was conducted in 25 mM Bis-tris propane, 200 mM NaCl, 0.5 µM methyl viologen, pH 7 at 20-23 °C.

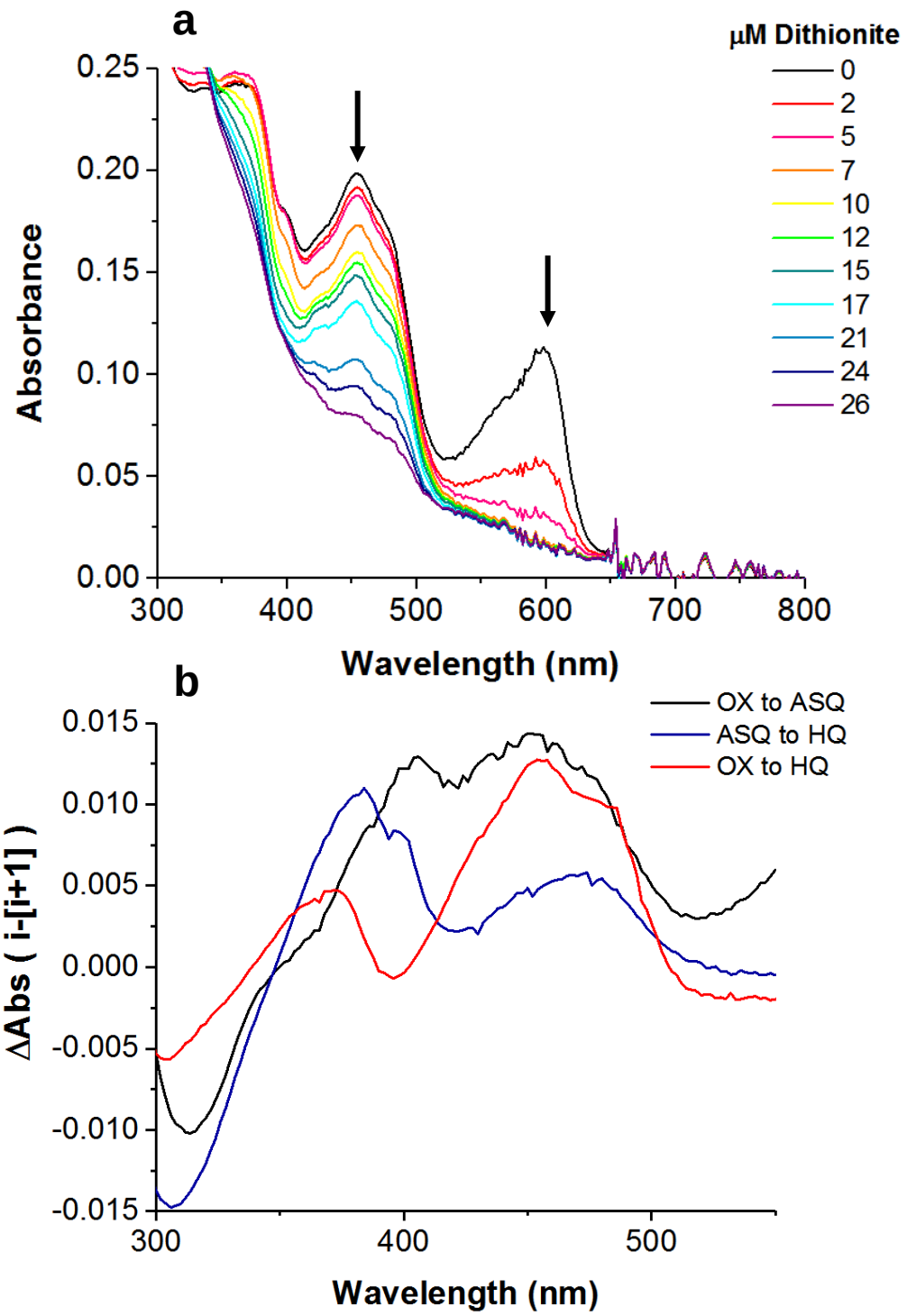

Figure 5.8: Potentiometric dithionite titration of 6.5 μM reconstituted *Pae* EtfAB (jph-5-44; UG-102) in the presence of near equimolar thionine (**a**). Arrows denote the direction of signal change during the titration. For titration steps 7, 12 and 26 μM, difference spectra (**b**) were produced by subtraction from the spectra of the preceding titration steps 5, 10, and 24 μM (i.e., spectra 5 μM minus spectra 7μM). The difference spectra more clearly illustrate the flavin redox transitions (oxidized, OX; anionic semiquinone, ASQ; hydroquinone (HQ). The

titration was conducted in 25 mM Bis-tris propane, 200 mM NaCl, 0.5 µM methyl viologen, pH 7 at 20-23 °C.

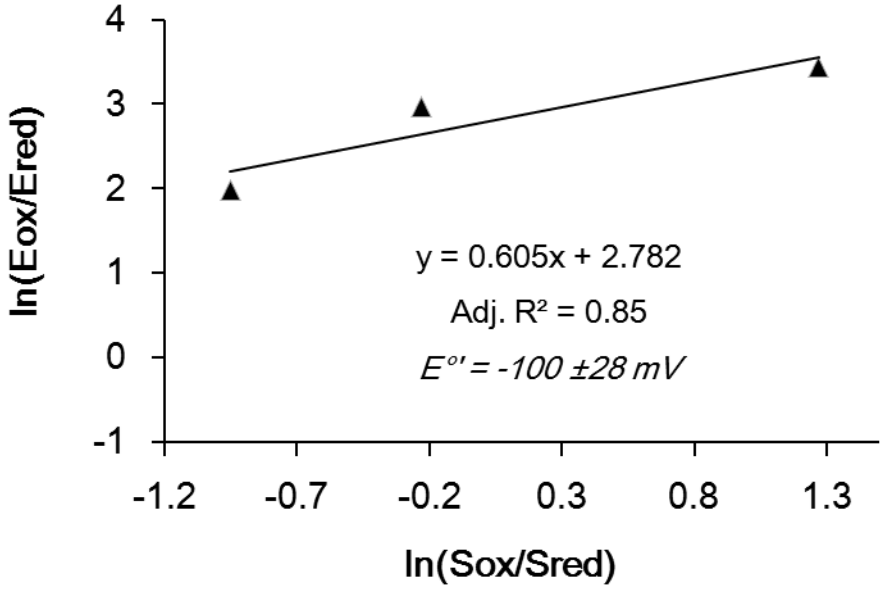

Figure 5.9: Plot of the linear best fit of $\ln(E_{ox}/E_{red})$ versus $\ln(S_{ox}/_{red})$ used in the calculation of *E°'* ($E_{ASQ/HQ}$) for reconstituted *Pae* EtfAB (jph-5-44; UG-102) in the presence of equimolar thionine. Data shown in **Figure 5.8a** for 2, 5, and 7 µM dithionite was used for plotting and analysis. The slope of the linear best fit is 0.6, indicating that one electron is involved in the reduction. The titration was conducted in 25 mM Bis-tris propane, 200 mM NaCl, 0.5 µM methyl viologen, pH 7 at 20-23 °C.

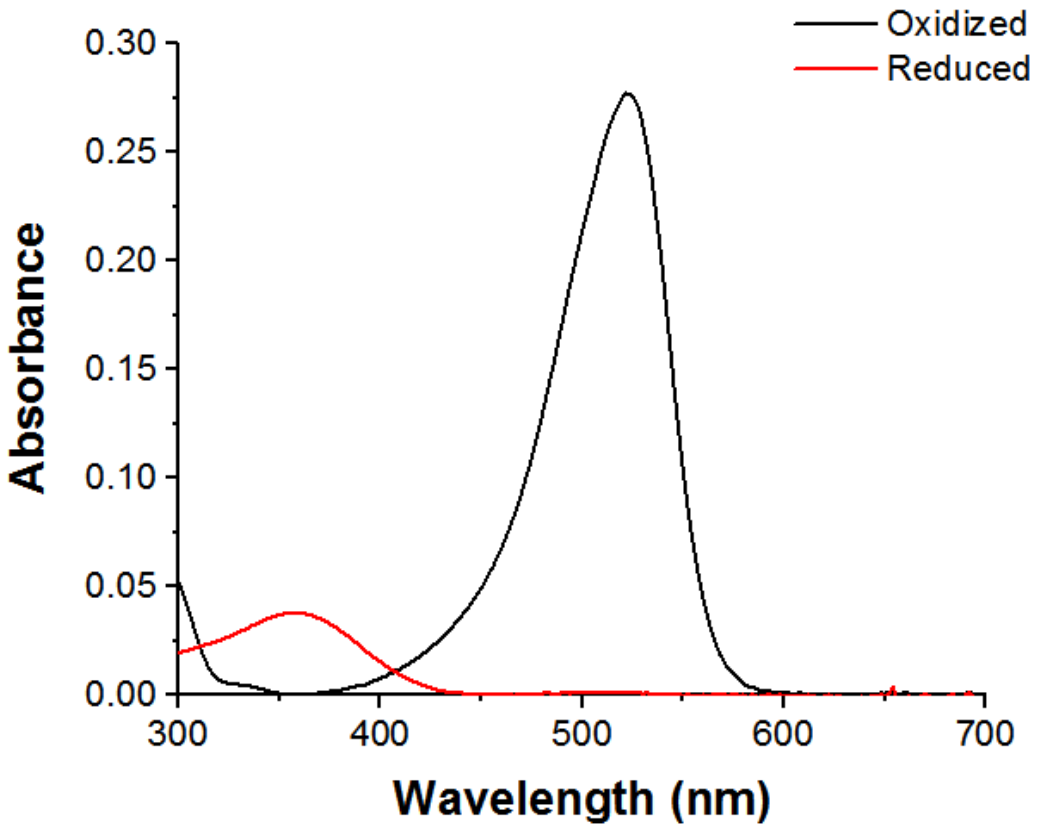

Figure 5.10: Phenosafranin in the oxidized and reduced states. The titration was conducted in 25 mM Bis-tris propane, 200 mM NaCl, 0.5 µM methyl viologen, pH 7 at 20-23 °C.

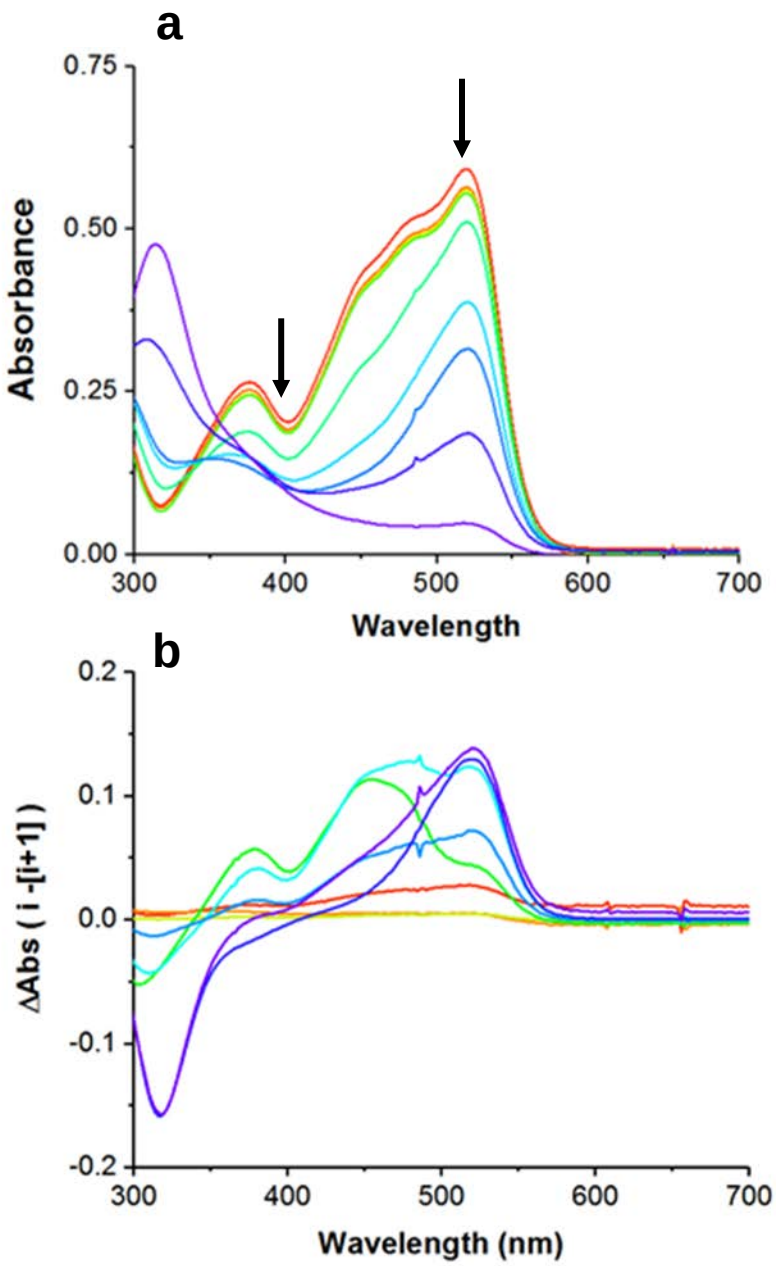

Figure 5.11: Potentiometric reductive titration for reconstituted *Pae* EtfAB (jph-5-59; UG-102) (**a**) and the resulting difference spectra (**b**) in the presence of equimolar phenosafranin by a xanthine/xanthine oxidase reducing system. Difference spectra were calculated by subtracting successive spectra from each other (e.g., the spectrum at 5 min was subtracted by the proceeding spectrum at 10 min). Arrows denote the direction of signal change during the titration and the wavelengths used for analysis (bound flavin was monitored at 408 nm, the isosbestic point of phenosafranin, and phensafranin was monitored at 520 nm). The titration was conducted in 25 mM Bis-tris propane, 200 mM NaCl, 0.5 µM methyl viologen, pH 7 at 20-23 °C. The xanthine/xanthine oxidase reducing

system was initiated by the addition of ~3 ng of xanthine oxidase to 500 µL of a protein solution containing 400 µM xanthine and monitored for at least 75 min.

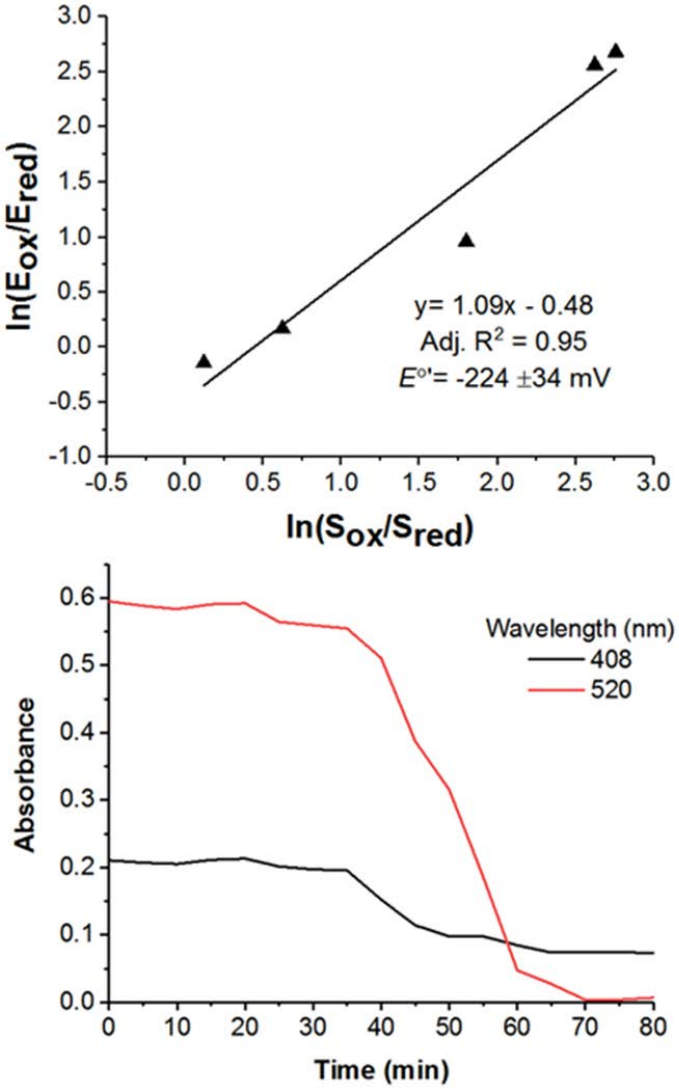

Figure 5.12: Plot of the linear best fit of $\ln(E_{ox}/E_{red})$ versus $\ln(S_{ox}/_{red})$ used in the calculation of *E°'* ($E_{OX/HQ}$) for reconstituted *Pae* EtfAB (jph-5-59; UG-102) in the presence of near equimolar phenosafranin (a). Analysis was limited to the portion of data where the enzyme (E) and redox standard dye (S) were both partially reduced (30 to 50 min) as evidenced by the loss of absorbance at 408 nm (phenosafranin isosbestic point) and 520 nm (oxidized phenosafranin) (b). Data shown in **Figure 5.11** was used for plotting and analysis. The slope of the plot is 1.09, indicating that two electrons are involved in the reduction.

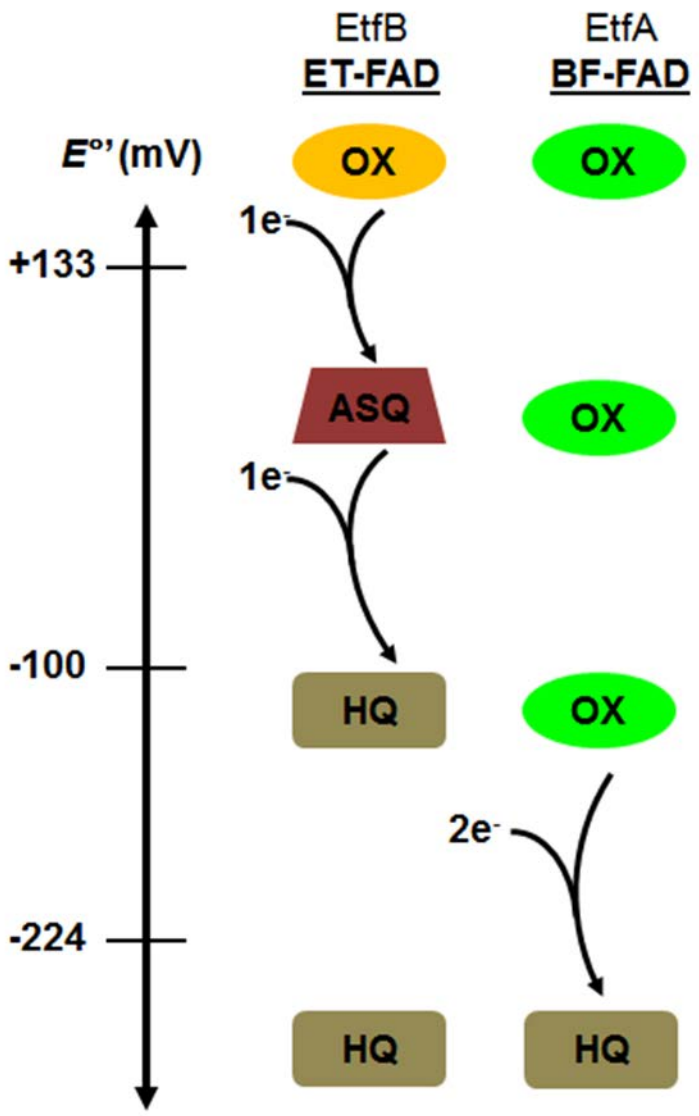

Figure 5.13: Graphical depiction of the redox transitions observed and their assignment to each flavin site. The measured values for the reduction midpoint potentials are provided for each of the three flavin redox transitions observed: $E_{OX/ASQ}$= +133 ±10 mV; $E_{ASQ/HQ}$= -100 ±28 mV; $E_{OX/HQ}$= -224 ±34 mV. The standard deviation for $E_{OX/ASQ}$ results from the calibration of the oxidation reduction probe. For $E_{ASQ/HQ}$ and $E_{OX/HQ}$, the standard deviation is from the linear best fit shown in **Figure 5.9** and **5.12** .
Abbreviations: Bf-FAD, bifurcating flavin; ET-FAD, electron transfer flavin; OX, oxidized; ASQ, anionic semiquinone; HQ, hydroquinone.

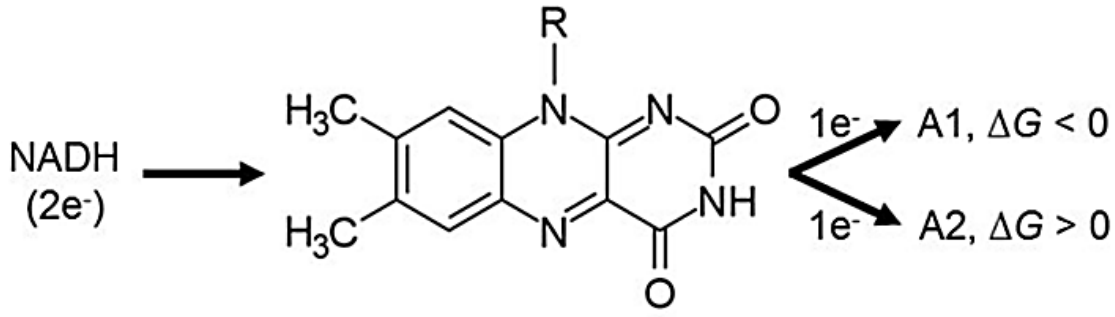

Scheme 5.1: Flavin-based electron bifurcation (FBEB) scheme showing the splitting of a pair of electrons from NADH. The intermediate reduction midpoint potential of NADH results in the exergonic reduction ($\Delta G < 0$) of an acceptor at a higher reduction midpoint potential (A1) which in turn drives the endergonic reduction ($\Delta G > 0$) of an acceptor at a lower reduction midpoint potential (A2).

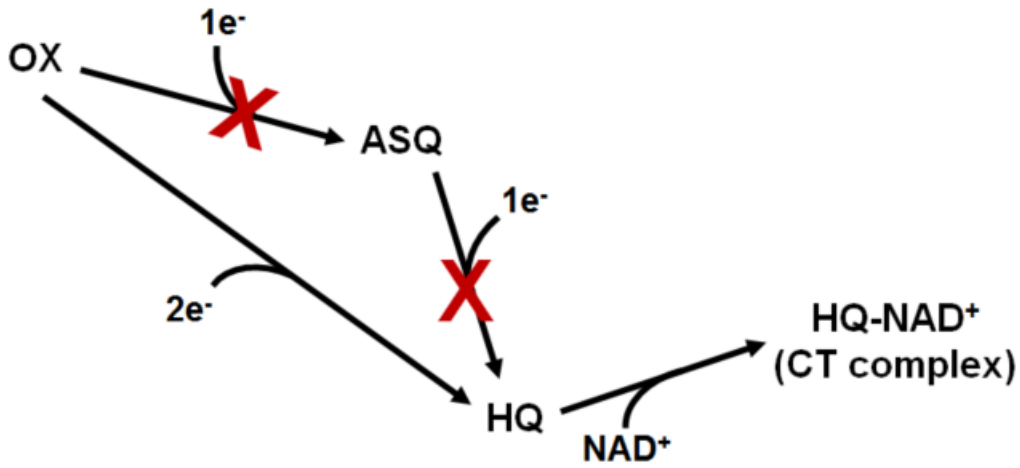

Scheme 5.2: Formation of the charge transfer (CT) complex proposed between the bifurcating flavin (Bf-FAD) hydroquinone (HQ) and the oxidized form of nicotinamide adenine dinucleotide (NAD^+) for fully occupied reconstituted *Pae* EtfAB first reduced with dithionite. One-electron reduction steps (noted by a *red "X"*) are proposed to be unfavorable due to semiquinone (SQ) suppression by Bf-FAD. Two-electron reduction of Bf-FAD to form HQ results from equilibration with excess dithionite and the redox mediator methyl viologen. (oxidized, OX; anionic semiquinone, ASQ).

CHAPTER 6 SUMMARY AND OUTLOOK

Our work provides specific insight into the redox properties governing semiquinone (SQ) suppression and the ability to bifurcate electrons. Unlike other studies on biological electron bifurcation, we employed both nonbifurcating and bifurcating protein systems to help inform what flavin redox properties are likely prerequisite for bifurcation.

NADOX

In addition to using NADH oxidase (NADOX) from *Thermus thermophilus* to ask fundamental questions surrounding reduction midpoint potential tuning, continued effort is motivated by applications in the biosynthesis of aromatic amines. The NADOX results presented herein support previous findings that NADOX could serve as a more robust nitroreductase (NR) homolog with a higher degree of tolerance to mutation (68), pH (50), temperature (52), and high concentrations of chaotropic agents (123). A large amount of research on NR has shown promise in exploiting the large substrate repertoire of NR for the near full conversion of nitroaromatics to aromatic amines for use in the production of active pharmaceutical ingredients (16,19,25,47,124,125). Of all drugs marketed in 2009, 13% were aromatic amines (126). Biosynthesis with NR and, possibly, NADOX has potential advantages over more common inorganic catalysts (127) which must be fully removed to achieve the high purity standards for pharmaceutical application (128).

Successful application of NR and its homologs in biodegradation, biosynthesis, and prodrug therapy would be limited by flavin reductase activity arising from a flavin shuttle mechanism. Such catalysis by NADOX would produce reduced free flavin which could participate in undesired side reactions

resulting in toxic products (e.g., H_2O_2) at the cost of starting materials. However, if NADOX proves to perform much of the same chemistry as NR and shares NR's large substrate repertoire, the thermophilic NR homolog could prove useful as a more robust NR. Of the possible NR/NADOX applications, biosynthesis of aromatic amines is particularly promising for the production of active pharmaceutical ingredients. Within a multistep synthesis scheme employing traditional synthetic methods as well as enzymes, the large substrate repertoire of NR and likely NADOX can be exploited for the biosynthesis of aromatic amines. NADOX does not suffer the same protein precipitation problems as NR and can be exposed to a variety of conditions while maintaining catalytic activity. In the case of NADOX, catalysis can be turned on and off (i.e., switchable) depending on pH (50), temperature (52), and buffer reagents (123). Further work on NADOX mutants and/or solvent conditions could lead to a system that can be switched on or off depending on solvent conditions without protein precipitation or loss of activity.

To our knowledge, there is only one other report of nitroreductase activity by NADOX and the mechanism of secondary substrate reduction remains unclear (57). In the previous report and in our work, the assays monitored the rate of NADH oxidation which increased when secondary nitroaromatics were present. Follow up studies are needed to confirm nitroreductase activity by direct detection of nitroso, hydroxylamine, and/or amine products resulting from nitroaromatic starting materials.

Further clarification of the role excess FMN plays would substantiate the results for NADOX presented herein. We propose future work should include experiments to test the hypothesis of NADOX acting as a flavin reductase by

testing the effect of oxygen concentration and of FMN competition with secondary substrates. In the case of NADOX activity resulting from an FMN shuttle mechanism, product concentrations would be expected to steadily increase following a lag period during which reduced FMN contractions reach a maximum. Reduction of a second FMN under a flavin shuttle mechanistic regime would be followed by product dissociation. Conversely, true nitroreductase activity as defined by the ping-pong kinetic mechanism established for *Enterobacter cloacae*'s NR (23) would produce a smaller magnitude for the rate of reduction of nitroaromatics when FMN concentrations are increased (i.e., secondary substrate competition).

While NR and NADOX do not appear to have the reducing power to drive the reduction of aromatic nitro groups to amines (25), further research effort to increase the substrate binding of aromatic hydroxylamines and to lower the reduction potential of the oxidized-hydroquinone couple ($E_{OX/HQ}$) could allow for such catalysis. Several NADOX mutants were prepared but have yet to be characterized. Our initial approach was to test the hypothesis that proline 156 participates in the observed destabilization of SQ by sterically straining bound flavin and contributing to the observed butterfly bend observed in the crystal structure (63). Mutation to glycine (P156G) produced transient absorbance spectroscopy (TAS) kinetics that were on average two times faster than the wild type. Adding larger amino acids back to the proline site would be expected to provide kinetics proportional to amino acid size. Mutation to alanine and valine should be part of future NADOX work. The conserved proline 156 residue within 3.5 Å of C9 is believed to be involved in conformational control of the flavin (63). Glycine should provide maximum backbone flexibility while minimizing volume to,

in turn, relieve strain applied to the flavin by the protein. Alanine and valine provide less flexibility but may lend themselves to detecting a trend as a function of residue volume (glycine > alanine > valine ≈ proline). By controlling planarity in a non-covalently bound flavin-enzyme system, we hope to empirically verify calculations regarding redox tuning and SQ suppression for the first time (129-131). We hypothesize that such mutations will increase the $E_{OX/SQ}$ and/or decrease the $E_{SQ/HQ}$ and, in turn, stabilize SQ.

Electron transfer kinetics observed in TAS and the underlying thermodynamic control of redox cofactors is not clearly understood. The proposed mutants would be ideal to study the relationship between SQ formed under photoexcitation in TAS and reduction midpoint potentials.

PaeEtfAB

Early success in characterizing *Pae*EtfAB reduction midpoint potentials was prevented by protein precipitation upon reduction and batch-to-batch variability we attribute to as isolated flavin occupancy which ranged from 0.56 to 2.34 FAD per dimer (**Table 5.1**). Later success was achieved by optimization of buffer conditions and flavin reconstitution that produced 2.12±0.17 (n= 3) FAD per dimer reproducibly. All studies were conducted with ≤20 mg *Pae*EtfAB.

Possible Dual Bifurcation and Canonical Etf Function by a Single Protein in Response to Environmental Conditions In Vivo

Failure to isolate material directly from cell lysate with full occupancy (i.e., 2 FAD per heterodimer) suggests the flavin microenvironment and flavin binding is sensitive to growth and/or purification conditions. While reconstitution conditions were developed to obtain fully occupied material in vitro, questions remain regarding the properties and possible physiological relevance of the as isolated

preparation with only 1 FAD per heterodimer. Under certain growth conditions (e.g. more oxidizing solution potentials, ≥E_m of ET-FAD OX/SQ couple) AMP binding may be promoted over FAD binding at the Bf-FAD site, essentially switching off the capacity to bifurcate. Dual function from a single Etf in response to environmental cues such as solution reduction potential may be of special importance given that *Pae* is a facultative microaerobe and a member of a genus dominated by strict anaerobes (132). In addition to growth under anaerobic and aerobic conditions, *Pae* can utilize both inorganic and organic substrates using a large number of terminal electron acceptors (O_2, NO^{3-}, NO^{2-}, As(V), Se(VI), Se(IV), $S_2O_3^{2-}$, Fe(III)-citrate, and FeOOH) (133-139). *Pae* appears to the most metabolically versatile member of *Pyrobaculum* which is a genus known for its high degree of respiratory versatility (133). Such versatility may be due in part to the complex nature of *Pae's* Etf and other redox systems capable of supporting bioenergetic pathways that exploit electron bifurcation.

Role of Charge-Transfer Complex

To our knowledge, we are the first to report on the observation of a NAD^+-FAD charge-transfer (CT) complex in a system with the capacity to bifurcate. While a mechanistic role for a CT complex in bifurcation has not been previously suggested, we propose that flavin electron delocalization at the proposed site of bifurcation (Bf-FAD) could play a role in yet to be discovered alternative mechanisms specific to hyperthermophilic archaea whereby HQ formation is stabilized by bound NAD^+ and serves as a driving force for FAD reduction. While the results reported herein fail to establish a K_d for NAD^+ binding at Bf-FAD, half-saturation appears to occur at NAD^+ concentrations near the physiological range (140). In further support of possible physiological relevance, the CT complex is stable and formation occurs on time scales relevant for catalysis unlike the well-studied nicotinamide CT complexes formed in lipoyl dehydrogenase (119).

Future Work

We explored and confirmed mechanistic details that may give rise to flavin-based electron bifurcation and elucidated requirements for electron bifurcation to occur. However, additional studies are needed to better understand mechanisms of electron transfer and the role of specific amino acids within the flavin environment at the level of individual electrons. To better understand the TAS results and to obtain species associated difference spectra, global and target analysis was initiated using the open source R package TIMP and the related Java-based tool Glotaran (141,142). However, the effort remains incomplete. We were able to find a statistically significant global fit for NR (**Figure 6.1**). Two of the components (decay associated spectra 1 and 3) for the parallel model had significant anionic SQ character at the expected lifetimes for a nitroreductase flavin site (**see Chapter 4**). The parallel model describes a multi-component system where each component decays independently (143). While global analysis did not produce a statistically significant model for the other proteins subjected to TAS, continued analysis effort may prove useful. Such effort may lead to the ability to obtain species associated spectra which can best inform on the nature and mechanism of electron transfer.

Inclusion of a bifurcating and nonbifurcating Etf in the TAS studies followed by global analysis would make a significant contribution to understanding the role of flavin in bifurcation. Such experimentation could help establish the role of flavin kinetics in bifurcation. Transient absorbance spectroscopy is well suited to answer questions which remain on the topic of SQ suppression. One such question is whether or not there is a specific lifetime of transiently formed SQ which differentiates a bifurcating Etf from a nonbifurcating Etf. In the case of bifurcating Etfs, the rates of SQ decay as a function of ferredoxin and/or flavodoxin (the physiologically relevant electron acceptors) would provide mechanistic insight. We hypothesize that the presence of such electron acceptors would increase the rate of SQ decay observed by TAS.

Due to limitations of time and *Pae* EtfAB availability, a number of experiments were not performed. To fully characterize the as isolated material and the effects of flavin reconstitution additional work is needed. One priority of such work should be in the assignment of flavin spectral features to either the ET-FAD or the Bf-FAD site. Circular dichroism methods have been developed for the EtfAB from *Rhodopseudomonas palustris* which allowed the authors to deconvolute the spectra from each of the flavin sites and ultimately assign spectral features to either the ET-FAD or the Bf-FAD site (36). Similar effort on *Pae* EtfAB would help substantiate some of the assignments made in the work presented herein.

Significance

The studies described herein represent a substantial step forward in our understanding of flavin-based electron bifurcation, the newly discovered third form of biological energy-conservation. Only two other labs have reported on the reduction midpoint potentials for bifurcating flavoenzymes, ours and the Shiga group (Kumamoto University). Those reports provided thermodynamic insight on NADH-dependent ferredoxin-NADP+ oxidoreductase I (Nfn) from *Pyrococcus furiosus* (39), EtfAB from *Rhodopseudomonas palustris* (36), and EtfAB from *Megasphaera elsdenii* (122). The findings presented here provide estimates for reduction midpoint potentials of a fourth system (i.e., *Pae*EtfAB), in which we propose also has the capacity to perform electron bifurcation.

Previous work on biological electron bifurcation has established the importance of the mechanism in the anaerobic metabolism of microbes (30-32,74). Bifurcation is likely ancient within biological systems and possibly pre-dates the Great Oxidation Event; this also suggests its importance in anaerobic metabolism (74,102,144). However, more recent findings on the ETF from the soil aerobe *Azotobacter vinelandii* (37) and on the ETFs from the metabolically versatile microbes *Rhodopseudomonas palustris* (36) and *Pae* (this study) challenge the notion that flavin-based bifurcation is only relevant in anaerobic

environments. Biological electron bifurcation, mediated by flavin active sites, may be more widespread among microbes and occur throughout the gradient of oxygen concentrations which are found in terrestrial and aquatic habitats.

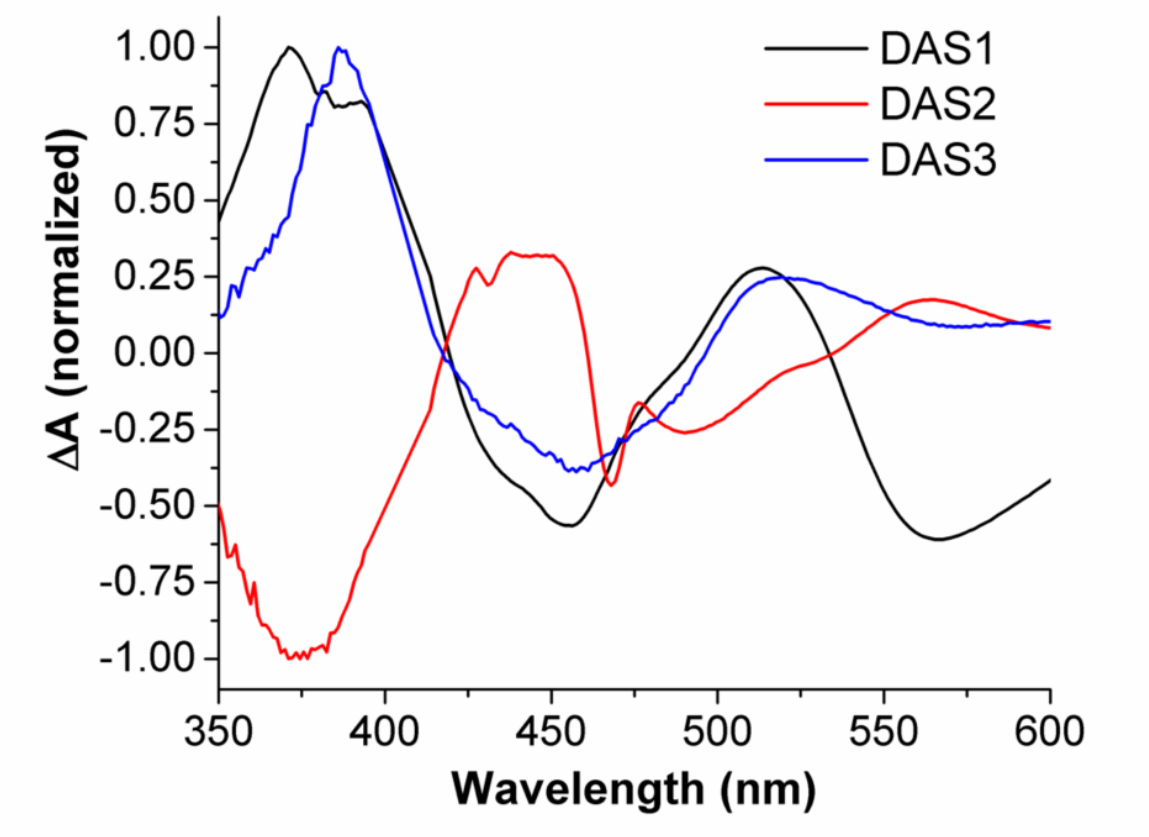

Figure 6.1: Transient absorbance spectroscopy results from global analysis using a parallel three component model of 250 μM nitroreductase at room temperature. The decay associated spectra (DAS) have lifetimes of 403 ps (DAS1), 0.8 ps (DAS2), and 2852 ps (DAS3).

REFERENCES

1. Hefti, M. H., Vervoort, J., and van Berkel, W. J. H. (2003) Deflavination and reconstitution of flavoproteins - Tackling fold and function. *Eur. J. Biochem.* **270**, 4227-4242
2. Senda, T., Senda, M., Kimura, S., and Ishida, T. (2009) Redox Control of Protein Conformation in Flavoproteins. *Antioxid. Redox Signal.* **11**, 1741-1766
3. Krebs, H. A. (1935) Metabolism of Amino Acids: Deamination of Amino Acids. *Biochemical Journal* **29**, 1620-1625
4. Warburg, O., and Christian, W. (1933) Yellow enzyme and its effects. *Biochem. Z.* **266**, 377-411
5. Aliverti, A., Curti, B., and Vanoni, M. A. (1999) Identifying and Quantitating FAD and FMN in Simple and in Iron-Sulfur-Containing Flavoproteins. in *Flavoprotein Protocols* (Chapman, S. K., and Reid, G. A. eds.), Humana Press, Totowa, NJ. pp 9-23
6. Sobrado, P., and Gadda, G. (2017) Introduction to flavoproteins: Beyond the classical paradigms. *Arch. Biochem. Biophys.* **632**, 1-3
7. Chaiyen, P., Fraaije, M. W., and Mattevi, A. (2012) The enigmatic reaction of flavins with oxygen. *Trends in Biochemical Sciences* **37**, 373-380
8. Ghisla, S., and Massey, V. (1986) New flavins for old - artificial flavins as active-site probes of flavoproteins. *Biochemical Journal* **239**, 1-12
9. Mansoorabadi, S. O., Thibodeaux, C. J., and Liu, H. W. (2007) The diverse roles of flavin coenzymes-nature's most versatile thespians. *J. Org. Chem.* **72**, 6329-6342
10. Mayhew, S. G. (1999) The effects of pH and semiquinone formation on the oxidation-reduction potentials of flavin mononucleotide - A reappraisal. *Eur. J. Biochem.* **265**, 698-702
11. Akiva, E., Copp, J. N., Tokuriki, N., and Babbitt, P. C. (2017) Evolutionary and molecular foundations of multiple contemporary functions of the nitroreductase superfamily. *Proc. Natl. Acad. Sci. U. S. A.* **114**, E9549-E9558
12. Friedman, J. E., Watson, J. A., Jr., Lam, D. W., and Rokita, S. E. (2006) Iodotyrosine deiodinase is the first mammalian member of the NADH oxidase/flavin reductase superfamily. *The Journal of biological chemistry* **281**, 2812-2819
13. Bryant, C., and DeLuca, M. (1991) Purification and characterization of an oxygen-insensitive NAD(P)H nitroreductase from Enterobacter cloacae. *The Journal of biological chemistry* **266**, 4119-4125
14. Bryant, D. W., McCalla, D. R., Leeksma, M., and Laneuville, P. (1981) Type-i nitroreductases of *Escherichia coli*. *Can. J. Microbiol.* **27**, 81-86
15. Kim, H. Y., and Song, H. G. (2005) Purification and characterization of NAD(P)H-dependent nitroreductase I from *Klebsiella* sp. C1 and

enzymatic transformation of 2,4,6-trinitrotoluene. *Appl Microbiol Biotechnol* **68**, 766-773
16. Yanto, Y., Hall, M., and Bommarius, A. S. (2010) Nitroreductase from Salmonella typhimurium: characterization and catalytic activity. *Org. Biomol. Chem.* **8**, 1826-1832
17. Manina, G., Bellinzoni, M., Pasca, M. R., Neres, J., Milano, A., Ribeiro, A. L. J. L., Buroni, S., Skovierova, H., Dianiskova, P., Mikusova, K., Marak, J., Makarov, V., Giganti, D., Haouz, A., Lucarelli, A. P., Degliacomi, G., Piazza, A., Chiarelli, L. R., De Rossi, E., Salina, E., Cole, S. T., Alzari, P. M., and G., R. (2010) Biological and structural characterization of the *Micobacterium smegmatis* nitroreductase NfnB, and its role in benzothiozinone resistance. *Mol. Microbiol.* **77**, 1172-1185
18. LinWu, S. W., Wu, C. A., Peng, F. C., and Wang, A. H. (2012) Structure-based development of bacterial nitroreductase against nitrobenzodiazepine-induced hypnosis. *Biochemical pharmacology* **83**, 1690-1699
19. Pitsawong, W., Hoben, J. P., and Miller, A. F. (2014) Understanding the Broad Substrate Repertoire of Nitroreductase Based on Its Kinetic Mechanism. *J. Biol. Chem.* **289**, 15203-15214
20. Nivinskas, H., Koder, R. L., Anusevicius, Z., Sarlauskas, J., Miller, A. F., and Cenas, N. (2001) Quantitative structure-activity relationships in two-electron reduction of nitroaromatic compounds by Enterobacter cloacae NAD(P)H : nitroreductase. *Arch. Biochem. Biophys.* **385**, 170-178
21. Bryant, C., Hubbard, L., and McElroy, W. D. (1991) Cloning, nucleotide sequence, and expression of the nitroreductase gene from Enterobacter cloacae. *The Journal of biological chemistry* **266**, 4126-4130
22. Koder, R. L., Haynes, C. A., Rodgers, M. E., Rodgers, D. W., and Miller, A. F. (2002) Flavin thermodynamics explain the oxygen insensitivity of enteric nitroreductases. *Biochemistry* **41**, 14197-14205
23. Koder, R. L., Jr., and Miller, A.-F. (1998) Steady state kinetic mechanism, stereospecificity, substrate and inhibitor specificity of Enterobacter cloacae nitroreductase. *Biochim. Biophys. Acta* **1387**, 394-405
24. Race, P. R., Lovering, A. L., White, S. A., Grove, J. I., Searle, P. F., Wrighton, C. W., and Hyde, E. I. (2007) Kinetic and structural characterisation of Escherichia coli nitroreductase mutants showing improved efficacy for the prodrug substrate CB1954. *J. Mol. Biol.* **368**, 481-492
25. Miller, A. F., Park, J. T., Ferguson, K. L., Pitsawong, W., and Bommarius, A. S. (2018) Informing Efforts to Develop Nitroreductase for Amine Production. *Molecules* **23**, 22
26. Copp, J. N., Mowday, A. M., Williams, E. M., Guise, C. P., Ashoorzadeh, A., Sharrock, A. V., Flanagan, J. U., Smaill, J. B., Patterson, A. V., and Ackerley, D. F. (2017) Engineering a Multifunctional Nitroreductase for

Improved Activation of Prodrugs and PET Probes for Cancer Gene Therapy. *Cell Chemical Biology* **24**, 391-403
27. Bai, J., Yang, J., Liu, P., and Yang, Q. (2015) Transformation pathway of 2,4,6-trinitrotoluene by Escherichia coli nitroreductases and improvement of activity using structure-based mutagenesis. *Process Biochemistry* **50**, 705-711
28. Smets, B. F., Yin, H., and Esteve-Nunez, A. (2007) TNT biotransformation: when chemistry confronts mineralization. *Applied Microbiology and Biotechnology* **76**, 267-277
29. Chaignon, P., Cortial, S., Ventura, A. P., Lopes, P., Halgand, F., Laprevote, O., and Ouazzani, J. (2006) Purification and identification of a Bacillus nitroreductase: Potential use in 3,5-DNBTF biosensoring system. *Enzyme and Microbial Technology* **39**, 1499-1506
30. Herrmann, G., Jayamani, E., Mai, G., and Buckel, W. (2008) Energy conservation via electron-transferring flavoprotein in anaerobic bacteria. *Journal of Bacteriology* **190**, 784-791
31. Peters, J. W., Miller, A. F., Jones, A. K., King, P. W., and Adams, M. W. W. (2016) Electron bifurcation. *Current Opinion in Chemical Biology* **31**, 146-152
32. Buckel, W., and Thauer, R. K. (2018) Flavin-Based Electron Bifurcation, A New Mechanism of Biological Energy Coupling. *Chem. Rev.* **118**, 3862-3886
33. Garrett, R. H., and Grisham, C. M. (2017) *Biochemistry*,
34. Chowdhury, N. P., Mowafy, A. M., Demmer, J. K., Upadhyay, V., Koelzer, S., Jayamani, E., Kahnt, J., Hornung, M., Demmer, U., Ermler, U., and Buckel, W. (2014) Studies on the Mechanism of Electron Bifurcation Catalyzed by Electron Transferring Flavoprotein (Etf) and Butyryl- CoA Dehydrogenase (Bcd) of Acidaminococcus fermentans*. *Journal of Biological Chemistry* **289**, 5145-5157
35. Chowdhury, N. P., Klomann, K., Seubert, A., and Buckel, W. (2016) Reduction of Flavodoxin by Electron Bifurcation and Sodium Ion-dependent Reoxidation by NAD(+) Catalyzed by Ferredoxin-NAD(+) Reductase (Rnf). *J. Biol. Chem.* **291**, 11993-12002
36. Duan, H. D., Lubner, C. E., Tokmina-Lukaszewska, M., Gauss, G. H., Bothner, B., King, P. W., Peters, J. W., and Miller, A. F. (2018) Distinct properties underlie flavin-based electron bifurcation in a novel electron transfer flavoprotein FixAB from Rhodopseudomonas palustris. *J. Biol. Chem.* **293**, 4688-4701
37. Ledbetter, R. N., Costas, A. M. G., Lubner, C. E., Mulder, D. W., Tokmina-Lukaszewska, M., Artz, J. H., Patterson, A., Magnuson, T. S., Jay, Z. J., Duan, H. D., Miller, J., Plunkett, M. H., Hoben, J. P., Barney, B. M., Carlson, R. P., Miller, A. F., Bothner, B., King, P. W., Peters, J. W., and Seefeldt, L. C. (2017) The Electron Bifurcating FixABCX Protein Complex

from Azotobacter vinelandii: Generation of Low-Potential Reducing Equivalents for Nitrogenase Catalysis. *Biochemistry* **56**, 4177-4190

38. Costas, A. M. G., Poudel, S., Miller, A. F., Schut, G. J., Ledbetter, R. N., Fixen, K. R., Seefeldt, L. C., Adams, M. W. W., Harwood, C. S., Boyd, E. S., and Peters, J. W. (2017) Defining Electron Bifurcation in the Electron-Transferring Flavoprotein Family. *Journal of Bacteriology* **199**
39. Lubner, C. E., Jennings, D. P., Mulder, D. W., Schut, G. J., Zadvornyy, O. A., Hoben, J. P., Tokmina-Lukaszewska, M., Berry, L., Nguyen, D. M., Lipscomb, G. L., Bothner, B., Jones, A. K., Miller, A. F., King, P. W., Adams, M. W. W., and Peters, J. W. (2017) Mechanistic insights into energy conservation by flavin-based electron bifurcation. *Nat. Chem. Biol.* **13**, 655-659
40. Chang, F. C., Bradley, L. H., and Swenson, R. P. (2001) Evaluation of the hydrogen bonding interactions and their effects on the oxidation-reduction potentials for the riboflavin complex of the Desulfovibrio vulgaris flavodoxin. *Biochimica Et Biophysica Acta-Bioenergetics* **1504**, 319-328
41. Clarke, W. M. (1960) Oxidation Reduction Potentials of Organic Systems. *The Williams and Wilkins Co*, 1960
42. LinWu, S.-W., Wang, A. H. J., and Peng, F.-C. (2010) Flavin-containing reductase: new perspective on the detoxification of nitrobenzodiazepine. *Expert Opinion on Drug Metabolism & Toxicology* **6**, 967-981
43. Gasparic, J., Svobodova, D., and Pospisilova, M. (1977) Investigation of color-reaction of phenols with mbth reagent - identification of organic-compounds .86. *Mikrochimica Acta* **1**, 241-250
44. Elkommos, M. E., and Emara, K. M. (1987) Spectrophotometric determination of certain local-anesthetics using 3-methylbenzothiazolin-2-one hydrazone. *Analyst* **112**, 1253-1256
45. Koder, R. L., and Miller, A. F. (1998) Overexpression, isotopic labeling, and spectral characterization of Enterobacter cloacae nitroreductase. *Protein expression and purification* **13**, 53-60
46. Zhang, P. (2007) Nitroreductase: Evidence For A Fluxional Low-Temperature State And Its Possible Role In Enzyme Activity. *University of Kentucky Doctoral Dissertations.* **492**, 15-16
47. Pitsawong, W., Haynes, C. A., Koder, R. L., Jr., Rodgers, D. W., and Miller, A.-F. (2017) Mechanism-Informed Refinement Reveals Altered Substrate-Binding Mode for Catalytically Competent Nitroreductase. *Structure* **25**, 978-+
48. Munro, A. W., Noble, M. A., Robledo, L., Daff, S. N., and Chapman, S. K. (2001) Determination of the redox properties of human NADPH-cytochrome P450 reductase. *Biochemistry* **40**, 1956-1963
49. Park, H. J., Reiser, C. O. A., Kondruweit, S., Erdmann, H., Schmid, R. D., and Sprinzl, M. (1992) Purification and characterization of a NADH oxidase from the thermophile *Thermus thermophilus* HB8. *Eur. J. Biochem.* **205**, 881-885

50. Zoldak, G., Musatov, A., Stupak, M., Sprinzo, M., and Sedlak, E. (2005) pH-induced changes in activity and conformation of NADH oxidase from Thermus thermophilus. *General Physiology and Biophysics* **24**, 279-298
51. Henne, A., Bruggemann, H., Raasch, C., Wiezer, A., Hartsch, T., Liesegang, H., Johann, A., Lienard, T., Gohl, O., Martinez-Arias, R., Jacobi, C., Starkuviene, V., Schlenczeck, S., Dencker, S., Huber, R., Klenk, H. P., Kramer, W., Merkl, R., Gottschalk, G., and Fritz, H. J. (2004) The genome sequence of the extreme thermophile Thermus thermophilus. *Nature Biotechnology* **22**, 547-553
52. Zoldak, G., Sut'ak, R., Antalik, M., Sprinzl, M., and Sedlak, E. (2003) Role of conformational flexibility for enzymatic activity in NADH oxidase from Thermus thermophilus. *Eur. J. Biochem.* **270**, 4887-4897
53. Korbie, D. J., and Mattick, J. S. (2008) Touchdown PCR for increased specificity and sensitivity in PCR amplification. *Nature Protocols* **3**, 1452-1456
54. Seiler, C. Y., Park, J. G., Sharma, A., Hunter, P., Surapaneni, P., Sedillo, C., Field, J., Algar, R., Price, A., Steel, J., Throop, A., Fiacco, M., and LaBaer, J. (2014) DNASU plasmid and PSI: Biology-Materials repositories: resources to accelerate biological research. *Nucleic Acids Research* **42**, D1253-D1260
55. Cormier, C. Y., Park, J. G., Fiacco, M., Steel, J., Hunter, P., Kramer, J., Singla, R., and LaBaer, J. (2011) PSI:Biology-materials repository: a biologist's resource for protein expression plasmids. *Journal of Structural and Functional Genomics* **12**, 55-62
56. Cormier, C. Y., Mohr, S. E., Zuo, D., Hu, Y., Rolfs, A., Kramer, J., Taycher, E., Kelley, F., Fiacco, M., Turnbull, G., and LaBaer, J. (2010) Protein Structure Initiative Material Repository: an open shared public resource of structural genomics plasmids for the biological community. *Nucleic Acids Research* **38**, D743-D749
57. Siebner, M. (1997) *Struktur-Funktionsbeziehungen der NADH-Oxidase aus Thermus thermophiles.*Ph. D., Technische Universität Carolo-Wilhelmina zu Braunschweig
58. Hald, E., Lehmann, P., and Ziegenhorn, J. (1975) Molar Absorptivities of β-NADH and β-NAD at 260 nm. *Clinical Chemistry* **21**, 884-887
59. Kim, C., Crane, F. L., Faulk, W. P., and Morré, D. J. (2002) Purification and Characterization of a Doxorubicin-inhibited NADH-quinone (NADH-ferricyanide) Reductase from Rat Liver Plasma Membranes. *J. Biol. Chem.* **277**, 16441-16447
60. Zenno, S., Koike, H., Tanokura, M., and Saigo, K. (1996) Gene Cloning, Purification, and Characterization of NfsB, a Minor Oxygen-Insensitive Nitroreductase from Escherichia coli, Similar in Biochemical Properties to FRase I, the Major Flavin Reductase in Vibrio fischeri1. *Journal of Biochemistry* **120**, 736-744

61. Massey, V. (1991) A simple method for determination of redox potentials. in *Flavins and flavoproteins.* (Curti, B., Ronchi, S., and Zanetti, G. eds.), Walter de Gruyer, Berlin. pp 59-66
62. Park, H. J., Kreutzer, R., Reiser, C. O. A., and Sprinzl, M. (1992) Molecular cloning and nucleotide sequence of the gene encoding a H_2O_2-forming nadh oxidase from the extreme thermophilic *Thermos thermophilus* HB8 and its expression in *Escherichia coli*
Eur. J. Biochem. **205**, 875-879
63. Hecht, H.-J., Erdmann, H., Park, H. J., Sprinzl, M., and Schmid, R. D. (1995) Crystal structure of NADH oxidase from *Thermus thermophilus*. *Nat. Struct. Biol.* **2**
64. Massey, V., and Palmer, G. (1966) On existence of spectrally distinct classes of flavoprotein semiquinones . a new method for quantitative production of flavoprotein semiquinones. *Biochemistry* **5**, 3181-&
65. Toth, K., Sedlak, E., Musatov, A., and Zoldak, G. (2010) Activity of NADH oxidase from Thermus thermophilus in water/alcohol binary mixtures is limited by the stability of quaternary structure. *Journal of Molecular Catalysis B-Enzymatic* **64**, 60-67
66. Li, X., and Tu, S. C. (2006) Activity coupling of Vibrio harveyi luciferase and flavin reductase (FRP): Oxygen as a probe. *Arch. Biochem. Biophys.* **454**, 26-31
67. Jawanda, N., Ahmed, K., and Tu, S. C. (2008) Vibrio harveyi flavin reductase-luciferase fusion protein mimics a single-component bifunctional monooxygenase. *Biochemistry* **47**, 368-377
68. Merkley, E. D., Daggett, V., and Parson, W. W. (2012) A temperature-dependent conformational change of NADH oxidase from Thermus thermophilus HB8. *Proteins-Structure Function and Bioinformatics* **80**, 546-555
69. Buckel, W., and Thauer, R. K. (2013) Energy conservation via electron bifurcating ferredoxin reduction and proton/Na+ translocating ferredoxin oxidation. *Biochimica Et Biophysica Acta-Bioenergetics* **1827**, 94-113
70. Scott, J. D., and Ludwig, R. A. (2004) Azorhizobium caulinodans electron-transferring flavoprotein N electrochemically couples pyruvate dehydrogenase complex activity to N-2 fixation. *Microbiology-Sgm* **150**, 117-126
71. Huang, J. J., Heiniger, E. K., McKinlay, J. B., and Harwood, C. S. (2010) Production of Hydrogen Gas from Light and the Inorganic Electron Donor Thiosulfate by Rhodopseudomonas palustris. *Applied and Environmental Microbiology* **76**, 7717-7722
72. Edgren, T., and Nordlund, S. (2004) The fixABCX genes in Rhodospirillum rubrum encode a putative membrane complex participating in electron transfer to nitrogenase. *Journal of Bacteriology* **186**, 2052-2060
73. Mitchell, P. (1975) The protonmotive Q cycle: A general formulation. *FEBS Letters* **59**, 137-139

74. Nitschke, W., and Russell, M. J. (2012) Redox bifurcations: Mechanisms and importance to life now, and at its origin. *Bioessays* **34**, 106-109
75. Demmer, J. K., Huang, H., Wang, S., Demmer, U., Thauer, R. K., and Ermler, U. (2015) Insights into Flavin-based Electron Bifurcation via the NADH-dependent Reduced Ferredoxin:NADP Oxidoreductase Structure. *J. Biol. Chem.* **290**, 21985-21995
76. Curley, G. P., Carr, M. C., Mayhew, S. G., and Voordouw, G. (1991) Redox and flavin-binding properties of recombinant flavodoxin from Desulfovibrio vulgaris (Hildenborough). *Eur. J. Biochem.* **202**, 1091-1100
77. Cui, D. (2010) *15N Solid-state NMR Detection of Flavin Perturnation by H-bonding in Models and Enzyme Active Sites.* Ph.D., University of Kentucky
78. Mayhew, S. G., Foust, G. P., and Massey, V. (1969) Oxidation-Reduction Properties Of Flavodoxin From *Peptostreptococcus Elsdenii*. *J. Biol. Chem.* **244**, 803-810
79. Pitsawong, W., Hoben, J. P., and Miller, A.-F. (2014) Understanding the broad substrate repertoire of nitroreductase based on its simple mechanism. *J. Biochem. Chem.* **289**, 15203-15214
80. Aliverti, A., Curti, B., and Vanoni, M. A. (1999) Identifying and quantitating FAD and FMN in simple and in iron-sulfur-containing flavoproteins. in *Methods in Molecular Biology* (Chapman, S. K., and Reid, G. A. eds.), Humana Press Inc., Totowa, NJ. pp 9-23
81. La Mer, V. K., and Parsons, T. R. (1923) The application of the quinhydrone electrode to electrometric acid- base titrations in the presence of air, and the factors limiting its use in alkaline solution. *J. Biol. Chem.* **57**, 613-631
82. Lakowicz, J. R. (2007) Ch 6. Solvent and Environmental Effects. in *Principles of Fluorescence Spectroscopy.* Springer Science & Business Media. pp 205-235
83. Liu, Z. Y., Tan, C., Guo, X. M., Li, J., Wang, L. J., Sancar, A., and Zhong, D. P. (2013) Determining complete electron flow in the cofactor photoreduction of oxidized photolyase. *Proc. Natl. Acad. Sci. U. S. A.* **110**, 12966-12971
84. Mathes, T., van Stokkum, I. H. M., Stierl, M., and Kennis, J. T. M. (2012) Redox Modulation of Flavin and Tyrosine Determines Photoinduced Proton-coupled Electron Transfer and Photoactivation of BLUF Photoreceptors. *J. Biol. Chem.* **287**, 31725-31738
85. Hardman, S. J. O., Pudney, C. R., Hay, S., and Scrutton, N. S. (2013) Excited State Dynamics Can Be Used to Probe Donor-Acceptor Distances for H-Tunneling Reactions Catalyzed by Flavoproteins. *Biophys. J.* **105**, 2549-2558
86. Gauden, M., Grinstead, J. S., Laan, W., van Stokkum, I. H. M., Avila-Perez, M., Toh, K. C., Boelens, R., Kaptein, R., van Grondelle, R., Hellingwerf, K. J., and Kennis, J. T. M. (2007) On the role of aromatic side

chains in the photoactivation of BLUF domains. *Biochemistry* **46**, 7405-7415
87. Gray, H. B., and Winkler, J. R. (1996) Electron transfer in proteins. *Annu. Rev. Biochem.* **65**, 537-561
88. He, T. F., Guo, L. J., Guo, X. M., Chang, C. W., Wang, L. J., and Zhong, D. P. (2013) Femtosecond Dynamics of Short-Range Protein Electron Transfer in Flavodoxin. *Biochemistry* **52**, 9120-9128
89. Crozier-Reabe, K., and Moran, G. R. (2012) Form Follows Function: Structural and Catalytic Variation in the Class A Flavoprotein Monooxygenases. *Int. J. Mol. Sci.* **13**, 15601-15639
90. Enescu, M., Lindqvist, L., and Soep, B. (1998) Excited-state dynamics of fully reduced flavins and flavoenzymes studied at subpicosecond time resolution. *Photochem. Photobiol.* **68**, 150-156
91. Mataga, N., Chosrowjan, H., Taniguchi, S., Tanaka, F., Kido, N., and Kitamura, M. (2002) Femtosecond fluorescence dynamics of flavoproteins: Comparative studies on flavodoxin, its site-directed mutants, and riboflavin binding protein regarding ultrafast electron transfer in protein nanospaces. *Journal of Physical Chemistry B* **106**, 8917-8920
92. Petushkov, V. N., van Stokkum, I. H. M., Gobets, B., van Mourik, F., Lee, J., van Grondelle, R., and Visser, A. J. W. G. (2003) Ultrafast Fluorescence Relaxation Spectroscopy of 6,7-Dimethyl-(8-ribityl)-lumazine and Riboflavin, Free and Bound to Antenna Proteins from Bioluminescent Bacteria. *The Journal of Physical Chemistry B* **107**, 10934-10939
93. Gauden, M., van Stokkum, I. H. M., Key, J. M., Luhrs, D. C., Van Grondelle, R., Hegemann, P., and Kennis, J. T. M. (2006) Hydrogen-bond switching through a radical pair mechanism in a flavin-binding photoreceptor. *Proc. Natl. Acad. Sci. U. S. A.* **103**, 10895-10900
94. Fenimore, P. W., Frauenfelder, H., McMahon, B. H., and Parak, F. G. (2002) Slaving: Solvent fluctuations dominate protein dynamics and functions. *Proceedings of the National Academy of Sciences* **99**, 16047-16051
95. Butterwick, J. A., Patrick Loria, J., Astrof, N. S., Kroenke, C. D., Cole, R., Rance, M., and Palmer, A. G. (2004) Multiple Time Scale Backbone Dynamics of Homologous Thermophilic and Mesophilic Ribonuclease HI Enzymes. *J. Mol. Biol.* **339**, 855-871
96. Abramovitz, A. S., and Massey, V. (1976) Interaction of phenols with old yellow enzyme - physical evidence for charge-transfer complexes. *J. Biol. Chem.* **251**, 5327-5336
97. Hay, S., Pudney, C. R., McGrory, T. A., Pang, J. Y., Sutcliffe, M. J., and Scrutton, N. S. (2009) Barrier Compression Enhances an Enzymatic Hydrogen-Transfer Reaction. *Angewandte Chemie-International Edition* **48**, 1452-1454
98. Miura, R. (2001) Versatility and specificity in flavoenzymes: Control mechanisms of flavin reactivity. *Chem. Rec.* **1**, 183-194

99. Swenson, R. P., and Krey, G. D. (1994) Site-Directed Mutagenesis of Tyrosine-98 in the Flavodoxin from Desulfovibrio vulgaris (Hildenborough): Regulation of Oxidation-Reduction Properties of the Bound FMN Cofactor by Aromatic, Solvent, and Electrostatic Interactions. *Biochemistry* **33**, 8505-8514
100. Haynes, C. A., Koder, R. L., Jr., Miller, A.-F., and Rodgers, D. W. (2002) Structures of Nitroreductase in Three States: Effects of Inhibitor Binding and Reduction. *J. Biol. Chem.* **277**, 11513-11520
101. Penzkofer, A., Bansal, A. K., Song, S. H., and Dick, B. (2007) Fluorescence quenching of flavins by reductive agents. *Chem. Phys.* **336**, 14-21
102. Schoepp-Cothenet, B., van Lis, R., Atteia, A., Baymann, F., Capowiez, L., Ducluzeau, A.-L., Duval, S., ten Brink, F., Russell, M. J., and Nitschke, W. (2013) On the universal core of bioenergetics. *Biochimica et Biophysica Acta (BBA) - Bioenergetics* **1827**, 79-93
103. Lukacs, A., Zhao, R. K., Haigney, A., Brust, R., Greetham, G. M., Towrie, M., Tonge, P. J., and Meech, S. R. (2012) Excited State Structure and Dynamics of the Neutral and Anionic Flavin Radical Revealed by Ultrafast Transient Mid-IR to Visible Spectroscopy. *Journal of Physical Chemistry B* **116**, 5810-5818
104. Artali, R., Bombieri, G., Meneghetti, F., Gilardi, G., Sadeghi, S. J., Cavazzini, D., and Rossi, G. L. (2002) Comparison of the refined crystal structures of wild-type (1.34 A) flavodoxin from Desulfovibrio vulgaris and the S35C mutant (1.44 A) at 100 K. . *Acta Crystallogr D Biol Crystallogr* **58**, 1787-1792
105. Syrokomsky, W. S., and Stiepin, V. V. (1936) New Oxidation—Reduction Indicators. I. Phenylanthranilic Acid (o-Diphenylamine Carbonic Acid). *J. Am. Chem. Soc.* **58**, 928-929
106. Chobot, V., Hadacek, F., Weckwerth, W., and Kubicova, L. (2015) Iron chelation and redox chemistry of anthranilic acid and 3-hydroxyanthranilic acid: A comparison of two structurally related kynurenine pathway metabolites to obtain improved insights into their potential role in neurological disease development. *J. Organomet. Chem.* **782**, 103-110
107. Montilla , F., Morallón, E., and Vázquez, J. L. (2003) Electrochemical Behaviour of Benzoic Acid on Platinum and Gold Electrodes. *Langmuir* **19**, 1021-10246
108. Armenta, M. E., and Diaz, A. F. (2005) Oxidation of benzoic acid by electrochemically generated Ce(IV). *Environ Sci Technol* **1**, 5872-5877
109. Pettersen, E. F., Goddard, T. D., Huang, C. C., Couch, G. S., Greenblatt, D. M., Meng, E. C., and Ferrin, T. E. (2004) UCSF Chimera - a visualization system for exploratory research and analysis. *J. Comput. Chem.* **25**, 1605-1612
110. Lehninger, A. L. (1971) *Bioenergetics: The Molecular Basis of Biological Energy Transformations*, W. A. Benjamin

111. Paulsen, I. T., Sliwinski, M. K., and Saier, M. H. (1998) Microbial genome analyses: Global comparisons of transport capabilities based on phylogenies, bioenergetics and substrate specificities. *J. Mol. Biol.* **277**, 573-592
112. Peters, J. W., Miller, A.-F., Jones, A. K., King, P. W., and Adams, M. W. W. (2016) Electron bifurcation. *Current Opinion in Chemical Biology* **31**, 146-152
113. Chowdhury, N. P., Kahnt, J., and Buckel, W. (2015) Reduction of ferredoxin or oxygen by flavin-based electron bifurcation in Megasphaeraelsdenii. *Febs Journal* **282**, 3149-3160
114. Sato, K., Nishina, Y., and Shiga, K. (2003) Purification of electron-transferring flavoprotein from Megasphaera elsdenii and binding of additional FAD with an unusual absorption spectrum. *Journal of Biochemistry* **134**, 719-729
115. Thauer, R. K. (2015) My Lifelong Passion for Biochemistry and Anaerobic Microorganisms. *Annual Review of Microbiology* **69**, 1-30
116. Metcalf, W. W. (2016) Classic Spotlight: Electron Bifurcation, a Unifying Concept for Energy Conservation in Anaerobes. *Journal of Bacteriology* **198**, 1358-1358
117. Lipscomb, G. L., Stirrett, K., Schut, G. J., Yang, F., Jenney, F. E., Scott, R. A., Adams, M. W. W., and Westpheling, J. (2011) Natural Competence in the Hyperthermophilic Archaeon Pyrococcus furiosus Facilitates Genetic Manipulation: Construction of Markerless Deletions of Genes Encoding the Two Cytoplasmic Hydrogenases. *Applied and Environmental Microbiology* **77**, 2232-2238
118. Verhagen, M., Menon, A. L., Schut, G. J., and Adams, M. W. W. (2001) Pyrococcus furiosus: Large-scale cultivation and enzyme purification. *Methods Enzymol.* **330**, 25-30
119. Massey, V., and Palmer, G. (1962) Charge Transfer Complexes of Lipoyl Dehydrogenase and Free Flavins. *J. Biol. Chem.* **237**, 2347-2358
120. Loach, P. A. (1973) Oxidation-reduction potentials: Absorbance bands and molar absorbance of compounds used in biochemical studies. in *Handbook of Biochemistry Selected Data for Molecular Biology* (Sorber, H. A., Ed. ed. ed.), The Chemical Rubber Co. (CRC Press), Cleveland, OH. pp J-33 - J-40
121. Minnaert, K. (1965) Measurement of the equilibrium constant of the reaction between cytochrome c and cytochrome a. *Biochimica et Biophysica Acta (BBA) - Enzymology and Biological Oxidation* **110**, 42-56
122. Sato, K., Nishina, Y., and Shiga, K. (2013) Interaction between NADH and electron-transferring flavoprotein from Megasphaera elsdenii. *Journal of Biochemistry* **153**, 565-572
123. Toth, K., Sedlak, E., Sprinzl, M., and Zoldak, G. (2008) Flexibility and enzyme activity of NADH oxidase from Thermus thermophilus in the

presence of monovalent cations of Hofmeister series. *Biochimica Et Biophysica Acta-Proteins and Proteomics* **1784**, 789-795
124. Bang, S. Y., Kim, J. H., Lee, P. Y., Bae, K.-H., Lee, J. S., Kim, P.-S., Lee, D. H., Myung, P. K., Parka, B. C., and Park, S. G. (2012) Confirmation of Frm2 as a novel nitroreductase in Saccharomyces cerevisiae. *Biochemical and Biophysical Research Communications* **423**, 638-641
125. Yang, Y., Lin, J., and Wei, D. (2016) Heterologous Overexpression and Biochemical Characterization of a Nitroreductase from Gluconobacter oxydans 621H. *Molecular Biotechnology* **58**, 428-440
126. Mirza, A., Desai, R., and Reynisson, J. (2009) Known drug space as a metric in exploring the boundaries of drug-like chemical space. *Eur. J. Med. Chem.* **44**, 5006-5011
127. Corma, A., Concepcion, P., and Serna, P. (2007) A different reaction pathway for the reduction of aromatic nitro compounds on gold catalysts. *Angewandte Chemie-International Edition* **46**, 7266-7269
128. Alsante, K. M., Huynh-Ba, K. C., Baertschi, S. W., Reed, R. A., Landis, M. S., Furness, S., Olsen, B., Mowery, M., Russo, K., Iser, R., Stephenson, G. A., and Jansen, P. (2014) Recent Trends in Product Development and Regulatory Issues on Impurities in Active Pharmaceutical Ingredient (API) and Drug Products. Part 2: Safety Considerations of Impurities in Pharmaceutical Products and Surveying the Impurity Landscape. *Aaps Pharmscitech* **15**, 237-251
129. Hasford, J. J., Kemnitzer, W., and Rizzo, C. J. (1997) Conformational Effects on Flavin Redox Chemistry. *The Journal of Organic Chemistry* **62**, 5244-5245
130. Reibenspies, J. H., Guo, F., and Rizzo, C. J. (2000) X-ray Crystal Structures of Conformationally Biased Flavin Models. *Organic Letters* **2**, 903-906
131. Walsh, J. D., and Miller, A.-F. (2003) Flavin reduction potential tuning by substitution and bending. *Journal of Molecular Structure: THEOCHEM* **623**, 185-195
132. Völkl, P., Huber, R., Drobner, E., Rachel, R., Burggraf, S., Trincone, A., and Stetter, K. O. (1993) Pyrobaculum aerophilum sp. nov., a novel nitrate-reducing hyperthermophilic archaeum. *Applied and Environmental Microbiology* **59**, 2918-2926
133. Cozen, A. E., Weirauch, M. T., Pollard, K. S., Bernick, D. L., Stuart, J. M., and Lowe, T. M. (2009) Transcriptional Map of Respiratory Versatility in the Hyperthermophilic Crenarchaeon Pyrobaculum aerophilum. *Journal of Bacteriology* **191**, 782-794
134. Afshar, S., Kim, C., Monbouquette, H. G., and Schröder, I. (1998) Effect of Tungstate on Nitrate Reduction by the Hyperthermophilic Archaeon Pyrobaculum aerophilum. *Applied and Environmental Microbiology* **64**, 3004-3008

135. Feinberg, L. F., Srikanth, R., Vachet, R. W., and Holden, J. F. (2008) Constraints on Anaerobic Respiration in the Hyperthermophilic Archaea Pyrobaculum islandicum and Pyrobaculum aerophilum. *Applied and Environmental Microbiology* **74**, 396-402
136. Feinberg, L. F., and Holden, J. F. (2006) Characterization of Dissimilatory Fe(III) versus NO₃[−] Reduction in the Hyperthermophilic Archaeon Pyrobaculum aerophilum. *Journal of Bacteriology* **188**, 525-531
137. Huber, R., Sacher, M., Vollmann, A., Huber, H., and Rose, D. (2000) Respiration of Arsenate and Selenate by Hyperthermophilic Archaea. *Systematic and Applied Microbiology* **23**, 305-314
138. Kashefi, K., and Lovley, D. R. (2000) Reduction of Fe(III), Mn(IV), and Toxic Metals at 100°C by Pyrobaculum islandicum. *Applied and Environmental Microbiology* **66**, 1050-1056
139. Takai, K., and Horikoshi, K. (1999) Molecular Phylogenetic Analysis of Archaeal Intron-Containing Genes Coding for rRNA Obtained from a Deep-Subsurface Geothermal Water Pool. *Applied and Environmental Microbiology* **65**, 5586-5589
140. Nguyen, D., Schut, G., Zadvornyy, O., Tokmina-Lukaszewska, M., Poudel, S., L. Lipscomb, G., A. Adams, L., T. Dinsmore, J., J. Nixon, W., Boyd, E., Bothner, B., W. Peters, J., and W. W. Adams, M. (2017) *Two functionally distinct NADP + -dependent ferredoxin oxidoreductases maintain the primary redox balance of Pyrococcus furiosus*,
141. Mullen, K. M., and van Stokkum, I. H. M. (2007) TIMP: An R package for modeling multi-way spectroscopic measurements. *J. Stat. Softw.* **18**, 46
142. Snellenburg, J. J., Laptenok, S. P., Seger, R., Mullen, K. M., and van Stokkum, I. H. M. (2012) Glotaran: A Java-Based Graphical User Interface for the R Package TIMP. *J. Stat. Softw.* **49**, 1-22
143. van Stokkum, I. H. M., Larsen, D. S., and van Grondelle, R. (2004) Global and target analysis of time-resolved spectra. *Biochimica et Biophysica Acta (BBA) - Bioenergetics* **1657**, 82-104
144. Nitschke, W., and Russell, M. J. (2009) Hydrothermal Focusing of Chemical and Chemiosmotic Energy, Supported by Delivery of Catalytic Fe, Ni, Mo/W, Co, S and Se, Forced Life to Emerge. *J. Mol. Evol.* **69**, 481-496

CURRICULUM VITAE

John Patrick Hoben

EDUCATION

Ph.D. Chemistry, expected Fall 2018 3.7 GPA
Department of Chemistry, University of Kentucky, Lexington, KY
Advisor: Anne-Frances Miller, Ph.D.
Thesis: *Protein suppression of flavin semiquinone as a mechanistically important control of reactivity: a study comparing flavoenzymes which differ in redox properties, substrates, and ability to bifurcate electron*s

M.S. Soil Science, 2009 4.0 GPA
Department of Crop and Soil Sciences, Michigan State University, East Lansing, MI
Advisors: Ron Gehl, Ph.D.; Philip Robertson, Ph.D.
Thesis: *Field measurements of nitrous oxide emissions across a nitrogen fertilizer gradient for corn cropping systems.*

B.S. Agriculture (double major in Chemistry), 2004 3.7 GPA
Department of Plant and Soil Science, University of Kentucky, Lexington, KY
Advisor: Arthur Cammers, Ph.D.
Thesis: *The nature of global conformation in peptidomimetic oligoureas.*

EXPERIENCE

GRADUATE RESEARCH ASSISTANT, May 2013 – December 2018
Department of Chemistry, University of Kentucky.

CORE FACILITIES MANAGER, February 2012 – May 2017
Department of Chemistry, University of Kentucky.

GRADUATE TEACHING ASSISTANT, August 2011 - May 2013
Department of Chemistry, University of Kentucky.

LAB MANAGER, January 2010 - June 2011.
Soil Testing Lab, Kansas State University.

GRADUATE RESEARCH ASSISTANT, January 2007 - December 2009.
Department of Crop and Soil Sciences, Michigan State University.

LABORATORY TECHNICIAN, August 2006 - December 2006.
Department of Plant and Soil Science, University of Kentucky.

SENIOR LABORATORY TECHNICIAN, October 2004 - April 2006.
Kentucky Tobacco Research and Development Center, University of Kentucky.

RESEARCH TECHNICIAN, June 2002 - September 2004.
Department of Chemistry, University of Kentucky.

LABORATORY TECHNICIAN, June 2001 - February 2004.
Department of Molecular and Cellular Biochemistry, University of Kentucky.

AWARDS

• Research Challenge Trust Fellowship. Graduate School, University of Kentucky; 2014 -present
• Innovation Award. Biological Electron Transfer and Catalysis (BETCy) Energy Frontiers Research Center (EFRC), Department of Energy (DOE); 2015
• Max Steckler Fellowship. Department of Chemistry, University of Kentucky; 2012 - 2014
• Graduate Recruitment Scholarship. Department of Chemistry, University of Kentucky; 2011 - 2012
• 100% Plus Award. Department of Chemistry, University of Kentucky; 2011
• Graduate Student Award. North Central Extension-Industry Soil Fertility Conference; 2007
• Graduate Recruitment Scholarship. Department of Crop and Soil Sciences, Michigan State
University; 2007
• Towle Bedford Scholarship. Department of Chemistry, University of Kentucky; 2004
• Willard Riggs Meredith Award. Department of Chemistry, University of Kentucky; 2004

PUBLICATIONS

Hoben, J. P., Lubner, C. E., Ratzloff, M. W., Schut, G. J., Nguyen, D. M. N., Hempel, K. W., Adams, M. W. W., King, P. W., and Miller, A. F. (2017) Equilibrium and ultrafast kinetic studies manipulating electron transfer: A short-lived flavin semiquinone is not sufficient for electron bifurcation. *J. Biol. Chem.* **292**, 14039-14049.

Hoben, J. P.; Wang, J. N.; Miller, A. F., Unboiling an Egg: An Introduction to Circular Dichroism and Protein Refolding. *Journal of Chemical Education* **2017**, *94* (3), 356-360.

Lubner, C. E.; Jennings, D. P.; Mulder, D. W.; Schut, G. J.; Zadvornyy, O. A.; **Hoben, J. P.**; Tokmina-Lukaszewska, M.; Berry, L.; Nguyen, D. M.; Lipscomb, G. L.; Bothner, B.; Jones, A. K.; Miller, A. F.; King, P. W.; Adams, M. W. W.; Peters, J. W., Mechanistic insights into energy conservation by flavin-based electron bifurcation. *Nature Chemical Biology* **2017**, *13* (6), 655-659.

Ledbetter, R. N., Costas, A. M. G., Lubner, C. E., Mulder, D. W., Tokmina-Lukaszewska, M., Artz, J. H., Patterson, A., Magnuson, T. S., Jay, Z. J., Duan, H. D., Miller, J., Plunkett, M. H., **Hoben, J. P.**, Barney, B. M., Carlson, R. P., Miller, A. F., Bothner, B., King, P. W., Peters, J. W., and Seefeldt, L. C. (2017) The Electron Bifurcating FixABCX Protein Complex from Azotobacter vinelandii: Generation of Low-Potential Reducing Equivalents for Nitrogenase Catalysis. *Biochemistry* **56**, 4177-4190

Pitsawong, W.; **Hoben, J. P.**; Miller, A. F., Understanding the Broad Substrate Repertoire of Nitroreductase Based on Its Kinetic Mechanism. *Journal of Biological Chemistry* **2014,** *289* (22), 15203-15214.

Thelen, K. D.; Gao, J.; **Hoben, J.**; Qian, L. L.; Saffron, C.; Withers, K., A spreadsheet-based model for teaching the agronomic, economic, and environmental aspects of bioenergy cropping systems. *Computers and Electronics in Agriculture* **2012,** *85*, 157-163.

Hoben, J. P.; Gehl, R. J.; Millar, N.; Grace, P. R.; Robertson, G. P., Nonlinear nitrous oxide (N2O) response to nitrogen fertilizer in on-farm corn crops of the US Midwest. *Global Change Biology* **2011,** *17* (2), 1140-1152.

Grace, P. R.; Robertson, G. P.; Millar, N.; Colunga-Garcia, M.; Basso, B.; Gage, S. H.; **Hoben, J.**, The contribution of maize cropping in the Midwest USA to global warming: A regional estimate. *Agricultural Systems* **2011,** *104* (3), 292-296.

Millar, N.; Robertson, G. P.; Grace, P. R.; Gehl, R. J.; **Hoben, J. P.**, Nitrogen fertilizer management for nitrous oxide (N2O) mitigation in intensive corn (Maize) production: an emissions reduction protocol for US Midwest agriculture. *Mitigation and Adaptation Strategies for Global Change* **2010,** *15* (2), 185-204.